Storm Track Response to Perturbations in Climate

Thesis by

Cheikh Oumar Mbengue

In Partial Fulfillment of the Requirements

for the Degree of

Doctor of Philosophy

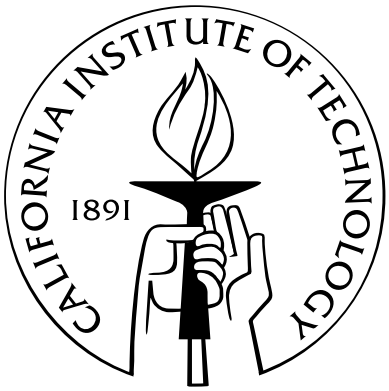

California Institute of Technology

Pasadena, California

2015

(Defended May 6, 2015)

To Elizabeth J. C. Mbengue

Acknowledgements

First, I would like to thank my mother, Elizabeth J. C. Mbengue, for providing me with all of the tools that I needed to make it this far.

A big thank you to my thesis advisor, Professor Tapio Schneider. I am extremely grateful for your support and guidance over the past four years. Your leadership, wisdom, and broad knowledge were an inspiration. Thank you for granting me the opportunity to grow and develop as a researcher.

I am grateful to the members of my research group, past and present, whom I encountered on my PhD-research journey. You made my time at Caltech and at ETH very memorable.

I would like to thank the members of my thesis advisory committee for their time, support, and advice. Your comments vastly improved this thesis. For the work done in chapter 1, I am grateful for the financial support provided by the National Science Foundation (grant AGS-1019211) and for the helpful discussions with Dr. Xavier Levine.

Abstract

This thesis advances our understanding of midlatitude storm tracks and how they respond to perturbations in the climate system. The midlatitude storm tracks are regions of maximal turbulent kinetic energy in the atmosphere. Through them, the bulk of the atmospheric transport of energy, water vapor, and angular momentum occurs in midlatitudes. Therefore, they are important regulators of climate, controlling basic features such as the distribution of surface temperatures, precipitation, and winds in midlatitudes. Storm tracks are robustly projected to shift poleward in global-warming simulations with current climate models. Yet the reasons for this shift have remained unclear. Here we show that this shift occurs even in extremely idealized (but still three-dimensional) simulations of dry atmospheres. We use these simulations to develop an understanding of the processes responsible for the shift and develop a conceptual model that accounts for it.

We demonstrate that changes in the convective static stability in the deep tropics alone can drive remote shifts in the midlatitude storm tracks. Through simulations with a dry idealized general circulation model (GCM), midlatitude storm tracks are shown to be located where the mean available potential energy (MAPE, a measure of the potential energy available to be converted into kinetic energy) is maximal.

As the climate varies, even if only driven by tropical static stability changes, the MAPE maximum shifts primarily because of shifts of the maximum of near-surface meridional temperature gradients. The temperature gradients shift in response to changes in the width of the tropical Hadley circulation, whose width is affected by the tropical static stability. Storm tracks generally shift in tandem with shifts of the subtropical terminus of the Hadley circulation.

We develop a one-dimensional diffusive energy-balance model that links changes in the Hadley circulation to midlatitude temperature gradients and so to the storm tracks. It is the first conceptual model to incorporate a dynamical coupling between the tropical Hadley circulation and midlatitude turbulent energy transport. Numerical and analytical solutions of the model elucidate the circumstances of when and how the storm tracks shift in tandem with the terminus of the Hadley circulation. They illustrate how an increase of only the convective static stability in the deep tropics can lead to an expansion of the Hadley circulation and a poleward shift of storm tracks.

The simulations with the idealized GCM and the conceptual energy-balance model demonstrate a clear link between Hadley circulation dynamics and midlatitude storm track position. With the help of the hierarchy of models presented in this thesis, we obtain a closed theory of storm track shifts in dry climates. The relevance of this theory for more realistic moist climates is discussed.

Contents

List of Tables

List of Figures

Thesis summary

In this thesis, we insert ourselves into the debate on the mechanisms that control shifts in midlatitude storm tracks as the climate changes. In chapter 1, we define storm tracks and give some background, which places our interest in storm track shifts into context.

In chapter 2, we present results of several climate change simulations using an idealized dry general circulation model (GCM). We quantify the degree to which large-scale dry processes account for the observed and simulated shifts in the storm tracks as the climate changes. Further, we demonstrate that changes in convective stability in the deep tropics alone can drive remote shifts in the storm tracks. The work in this chapter was published in the Journal of Climate[1].

In chapter 3, we use mean available potential energy (MAPE) to focus our investigation of storm track shifts. Through simulations with the dry GCM, midlatitude storm tracks are shown to be located where MAPE, a measure of the potential energy available to be converted into kinetic energy, is maximal. As the climate varies, shifts in the MAPE maximum occur primarily because of shifts in near-surface meridional temperature gradients. Hence, investigating shifts in near-surface temperature gradi-

[1]Mbengue, C. O., and T. Schneider, 2013: **Storm track shifts under climate change: what can be learned from large-scale dry dynamics**. *Journal of Climate*, **26**, 9923–9930.

ents helps simplify and focuses our investigation of storm track shifts. This chapter culminates in the hypothesis that expansions of the Hadley cell, through its effect on midlatitude near-surface meridional temperature gradients, shift storm tracks poleward. The work in chapter 3 is being prepared for submission to the Journal of the Atmospheric Sciences[2].

In chapter 4, we develop and use a simple conceptual model to test our hypothesis that expansions of the Hadley cell shift storm tracks poleward. We propose a simple mechanism of storm track shifts that is largely consistent with observations and prior work. We demonstrate a clear link between Hadley circulation dynamics and storm track position. We show that expansions of the Hadley cell, induced, for example, by increases in tropical static stability, can shift the storm tracks poleward. Thus, with the aid of a hierarchy of models, we obtain a closed theory of storm track shifts in dry climates. The work in this chapter is being prepared for submission to the Journal of the Atmospheric Sciences[3].

[2]Mbengue, C. O., and T. Schneider, 2015: **Toward a mechanistic understanding of storm track shifts using local measures of mean available potential energy**. In prep.

[3]Mbengue, C. O., and T. Schneider, 2015: **Linking Hadley circulation and storm tracks in an energy-balance model**. In prep.

Chapter 1

Introduction

1.1 Storm track response to climate change

The midlatitude storm tracks establish the day-to-day weather over vast regions of the Earth's surface. Any change in their location will have far reaching impacts. Precipitation distributions could change, as could the distribution of severe weather associated with the storm tracks. As the climate changes, the storm tracks will change, whether or not the changes are human induced or a function of internal variability.

There is growing observational (Bender et al., 2012) and strong modeling (Yin, 2005; Bengtsson et al., 2006; Tsushima et al., 2006; Schneider et al., 2010; Swart and Fyfe, 2012; Barnes and Polvani, 2013) evidence that the storm tracks will shift poleward as the climate warms. On the modeling side, Yin (2005) demonstrates the poleward shift of storm tracks seen in an ensemble of 15 of the GCMs used for the Intergovernmental Panel on Climate Change (IPCC) fourth assessment report; but, the dynamical mechanisms responsible for this shift remain unclear.

Another, albeit less robust, response of the storm tracks to warming is a reduction

in the frequency of cyclones, but an increase in their intensity (Geng and Sugi, 2003; O'Gorman, 2010; Chang, 2013).

1.1.1 Existing theories on storm track shifts

Since Yin (2005) documented the consistent poleward shift of storm tracks in 2004–5, there has been an eruption of proposals for mechanisms to explain the observed and simulated shifts in the storm tracks. Yin (2005) offered the partial explanation that shifts in maximum baroclinicity, and thus the storm tracks, are dominated by shifts in the meridional temperature gradient, which shifts the storm tracks. He did this by decomposing a measure for storm track activity known as the Eady growth rate, $\Gamma = 0.31\ g\ (N\ T)^{-1}|\partial_y T|$, where $N = \sqrt{g\ \theta^{-1}\ \partial_z \theta}$ is a measure of stability called the Brunt-Väisälä frequency, into its components. This explanation is incomplete since it offered no mechanism for the shifts in the meridional temperature gradients themselves.

Interestingly, another study (Lu et al., 2010) used a different measure to study the storm tracks; the potential vorticity ($PV = \nabla \cdot F$, where $F = -\overline{u'v'}\ \mathbf{j} + f\ \overline{\theta}^{-1}\ \overline{v'\theta'}\ \mathbf{k}$), and concluded that shifts in the subtropical and midlatitude stability dominate the shifts of the storm tracks—as opposed to the meridional temperature gradients.

Several studies suggest that the strength and location of anomalous sea surface temperatures and sea surface temperature gradients are responsible for shifts in the storm tracks (Brayshaw et al., 2008). This perspective argues that shifts in the storm tracks follow shifts in the surface baroclinicity without explaining how or why the

shifts in surface temperature gradients would occur in a warming world in the first place; thus, it is more of an association than a mechanism.

Lorenz and DeWeaver (2007) noted that poleward shifts in the storm tracks are accompanied by a rise in the height of the tropopause and suggested that the rising tropopause caused the shift in the storm tracks. However, the mechanism by which this was done was not offered, and one counterexample occurs during El Niño when tropical warming leads to an increase in the tropopause height, but storm tracks migrate equatorward (Seager et al., 2003; Tandon et al., 2012; Adam et al., 2014).

A large segment of the storm track community subscribes to a top-down control perspective on the midlatitude storm tracks (even though the mass of the atmosphere is an exponentially decreasing function of height). Changes in the near-surface baroclinicity are, in this view, coupled to the upper troposphere through the thermal wind relation, which relates temperature gradients to the vertical shear of the flow. They suggest that changes in the upper troposphere and lower stratosphere modify wave propagation characteristics and thus lead to storm track shifts (e.g., Kushner and Polvani, 2004; Chen and Held, 2007; Chen et al., 2008; Butler et al., 2010). For example, Chen et al. (2007); Chen and Held (2007) use reanalysis data and a GCM to show that increases in eddy phase speeds are associated with a poleward shift of the storm tracks. They suggest that an increase in the phase speed limits the meridional propagating distance of the waves, since waves will break at the latitude where their phase speed equals the background flow speed, i.e., their critical latitude. These breaking waves decelerate the flow and reduce baroclinicity below. The net effect is

to push the baroclinic zones poleward. Nonetheless, the authors admit that they are unable to establish cause and effect, that is, whether the storm track shift causes an increase in phase speed or vice-versa.

Most of these critical-line arguments rely on the aforementioned mechanism. For example Kidston et al. (2010) show that changes in the eddy length scale can shift the storm tracks. But this rests on a change in phase speed that accompanies the change in wavelength. The most modern perspective shows that the reflecting level for waves may also be important for shifting the storm tracks (Lorenz, 2014).

The above-mentioned mechanisms are not mutually exclusive and some of them act simultaneously, making it difficult to establish cause and effect. Nonetheless, we believe that insights into storm track shifts can be obtained by approaching this problem using a hierarchy of models.

1.2 Observed storm tracks

1.2.1 Modes of meridional energy transport

To facilitate an adequate description of the midlatitude storm tracks, some context is first required. Total specific energy relevant to atmospheric fluid dynamics is defined as,

$$\mathcal{E} = c_v\, T + g\, z + 2^{-1}(u^2 + v^2 + w^2) + L\, q, \tag{1.1}$$

where the terms on the right hand side are, respectively, sensible heat, potential

energy, kinetic energy, and latent energy (all symbols in Eqn. 1.1 are standard; L is the latent heat of vaporization and q is the specific humidity). Understanding the evolution of the various modes of $\mathcal{E}$ is central to understanding the weather we experience, and climate in general.

Radiant fluxes incident on a spherical planet from the Sun result in an externally forced meridional temperature gradient on Earth. Earth receives more solar radiation, per unit area, at the equator than at the poles, in the annual mean. The meridional profile of emitted radiation and surface fluxes imply a net poleward energy transport from regions of net radiative surplus, in the tropics, to those of net deficit, in polar regions (Peixoto and Oort, 1992). The decomposed total meridional energy transport equation, Eqn. 1.2, shows some possible physically relevant modes of meridional energy transport. Respectively, they are the transport by the zonal-mean meridional overturning circulation, the transient eddy transports, the stationary eddy transports, and the transport associated with transient asymmetric eddies [see (Peixoto and Oort, 1992, Chpt. 4) for a discussion of analysis of variance in the climate dynamics context]. Hence, some combination of them is required to accomplish the needed poleward energy transport.

$$c_v \, \overline{[v \; T]} = c_v \, \overline{[v]} \; \overline{[T]} + c_v \, \overline{[v]' \; [T]'} + c_v \, [\overline{v}^* \; \overline{T}^*] + c_v \, \overline{[v'^* \; T'^*]}, \tag{1.2}$$

where $\overline{(\cdot)}$ represents a temporal average and $(\cdot)'$ represents a deviation therefrom; and $[(\cdot)]$ represents an average along a latitude circle and $(\cdot)^*$ is a deviation therefrom.

The spherical shape of the Earth combined with its rotation about its axis im-

plies that a meridional angular momentum gradient exists. Assuming solid body rotation, a global maximum in angular momentum exists at the equator, where the moment arm is the longest. Considering the observed distribution of surface winds, neglecting how that distribution came about, then the region of westerlies observed in midlatitudes, spinning faster than the solid Earth, loses momentum to the Earth, while the tropics and, to a lesser extent, the polar latitudes gain momentum. This configuration requires meridional transport of angular momentum from regions of net surplus (largely the tropics) to regions of net deficit (the midlatitudes) [see Peixoto and Oort (1992); Held (2000); Holton (2004) for a detailed discussion of angular momentum balance and its implications]. The decomposed total meridional momentum transport, Eqn. 1.3, shows some possible physically relevant modes of mean meridional momentum transport. The modes of momentum transport are analogous to the modes of energy transport.

$$\overline{[u\ v]} = \overline{[u]}\ \overline{[v]} + \overline{[u]'\ [v]'} + [\overline{u}^*\ \overline{v}^*] + \overline{[u'^*\ v'^*]} \tag{1.3}$$

Over a sufficiently long timescale, precipitation minus evaporation in a given latitude band must be balanced by the net flux out of it. There is an observed moisture surplus in the deep tropics (associated with the Inter-Tropical Convergence Zone, ITCZ) and in the polar regions. A moisture deficit exists in the subtropics and midlatitudes Peixoto and Oort (1992). An analogous water vapor transport equation is given by,

$$\overline{[v\ q]} = \overline{[v]}\ \overline{[q]} + \overline{[v]'\ [q]'} + [\overline{v}^*\ \overline{q}^*] + \overline{[v'^*\ q'^*]}. \tag{1.4}$$

These modes of meridional transport reduce the strong gradients that would otherwise have developed. In essence, they help define the weather we experience and, by extension, the climate. They are observed to have different domains of efficient operation (see Peixoto and Oort, 1992). For example, mean meridional transport is most effective in the tropics and is associated with the Hadley circulation. Thus, understanding how they change when the climate changes is important for understanding the associated response of several atmospheric phenomena. Next, we touch on an important concept for synoptic scale dynamics: baroclinic instability.

1.2.2 Baroclinic instability

Assume an air parcel is at an equilibrium point, then it is said to be advectively stable if a displacement from this point results in restoring forces that accelerate it back to that equilibrium point, it is unstable if it experiences a force that accelerates it away from that equilibrium point, and it is neutrally stable if it experiences no forces at all and remains at the new position to which it was displaced. Different forms of instability observed in Earth's atmosphere include convective, slantwise, and symmetric instabilities (Rogers and Yau, 1989; Peixoto and Oort, 1992).

The atmosphere has been shown to be baroclinically unstable (see Charney, 1947; Eady, 1949). This is a form of slantwise instability in which isentropic slopes (Eqn. 1.5) are steeper than the slope of a parcel's displacement; hence, the displaced parcel is

accelerated away from its origin. Accordingly, if the isentropic slope is shallower than the parcel's displacement slope, then the parcel is baroclinically stable, and neutral otherwise (Rogers and Yau, 1989; Peixoto and Oort, 1992). Thus, the degree of baroclinic instability is strongly determined by the slopes of isentropes,

$$\overline{I} = \frac{\partial_y \overline{\theta}}{\overline{\partial_p \theta}}, \tag{1.5}$$

where θ is potential temperature[1], and y is the meridional coordinate and p, which is pressure, is the vertical coordinate. It is easy to see from Eqn. 1.5 why the meridional temperature gradient, $\partial_y \overline{\theta}$, and the static stability, $\overline{\partial_p \theta}$, are central to the debate on storm track dynamics, i.e., they are components of important quantities related to the generation of synoptic cyclones, which comprise the storm tracks.

We are now in a position to define storm tracks.

1.2.3 Midlatitude storm tracks: the phenomenon

The midlatitude storm tracks are best described as regions of enhanced turbulent energy, moisture, and momentum transport. They are observed as areas of the highest density of extratropical cyclone and anticyclone activity. Cyclones are cold core systems, which should be differentiated from the warm core tropical cyclones, although it is possible for tropical warm-core cyclones (hurricanes/typhoons) to transition to extratropical cyclones.

[1]The potential temperature, $\theta = T\left(\frac{p_{\text{ref}}}{p}\right)^{\kappa}$, is the temperature that a parcel would have were it brought, adiabatically, to a reference pressure, usually 1000 hPa.

The storm tracks occur in localized regions in the Northern Hemisphere, and are more uniformly distributed in the Southern Hemisphere, around 50° latitude. In the Northern Hemisphere, the storm tracks are confined to the northern Pacific, the north Atlantic, and, to a lesser extent, the Mediterranean sea (Chang et al., 2002).

Generally, storm tracks occur in strongly baroclinic regions. On a zonally symmetric planet, that would simply be the latitude of strongest meridional temperature gradients, or, through thermal wind balance, of strongest vertical shear. Earth is not zonally symmetric and storm track location is complicated by this—they are more localized. Nonetheless, the question of the localized position of the storm tracks, especially as observed in the Northern Hemisphere, becomes tractable if it is separated into the following parts: storm track genesis, storm track maintenance, and storm track destruction.

1.2.3.1 Storm track genesis

Storm tracks form in strongly baroclinic regions. These regions are referred to as the entrance region of the storm tracks and are marked by strong temperature gradients and vertical shear. Strongly sheared flow on a rotating sphere is baroclinically unstable, as a linear stability analysis will show (Charney, 1947; Eady, 1949). Disturbances in these regions of strong baroclinicity will grow by converting available potential energy into turbulent/eddy kinetic energy (Lorenz, 1955; Phillips, 1956; Orlanski and Katzfey, 1991; Chang et al., 2002).

In the Northern Hemisphere, the genesis regions of the localized storm tracks are on the east coasts of Asia and of North America. There, especially during the

most baroclinically unstable season (winter time) the land-sea thermal contrast (aided by warm tropical currents) create regions of enhanced baroclinicity. Topographic features, like the Rocky mountain range, play a role as sources for disturbances. These disturbances are then amplified over the strong baroclinic regions. In Earth's southern hemisphere, ocean currents, the tips of continents in the Southern Hemisphere and regions of persistent convection, such as the South Pacific Convergence Zone (SPCZ) all provide potential sources of disturbances for baroclinic growth (Chang et al., 2002; Brayshaw et al., 2009, 2011).

Once the storm track disturbances are formed and grow, it is important to consider how they are maintained.

1.2.3.2 Storm track maintenance

An interesting conundrum exists with the storm tracks: if the storm tracks exist to transport energy from regions of net surplus to those of net deficit, thereby smoothing out gradients and destroying the very source of their existence, why do they persist (especially since the degree of energy transport increases with the degree of baroclinicity).

One answer is that the restorative timescale is shorter than the eddy transport timescale. This may be true for large-scale temperature gradients and may apply in the Southern Hemisphere, but proves an unsatisfactory explanation for the localized storm tracks in the Northern Hemisphere. A plausible explanation for the persistence of the localized storm tracks in the Northern Hemisphere is the spatial offset of the region of maximum baroclinicity and maximum turbulent transport (Hoskins and

Valdes, 1990), i.e., disturbances grow at the site of maximum baroclinicity but are advected downstream before attaining their maximum dissipative capacity. Modern ideas suggest that there is also a temporal offset between maximum baroclinicity and maximum eddy transport (Ambaum and Novak, 2014). This likens the storm tracks to a non-linear oscillator.

Stationary eddies have also been found to play a role in storm track maintenance by enhancing baroclinicity near the source region. This occurs inside one half Rossby wavelength downstream of the storm track entrance region (Kaspi and Schneider, 2013).

Hoskins and Valdes (1990) argue that diabatic heating near the storm track entrance region plays a role in its maintenance.

Other arguments suggest that disturbances may circumnavigate the globe and not only grow again in the baroclinic region, but also provide energy for other disturbances to grow (Chang et al., 2002).

1.2.3.3 Storm track destruction

The localized nature of the storm tracks in the Northern Hemisphere suggests that some mechanism exists to terminate it and defines a storm track exit region. The observed kinetic energy budget shows that friction and barotropic conversion of eddy kinetic energy into mean kinetic energy play a role in terminating the storm tracks (Orlanski and Katzfey, 1991; Chang et al., 2002). Modern ideas posit that stationary eddies, excited by zonal asymmetries in the vicinity of the storm tracks, interact with transient eddies along the storm tracks and act to terminate them at distance

controlled by the Rossby wavelength scale. They do this by reducing temperature gradients and enhancing static stability in the exit region of the storm tracks (Kaspi and Schneider, 2011, 2013).

1.2.4 Storm tracks variability

The midlatitude storm tracks are dynamic components of the general circulation. They have been observed to vary robustly on seasonal and inter-annual timescales.

During the annual cycle, the Northern Hemisphere storm tracks are observed to migrate equatorward during the winter (Chang et al., 2002). This occurs in both the Atlantic and the Pacific basins. In addition, the intensity of the storm tracks is observed to attain a minimum in turbulent energy transport during the winter, when the hemisphere is least baroclinically stable (Nakamura, 1992). This puzzle of the midwinter minimum remains an area of active research.

On inter-annual timescales, the storm tracks are observed to respond to and feedback on modes of inter-annual variability. Storm tracks are observed to migrate equatorward and downstream during El Niño events. During La Niña, on the other hand, they are observed to migrate poleward and upstream. (Chang et al., 2002).

1.3 Thesis structure

Storm track research can divided into three broad areas:

1. Understanding the observed structure of midlatitude storm tracks. This includes questions on the genesis, maintenance, localization of storm tracks and

on the dynamics of the individual cyclones and anticyclones of which the storm tracks are comprised.

2. Understanding the observed trends and variability of the storm tracks.

3. Storm track response to perturbations in climate.

Storm track researchers use many different ways to identify the storm tracks. These include low pressure centers (Wallace et al., 1988; Fyfe, 2003), surface vorticity (Hoskins and Hodges, 2002), geopotential (Chang et al., 2002), and bandpass filtered turbulent fields (Blackmon, 1976; Blackmon et al., 1977; Hoskins and Valdes, 1990; Yin, 2005; Kaspi and Schneider, 2011)—the filtering period is usually 2-7 days to capture synoptic waves (Hartmann, 1974). Here, we identify the midlatitude storm tracks using zonal and temporal averages of eddy kinetic energy (EKE).

In this thesis, we insert ourselves into the debate on the mechanisms that control shifts in the midlatitude storm tracks with changing climate. In the next chapter, we approach the question of storm track shifts from a simplified framework, using an idealized dry GCM. We show that storm tracks shift poleward in dry climates, and that the shift can be caused by changes in deep tropical stability. In chapter 3, we demonstrate that mean available potential energy, MAPE, scales and collocates with eddy kinetic energy—our storm track proxy. Using this finding, we decompose MAPE to establish the quantities that dominate the shifts in the storm tracks. Chapter 4 presents a conceptual energy-balance model that is used interactively with the GCM to establish the relationship between the tandem shifting storm tracks and the Hadley circulation. A conclusion then follows in chapter 5.

Chapter 2

Quantifying the role of large-scale dry processes in storm track shifts

2.1 Introduction

The cyclones and anticyclones that carry out the bulk of the heat, moisture, and momentum transport in Earth's extratropical atmosphere are concentrated in storm tracks: regions of enhanced eddy kinetic energy in midlatitudes (Blackmon, 1976; Blackmon et al., 1977). Storm tracks are found in the Northern Hemisphere primarily over the Atlantic and Pacific Oceans; in the Southern Hemisphere, they are more zonally uniform. In both hemispheres, the storm tracks, identified as regions of enhanced eddy kinetic energy, are currently centered around 50° latitude. There is clear modeling evidence that storm tracks shift poleward as the climate warms globally, on average by about 2° under a doubling of carbon dioxide concentrations (Yin, 2005; Bengtsson et al., 2006; Swart and Fyfe, 2012; Barnes and Polvani, 2013). It is unclear, however, what dynamical processes are responsible for this poleward shift.

Numerous mechanisms driving a poleward shift of storm tracks have been proposed. One group of studies posits that low-level baroclinicity controls where storm

tracks are located and that changes in it drive storm track shifts. For example, Yin (2005) suggests that a change in the meridional temperature gradients is responsible for a poleward shift of the maximum of a baroclinicity measure, implying a concomitant shift of storm tracks. By contrast, Lu et al. (2010) hold that an increase in the subtropical and midlatitude static stability is responsible for a poleward shift of the maximum of a similar baroclinicity measure and hence for a poleward shift of storm tracks. Furthermore, Brayshaw et al. (2008) posit that the strength and location of anomalous SST gradients relative to the location of the subtropical jet drive the poleward shift of storm tracks, while Butler et al. (2010, 2011) emphasize the role of tropical heating in modifying the low-level baroclinicity and storm track position. Another group of studies posits that changes in the upper troposphere and lower stratosphere modify wave propagation characteristics and thus lead to storm track shifts (e.g., Kushner and Polvani, 2004; Chen and Held, 2007; Lorenz and DeWeaver, 2007; Chen et al., 2008; Butler et al., 2010). Yet others suggest that increasing eddy length scales under global warming may play a role in storm track shifts (Kidston et al., 2010; Riviere, 2011).

These mechanisms are not mutually exclusive, and several of them may act simultaneously. Our goal in this chapter is to disentangle distinct dynamical processes that may act jointly in global-warming scenarios. For example, increased mean surface temperatures generally lead to a higher tropopause (Held, 1982; Schneider, 2007), to increased lower-level static stability through increased latent heat release in phase changes of water, both in the tropics and extratropics (e.g., Xu and Emanuel,

1989; Emanuel, 2007; Schneider and O'Gorman, 2008), and typically to reduced pole-equator near-surface temperature contrasts through increased poleward latent heat transport (Pierrehumbert, 2002; Caballero and Langen, 2005; O'Gorman and Schneider, 2008a; Cabellero and Hanley, 2012). The presence of moisture in the atmosphere thus links surface temperature changes to static stability changes and to temperature-gradient changes, which have distinct dynamical effects. To separate such effects, and to demonstrate that at least part of the poleward shift of storm tracks can be understood irrespective of how large-scale dynamics affect latent heat release, we study the storm track response to various idealized climate changes in a dry GCM, similar to those used by Kushner and Polvani (2004), Chen and Held (2007), and Butler et al. (2010). In the GCM, we vary the mean surface temperatures separately from an adjustable but constant convective stability, which controls the tropical static stability but has a less direct effect on the extratropical static stability (Schneider and Walker, 2006; Schneider and O'Gorman, 2008). This allows us to more clearly separate tropical from extratropical mechanisms driving storm track shifts.

2.2 Idealized dry GCM and simulations

We conduct a series of simulations over a wide range of climates using the idealized dry GCM described in detail in Schneider (2004) and Schneider and Walker (2006). Here, we give a brief overview of some aspects of the GCM pertinent to this study. The GCM uses the dry dynamical core of GFDL's Flexible Modeling System and solves the primitive equations in a spherical shell using a spectral transform method, triangularly

truncated at 85 wave numbers. This truncation gives a horizontal resolution of about 1.5°. There are 30 vertical levels, and the vertical coordinate is σ, where $\sigma = p/p_{surf}$.

2.2.1 Mass conservation

The mass conservation equation solved in the GCM is given by,

$$\partial_t p_s = -\int_0^1 \nabla \cdot p_s \ \mathbf{v} \ d\sigma, \tag{2.1}$$

where p_s is the surface pressure, and the divergence operator acts in the horizontal.

2.2.2 Momentum equations

In spherical coordinates, the momentum equations solved by the GCM are,

$$\frac{Du}{Dt} = f \ v + \frac{u \ v \ tan(\varphi)}{a} - \frac{\partial_\lambda \Phi}{a \ cos(\varphi)} + \frac{\sigma \ \partial_\sigma \Phi \partial_\lambda p_s}{p_s \ a \ cos(\varphi)} - C_D \ \sigma_N(\sigma) \ ||\mathbf{v}|| \ u \tag{2.2}$$

$$\frac{Dv}{Dt} = -f \ u - \frac{u^2 \ tan(\varphi)}{a} - \frac{\partial_\varphi \Phi}{a} + \frac{\sigma \ \partial_\sigma \Phi \partial_\varphi p_s}{p_s \ a} - C_D \ \sigma_N(\sigma) \ ||\mathbf{v}|| \ v \tag{2.3}$$

$$\frac{\partial \Phi}{\partial \sigma} = -R \ T_v/\sigma \tag{2.4}$$

where (u, v) are the velocity components in latitude (λ) and in longitude (φ), respectively; a is the radius of the Earth, and $\Phi = g \ z$ is geopotential. C_D is a specified drag coefficient, $||v|| = \sqrt{u^2 + v^2}$, and $\sigma_N = (\sigma - \sigma_b)/(1 - \sigma_b)$ ensures that the drag acts below the level $\sigma = \sigma_b$. The latter equation results from using the hydrostatic approximation. This is justified by the small aspect ratio of the domain (NOAA/GFDL, cited 2015).

2.2.3 Radiative transfer

A Newtonian relaxation scheme represents radiative transfer and surface fluxes in an idealized way. Temperatures are relaxed to a radiative-equilibrium profile on a timescale of 7 days near the surface in low latitudes and 50 days in the rest of the atmosphere. The radiative-equilibrium temperature at the surface is given by

$$T_s^e(\phi) = \overline{T}_s^e + \Delta_h \left(\frac{1}{3} - \sin^2 \phi \right), \tag{2.5}$$

where ϕ is latitude, Δ_h is the pole-equator thermal contrast, and $\overline{T}_s^e$ is the mean near-surface temperature in radiative equilibrium. The radiative-equilibrium temperature away from the surface is given by

$$T^e(\phi, p) = T_t^e \left[1 + d_0(\phi) \left(\frac{p}{p_0} \right)^\alpha \right]^{1/4}, \tag{2.6}$$

where

$$d_0(\phi) = \left(\frac{T_s^e(\phi)}{T_t^e} \right)^4 - 1, \tag{2.7}$$

is a latitude-dependent optical thickness that depends on the near-surface radiative-equilibrium temperature $T_s^e(\phi)$. The optical depth is chosen so that the radiative-equilibrium temperature T_t^e at the top of the atmosphere is constant. In this study, it is set to $T_t^e = 200$ K in all simulations; that is, we assume a fixed longwave emission temperature, as the longwave emission temperature for a gray atmosphere is proportional to the temperature at the top of the atmosphere (Schneider, 2007). The ratio,

α, of the pressure scale height to the partial pressure scale height of the dominant infrared absorber controls the radiative-equilibrium lapse rate [see Schneider (2004) for a discussion of the role of optical thickness and α in this GCM]. The pole-equator thermal contrast, Δ_h, which is prescribed in the GCM, is set to 120 K, which is chosen to ensure sufficient (Earth-like) macroturbulence in midlatitudes.

2.2.4 Thermodynamic equation

Given the radiative forcing, the GCM solves the following thermodynamic equation,

$$\frac{DT}{Dt} = \frac{\kappa\ T_v\ \omega}{\sigma\ p_s} + \frac{Q}{c_p} - \tau_T^{-1}(\varphi, \sigma)\left(T - T^e\left(\phi, \sigma\right)\right) \tag{2.8}$$

where

$$\tau_T^{-1}(\varphi, \sigma) = \frac{1}{\tau} + \left(\frac{1}{\tau_{\text{trop}}} - \frac{1}{\tau}\right) \max\left(0, \frac{\sigma - \sigma_b}{1 - \sigma_b}\right)\ \cos^8(\varphi). \tag{2.9}$$

τ_T^{-1} represents the radiative time scale that is a function of height and latitude. Q represents any other diabatic source, like frictional heating. Finally, the GCM's system of equations is closed with ideal gas law, $\sigma\ p_s = \rho\ R\ T$ (NOAA/GFDL, cited 2015).

2.2.5 Dry convection

We use standard Earth values for physical parameters. There are no continents in the GCM, and moisture effects, such as latent heat release and transport, are

neglected[1]. The radiative-equilibrium profile of the dry GCM is unstable to thermal convection. The ensuing convection is represented by a quasi-equilibrium scheme, which relaxes temperatures in an atmospheric column toward a convective lapse rate given by $\gamma\Gamma_d$, whenever the column is less stable than one with this convective lapse. Here, $\Gamma_d = g/c_p$ is the dry adiabatic lapse rate, and γ is a rescaling parameter, which is inversely proportional to the local degree of stability. Decreasing γ increases the stability of the atmosphere, mimicking some of the effects of latent heat release in moist convection, except that the constant γ is an adjustable model parameter that does not depend, for example, on temperature (Schneider, 2004; Schneider and Walker, 2006). The convection scheme essentially sets the lapse rate in the tropics; it does not control but can influence the lapse rate in the extratropics, particularly in weakly baroclinic climates or when the rescaling parameter γ is small (Schneider and Walker, 2006; Schneider and O'Gorman, 2008).

2.2.6 Simulation parameters

In this study, we vary the rescaling parameter γ to study the effect of the convective lapse rate on storm track position. To disentangle the effect of convective lapse rate changes that are global from those that are confined to the tropics, we consider two scenarios: (i) We use a constant rescaling parameter γ globally and vary that. (ii) We use an equatorial rescaling parameter γ_e within 10° of the equator and an off-equatorial parameter γ_x outside this equatorial band, and we set $\gamma_x = 1$ and vary γ_e. Fig. 2.1 shows the partitioning of the planet. The second scenario resembles in

[1]Nonetheless, the GCM includes the effect of the mass of water vapor on the dynamics.

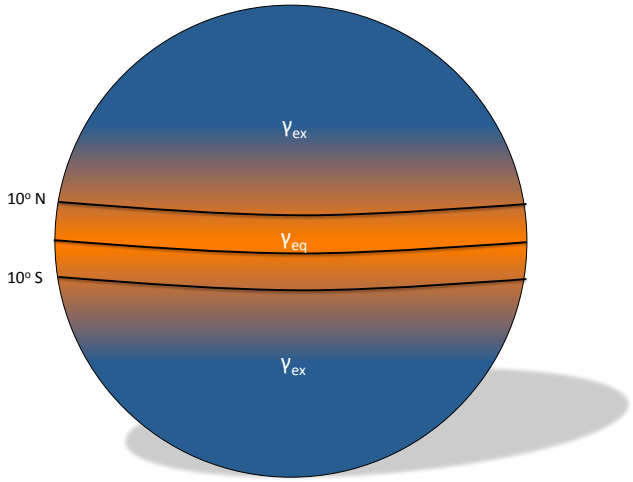

Figure 2.1: The idealized dry GCM is forced in a unique way, as shown in the schematic. Deep tropical and extratropical stability are varied independent of one another. Between the black bands $\gamma = \gamma_{eq}$, while outside, $\gamma = \gamma_{ex}$

some aspects the tropical heating simulations of Butler et al. (2010), but here we do not provide an additional enthalpy source to the tropical atmosphere, which would directly modify meridional temperature gradients.

Our goal is to investigate the mechanisms that may contribute to the poleward shift of storm tracks under global warming. Surface temperature increases have a number of consequences, among them an increase in the height of the tropopause if lapse rates remain fixed or decrease [see Held (1982) or, for a review, Schneider (2007)]. To study such effects separately, we perform two sets of simulations. In the first set, we vary the mean radiative-equilibrium surface temperature from $\overline{T}_s^e = 270\,\mathrm{K}$ to 365 K in increments of 5 K, implying an increasing optical thickness (3) in radiative equilibrium, as the temperature at the top of the atmosphere, T_t^e, is kept fixed. [While absolute temperatures do not affect dry dynamics, increasing the surface temperature in radiative equilibrium increases, for example, the tropopause height because the

Table 2.1: Simulation parameters (surface temperature ranges are incremented by 5 K and convective lapse rate ranges are incremented by 0.2 K km^{-1}).

Convection scenario	Surface temperature (K)	Tropical convective lapse rate (K km^{-1})	Extratropical convective lapse rate (K km^{-1})
$\gamma_e = 0.7$, $\gamma_x = 0.7$	270–365	6.9	6.9
$\gamma_e = 0.7$, $\gamma_x = 1$	270–365	6.9	9.8
$\gamma_e = 1$, $\gamma_x = 0.7$	270–365	9.8	6.9
$\gamma_e = 1$, $\gamma_x = 1$	270–365	9.8	9.8
γ_e variable, $\gamma_x = 1$	340	6.0–9.8	9.8
γ_e variable, γ_x variable	340	6.0–9.8	6.0–9.8

temperature at the top of the atmosphere T_t^e is kept fixed.] We perform this set of simulations for fixed convective lapse rates that are either globally constant or that assume different values near the equator and away from it (see Table 2.1), with the lower convective rescaling parameter $\gamma = 0.7$ roughly giving present-day moist-adiabatic convective lapse rates. In the second set of simulations, we keep the mean radiative-equilibrium surface temperature fixed ($\overline{T}_s^e = 340\,\mathrm{K}$) and vary the convective lapse rate by varying the rescaling parameter in increments of 0.03, either globally or varying it only near the equator while keeping $\gamma_x = 1$ fixed (see Table 2.1). All simulations are spun up for two years, after which flow variables are sampled four times daily over a further two years and are then temporally and zonally averaged.

2.3 Simulation results

Figures 2.2 and 2.3 show a sample of the simulated climates at the extremes of the scenarios investigated. It is apparent from the figures that the tropopause height and the subtropical jet speed increase with increasing mean radiative-equilibrium temperature and increasing convective stability, as expected from radiative equilibrium considerations (Schneider, 2007) and thermal wind shear extending over a deeper troposphere. The maximum of the eddy momentum flux convergence migrates poleward and upward. The Hadley cell strengthens with increasing radiative-equilibrium temperature, but it weakens with increasing convective stability. The shallow recirculation in the streamfunction seen in Figs. 2.2c, d and 2.3c results from flow separation induced by an adverse pressure gradient caused by the change in the convective lapse rate across 10° latitude (reversal of the near-surface meridional temperature gradient); however, our results are unaffected.

Table 2.2 (upper block of rows) and Fig. 2.4 show how the storm track location (as determined by the latitude of maximum barotropic EKE) responds to mean radiative-equilibrium temperature changes. The storm tracks migrate poleward with increasing radiative-equilibrium temperature in all convection scenarios; the magnitude of the poleward migration increases as the convective stability increases. These findings are qualitatively similar to those we obtain using other proxies for storm tracks, including extrema of the mean surface westerlies and of eddy heat fluxes (cf. Fig. 2.2). It is interesting that all storm track proxies studied migrate poleward in the statically neutral convection scenario: $\gamma_e = 1$ and $\gamma_x = 1$. This shows that changes in moist

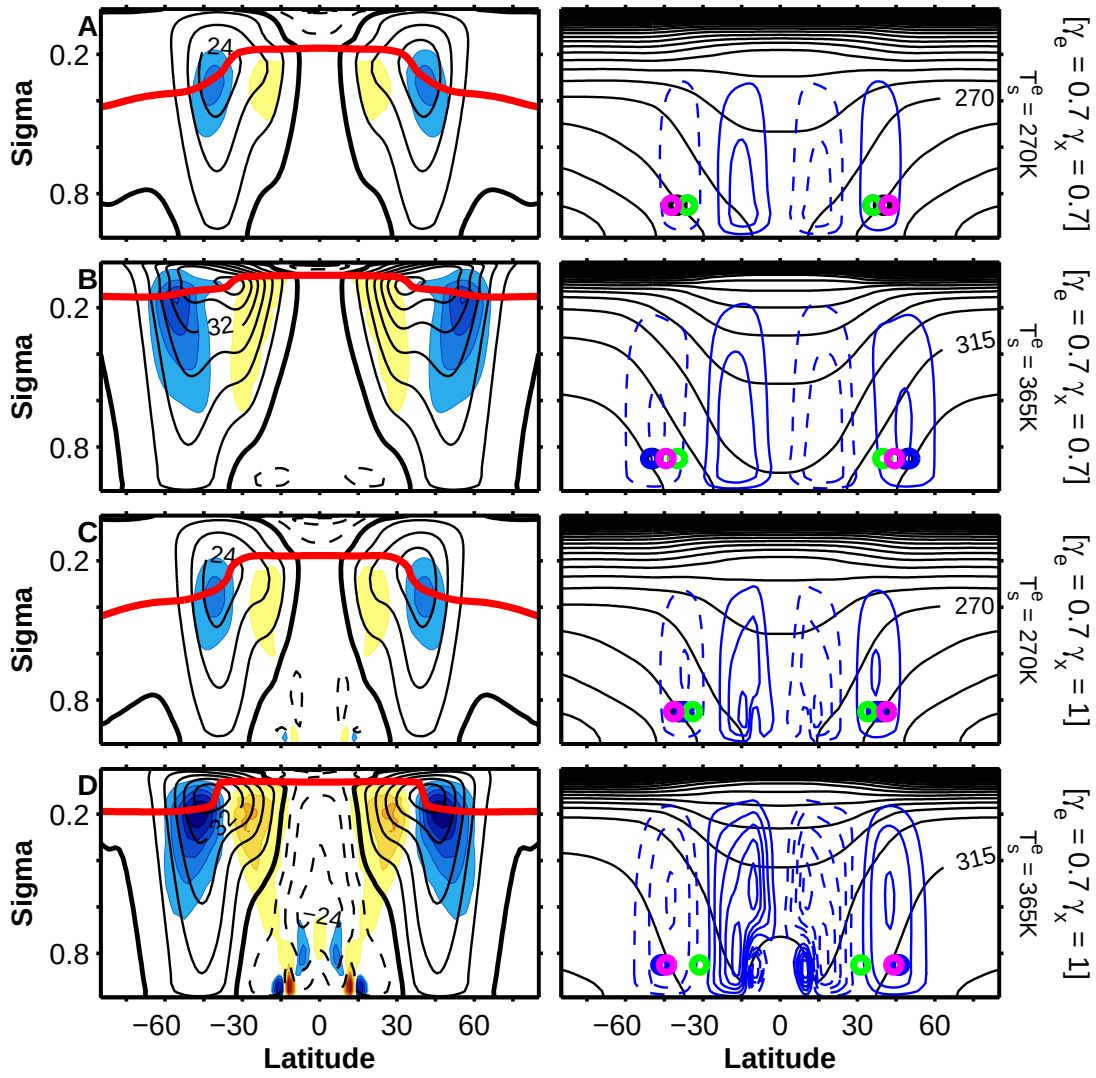

Figure 2.2: Sample of simulated climates as the mean radiative-equilibrium surface temperature is varied. (left column) Mean zonal wind (black contours with interval $8\,\mathrm{m\,s^{-1}}$), eddy momentum flux divergence (filled contours with interval $17 \times 10^{-6}\,\mathrm{m\,s^{-2}}$; yellow is positive), and tropopause (thick red line, WMO criterion). (right column) Potential temperature (black contours with interval 15 K), mass flux streamfunction (blue contours with interval $30 \times 10^9\,\mathrm{kg\,s^{-1}}$). (a) Coldest climate with $\gamma = 0.7$ globally. (b) Warmest climate with $\gamma = 0.7$ globally. (c) Coldest climate with $\gamma_e = 0.7$ and $\gamma_x = 1$. (d) Warmest climate with $\gamma_e = 0.7$ and $\gamma_x = 1$. Comparing panels (a) with (b) and (c) with (d) shows the response to mean radiative-equilibrium temperature changes. The circles show the location of the storm tracks as indicated by extrema in barotropic eddy kinetic energy (red), meridional eddy potential temperature flux (green), vertical heat flux (cyan), and surface westerlies (black).

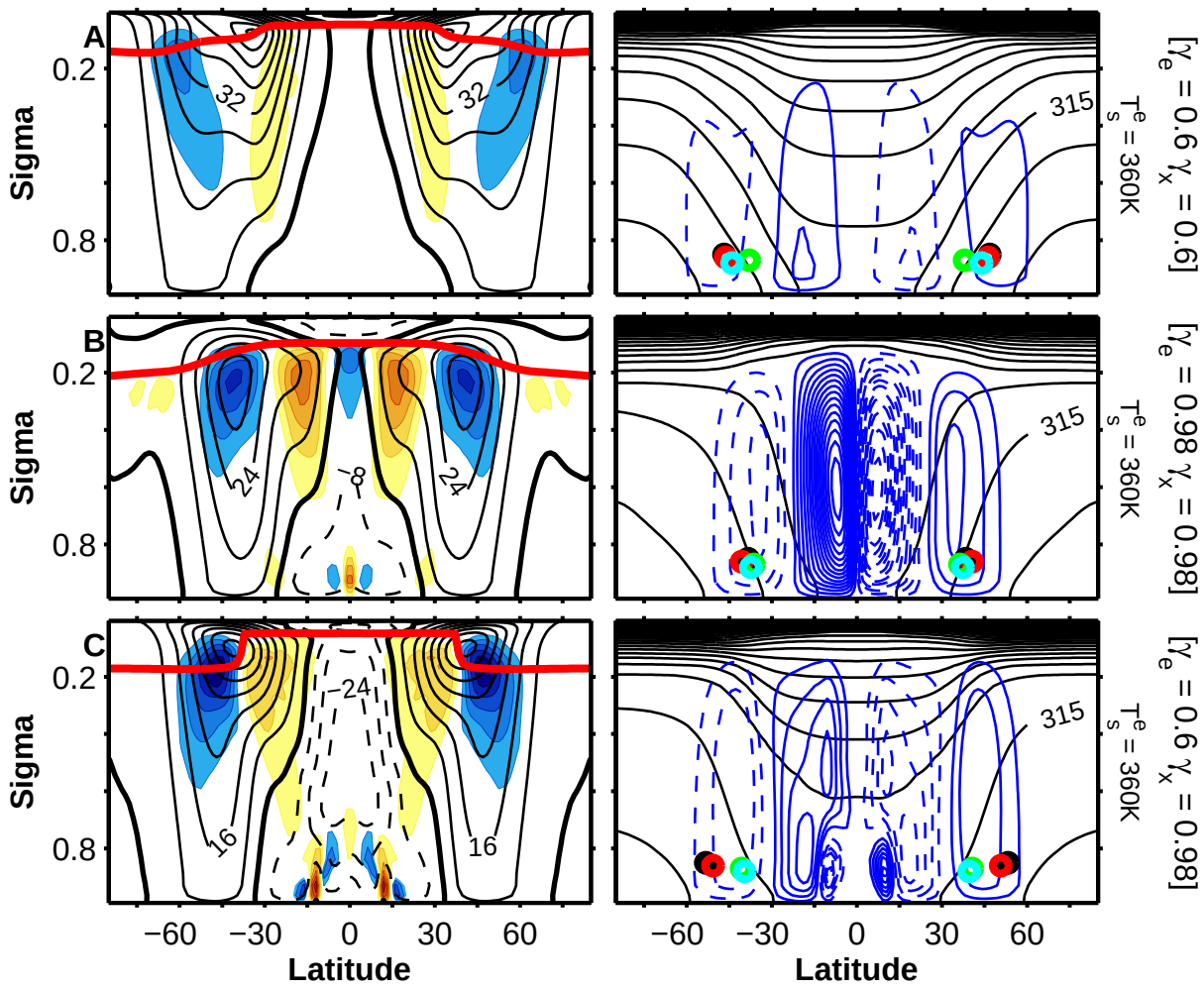

Figure 2.3: Sample of simulated climates as the convective stability is varied. (a, b) Most stable and least stable climates with variable γ_e and $\gamma_x = 1$. (c) Most stable climate with globally uniform convective stability, $\gamma = 0.6$. Plotting conventions as in Fig. 2.2 except that the contour interval of eddy momentum flux divergence is now $18 \times 10^{-6}\,\mathrm{m\,s^{-2}}$. Compare panels (a) with (b) for the response to global convective stability changes and (b) with (c) for the response to tropical convective stability changes.

processes are not a prerequisite for poleward migration of storm tracks. Dry dynamics can explain part of the storm track response to warming. It also shows that a fraction of the poleward migration of the storm tracks is independent of convective stability variations.

Figures 2.4 and 2.5 show the responses of barotropic EKE to increasing tropical

Table 2.2: Storm track response to variations in mean radiative-equilibrium temperature (upper block of rows) and to convective stability (lower block of rows). Columns from left to right show the convection scenario, the latitude of the storm tracks in the coldest/least stable climate, the latitude of the storm tracks in the warmest/most stable climate, the total storm track migration (degrees latitude) over the climate range, and the maximum latitudinal storm track excursion (the difference between the maximum and minimum latitudes reached by the storm tracks).

Convection scenario	Coldest	Warmest	Least stable	Most stable	Migration	Maximum excursion
$\gamma_e = 0.7$, $\gamma_x = 0.7$	36°	50°	—	—	14°	14°
$\gamma_e = 0.7$, $\gamma_x = 1$	34°	47°	—	—	13°	14°
$\gamma_e = 1$, $\gamma_x = 0.7$	37°	46°	—	—	9°	9°
$\gamma_e = 1$, $\gamma_x = 1$	33°	42°	—	—	9°	9°
γ_e variable, $\gamma_x = 1$	—	—	41°	46°	6°	6°
γ_e variable, γ_x variable	—	—	41°	50°	10°	11°

and global convective stability, respectively. The results show that the storm tracks generally migrate poleward with increasing global and tropical convective stability. On the interval $0.8 \lesssim \gamma_e \lesssim 0.9$, the storm track migration is essentially the same (a linear regression showing about 2° poleward per 1 $\mathrm{K\,km^{-1}}$) whether or not the extratropical convective stability (γ_x) is varied along with the tropical convective stability (γ_e). For $\gamma_e \lesssim 0.8$ (which include Earth-like climates), the poleward migration is enhanced by a further 1° per 1 $\mathrm{K\,km^{-1}}$ if γ_x is varied simultaneously with γ_e, showing the increasing influence of convection on the extratropical static stability and the storm track response (Schneider and Walker, 2006; Schneider and O'Gorman, 2008).

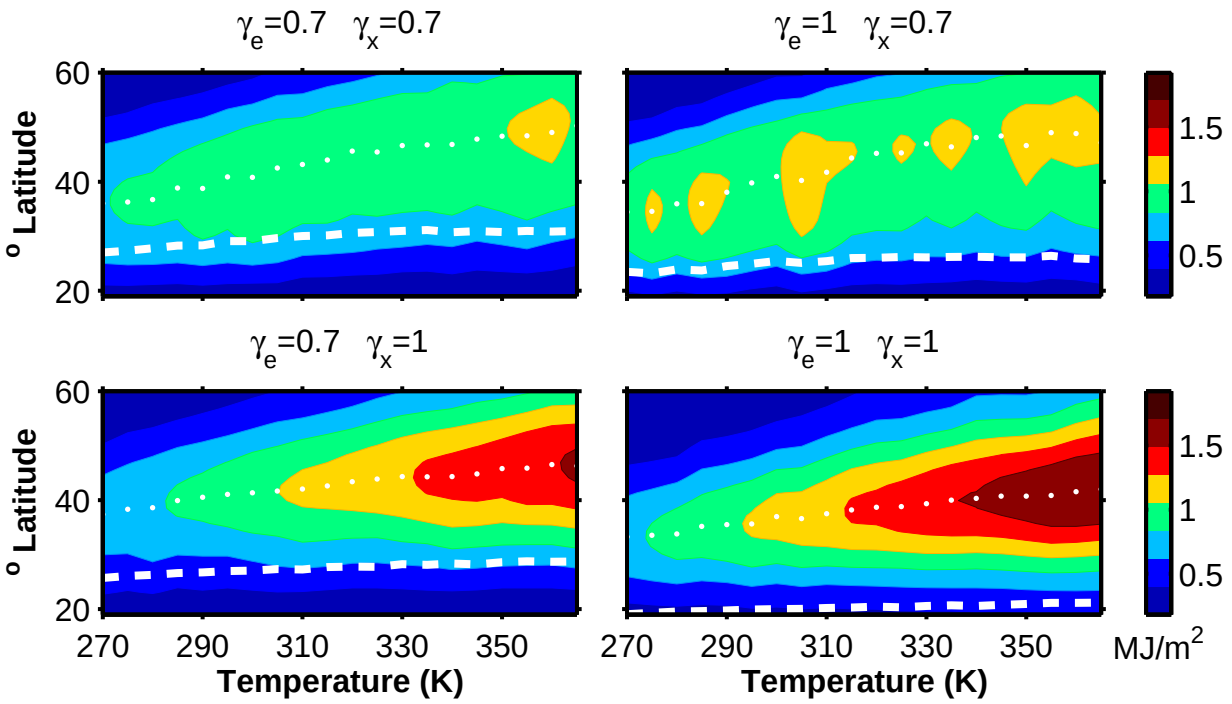

Figure 2.4: Barotropic eddy kinetic energy as a function of latitude plotted across climates with increasing mean surface temperature in radiative equilibrium. The convection scenario is stated above each plot. Here, γ_e is the convective stability rescaling parameter within $\pm 10°$ of the equator; γ_x is the value outside of this latitude band. The white dots show the EKE maxima, each marking the storm track location in the respective climate. The thick white dashed line shows the terminus of the Hadley cell, defined as the latitude at which the Eulerian mass streamfunction changes sign at the altitude where it achieves its extremum.

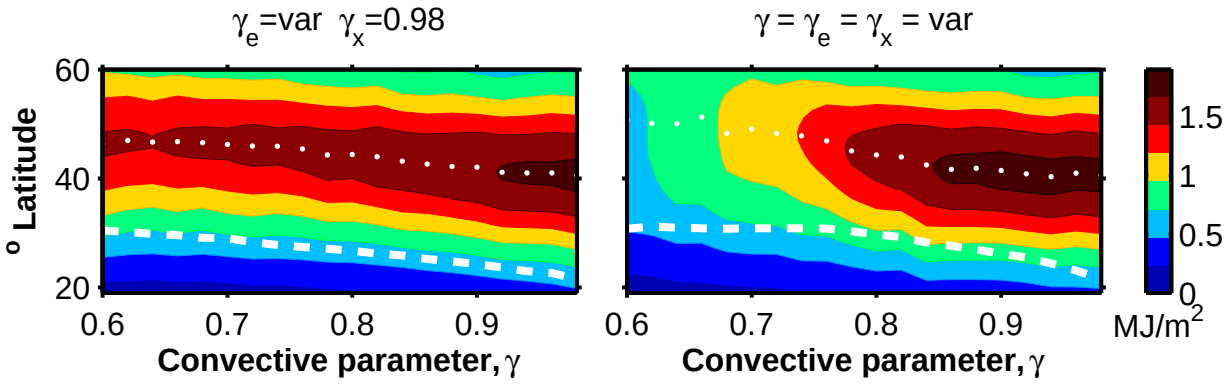

Figure 2.5: This figure is similar to Fig. 2.4, but showing storm track response to convective stability variations.

2.4 Discussion and synthesis

Changes in the height of the tropopause have been cited as a primary cause of the poleward migration of storm tracks (Williams, 2006; Lorenz and DeWeaver, 2007). We also find that increasing the radiative-equilibrium temperature leads to a rise in the height of the tropopause and a poleward migration of storm tracks (see also Schneider 2004). It is likely that the rising tropopause facilitates the dynamics necessary for a poleward migration of storm tracks, but the causality is not obvious. Furthermore, counterexamples exist; for example, during El Niño events (narrow tropical heating), the tropopause height increases while the storm tracks move equatorward. In this situation, tropical temperature gradient changes dominate over stability changes, leading to an equatorward shift of the jets and a contraction of the Hadley circulation (Seager et al., 2003; Tandon et al., 2012).

Previous studies have shown a dependence of storm track response on storm track latitude (Kidston and Gerber, 2010; Garfinkel et al., 2012). This result is qualitatively reproduced in our simulations varying convective stability (Fig. 2.5) and varying radiative-equilibrium temperatures (top right panel of Fig. 2.4): the storm track's poleward migration levels off at the highest latitudes. Additionally, storm tracks shift little as the convective stability is varied for $\gamma \gtrsim 0.9$; the reasons for this are unclear. Nevertheless, we suspect that this is because the distance between synoptic eddies and the Hadley cell is too large for the storm tracks to feel the effect of the expanding Hadley cell.

All simulations show that the Hadley circulation widens as the storm tracks mi-

grate poleward (Fig. 2.4 and 2.5)—a correlation noted previously by Kang and Polvani (2011) and Ceppi and Hartmann (2013). But Fig. 2.5 shows more particularly that storm tracks migrate in tandem with the Hadley cell terminus when varying only the tropical convective stability; however, the migration is less parallel when the convective stability is varied globally. Nonetheless, this suggests that the Hadley cell is responsible for communicating the variations in tropical convective stability to the storm tracks in the midlatitudes. The role of the tropical convective stability in eliciting a response in the midlatitude storm tracks has not been previously identified. This result complements the results found by Butler et al. (2010). It also raises questions about the mechanisms facilitating the requisite tropical-extratropical interactions.

Using our simulations, we estimate the individual contributions of changes in mean radiative-equilibrium temperature and tropospheric stability to the storm track response in a scenario similar to doubling CO_2 concentration on Earth. To do so, we assume a 287 K radiative-equilibrium temperature with $\gamma_e = 0.7$ and $\gamma_x = 1$ as the initial Earth-like conditions. Then, we assume a canonical 3 K global-mean temperature increase when CO_2 is doubled. The mean temperature sensitivity is obtained from the bottom left panel of Fig. 2.4 as the difference between the storm track latitudes $\phi\,(290\text{ K})$ and $\phi\,(287\text{ K})$. We use cubic spline interpolation to infer a 0.3° poleward migration for the 3-K mean temperature change.

The saturation vapor pressure is an exponential function of temperature, as shown

in the Clausius-Clapeyron relation,

$$\frac{de_s}{dT} = \frac{L}{T\left(\alpha_v - \alpha_l\right)}, \tag{2.10}$$

where e_s is the saturation vapor pressure and α_v and α_l are the specific volumes of water vapor and liquid water, respectively (Hartmann, 1994). This equation can be manipulated to show that,

$$\frac{\Delta q^*}{q^*} = \frac{\Delta e_s^*}{e_s^*} = \frac{L}{R_v\ T}\ \frac{\Delta T}{T}, \tag{2.11}$$

where $q^* \approx 0.622 e_s/p$ is the saturation mixing ratio (Peixoto and Oort, 1992) and R_v is the gas constant for water vapor. The moist adiabatic lapse rate can be computed using (Hartmann, 1994),

$$\Gamma_s = \Gamma_d\ \frac{1}{1 + \frac{L}{c_p}\ \frac{dq^*}{dT}}, \tag{2.12}$$

where $\Gamma_d = g/c_p$ is the dry adiabatic lapse rate.

Sensitivity to changes in tropospheric stability requires the change in γ with a doubling of CO_2. We use the Clausius-Clapeyron relation (Eqn. 2.10) to find the saturation vapor pressure and mixing ratio at a reference pressure (1000 mb) and calculate the moist adiabatic lapse rate (Eqn. 2.12) change going from 287 K to 290 K. This gives a 0.3-K km^{-1} decrease in lapse rate, or a 0.03 decrease in γ. Finally, we obtain the shift from the left panel of Fig. 2.5 as the difference between the storm track latitudes $\phi\left(\gamma_\mathrm{e} = 0.67, \gamma_\mathrm{x} = 1\right)$ and $\phi\left(\gamma_\mathrm{e} = 0.7, \gamma_\mathrm{x} = 1\right)$. This yields a 0.5° poleward migration due to tropical convective stability changes. To first order, we assume that

the two responses are additive; thus, our dry framework predicts a 0.8° poleward migration of the storm tracks under CO_2 doubling. This is less than what is found in studies with more comprehensive GCMs, but it is of the same order of magnitude (Yin, 2005; Tsushima et al., 2006; Schneider et al., 2010; Barnes and Polvani, 2013). The discrepancy is likely due to the linearity assumption made here, the neglect of extratropical static stability changes associated with global warming, or the many feedbacks associated with global warming in moist atmospheres. Nonetheless, if we consider the jet shifts reported in Barnes and Polvani (2013) using CMIP5 simulations, our dry model accounts for 40% of the shift in the storm tracks seen in the southern hemisphere, and for 80% percent of that in the northern hemisphere. The shift associated with tropical stability changes is found to be $\frac{2}{3}$ greater than the shift associated with mean temperature changes. This suggests that tropical stability changes are as, if not more, important.

2.5 Conclusion

We have presented a study that decouples mean temperature effects from convective stability effects, and tropical effects from extratropical ones. We used an idealized framework to investigate the storm tracks' response to changes in the radiative-equilibrium temperature and in the global and tropical convective stability—each varied independently. The storm tracks are found to generally migrate poleward with increasing radiative-equilibrium temperature and with increasing convective stability, even in the absence of moisture effects and with fixed pole-equator thermal contrast

in radiative equilibrium. Moreover, the storm tracks migrate poleward as the climate warms in the statically neutral scenario, meaning that dry dynamics may explain part of the storm track migration seen in moist models. Indeed, when our results are translated to what they imply for a moist framework, we found that the change in mean temperature alone accounts for roughly one third of the storm tracks' poleward migration, while convective stability changes (i.e., changes in the moist adiabatic lapse rate) account for the rest. Tropical convective stability has a surprisingly large effect on the storm tracks, suggesting that tropical-extratropical interactions are important. It begs the question of how varying the convective stability in a 10° zonal band around the equator leads to a poleward migration of the midlatitude storm tracks. One possibility is through the Hadley circulation, which was shown to expand in tandem with the storm tracks in many (but not all) of the simulations.

2.6 Appendix

2.6.1 Idealized dry GCM

The details of the GCM detailed in this chapter are derived from the GCM documentation (NOAA/GFDL, cited 2015), the GCM code itself, and from Schneider (2004); Schneider and Walker (2006).

2.6.1.1 Dry convection

A quasi-equilibrium dry convection scheme relaxes temperatures in an atmospheric column to a specified, but constant, lapse rate, $\Gamma_{\text{conv}} = \gamma\Gamma_{\text{d}}$. If a parcel raised from the surface has convective available potential energy relative to the convective lapse rate Γ_{d}, its convective available potential energy is relaxed to zero within a specified timescale τ_{conv}, which is 4 hrs in this study.

2.6.1.2 Time stepping

The GCM uses a standard semi-implicit leap-frog method combined with a Robert-Asselin-Williams (RAW) filter. The RAW filter corrects for spurious non-physical modes that manifest from the leap-frog method. It does this by reducing the curvature of the three values used during the time-stepping procedure (Robert, 1966; Asselin, 1972; Williams, 2009).

2.6.1.3 Sub-grid scale dissipation

Within the fixed planetary boundary layer (surface up to $\sigma = 0.84$), there is vertical diffusion of momentum and dry static energy, $M = c_p\ T + g\ z$, with a turbulent Prandtl number of one and default roughness of 5cm (Smagorinsky et al., 1965). The diffusivity is computed using the Mellor-Yamada 2.5 level turbulence closure (Mellor and Yamada, 1982). Quadratic drag is used to represent boundary layer friction. In the remainder of the atmosphere, horizontal hyper-diffusion, ∇^8, acts to dissipate momentum and energy at the smallest resolved scales (Schneider and Walker, 2006).

2.6.1.4 Boundary conditions

The boundary conditions of the GCM consist of momentum and buoyancy fluxes at the surface and zero flux at the top of the atmosphere. Monin-Obukov similarity theory provides the drag coefficients to compute surface drag and surface buoyancy fluxes using bulk aerodynamic formulae.

2.6.1.5 GCM validation

This GCM has been used in numerous published works including many cited in this thesis.

Chapter 3

Toward a mechanistic understanding of storm track shifts using local measures of mean available potential energy (MAPE)

3.1 Introduction

Midlatitude storm tracks respond in various ways to perturbations in the climate system: changes in the frequency and intensity of the cyclones and anticyclones of which they comprise (Geng and Sugi, 2003; O'Gorman, 2010; Chang, 2013), and changes in the latitudinal position. The mechanisms controlling storm track shifts with changes in climate are of particular interest, since a hierarchy of models show a robust poleward shift in storm tracks as the climate warms (Fyfe, 2003; Yin, 2005; Bengtsson et al., 2006; Tsushima et al., 2006; Schneider et al., 2010; Swart and Fyfe, 2012; Bender et al., 2012; Barnes and Polvani, 2013; Mbengue and Schneider, 2013). Several theories have been suggested (Kushner and Polvani, 2004; Yin, 2005; Chen and Held, 2007; Lorenz and DeWeaver, 2007; Chen et al., 2008; Lu et al., 2010; Butler

et al., 2010; Kidston et al., 2010; Riviere, 2011; Butler et al., 2011; Lorenz, 2014), the most recent of which highlights the importance of wave-reflecting level dynamics on shifting maxima in eddy-momentum flux convergence zones. Here, the authors use Rossby-wave chromatography in a linearized barotropic model to show how changes in upper-tropospheric wave characteristics can modify eddy-momentum flux convergence distributions, which may shift storm tracks (Lorenz, 2014). Nonetheless, to date, a generally accepted theory of storm track shifts remains elusive. In this study, we build upon the work of Mbengue and Schneider (2013) (henceforth referred to as MS13), in which a simple dry idealized framework is used to isolate quantities believed to be important drivers of storm track response to changes in climate.

Using the same simulations as in MS13, we employ the concept of mean available potential energy (MAPE) to explore and help explain the storm track shifts seen in this idealized dry context. Differential large-scale radiative forcing generates available potential energy, which can be decomposed into mean and eddy available potential energy (EAPE) (these are discussed in more detail later in this chapter). Midlatitude eddies then convert this available potential energy into eddy kinetic energy (EKE), primarily through baroclinic instability (Charney, 1947; Phillips, 1956; Orlanski and Katzfey, 1991; Chang et al., 2002). Thus, there is a physical (and well established) link between available potential energy and EKE. Further, prior studies have shown that bulk measures of MAPE and of EKE scale linearly when averaged over a baroclinic zone (Schneider and Walker, 2006, 2008). This is significant because it suggests that changes in MAPE may help dictate the changes in the magnitude of EKE.

Indeed, Lorenz (1955) thought it reasonable to expect large increases in MAPE to be accompanied by large increases in kinetic energy in midlatitudes, given the geostrophic nature of the flow. Furthermore, this linear scaling allows a simple relationship for EKE, a turbulent quantity, to be obtained in terms of MAPE, a mean-flow quantity, within the baroclinic region. This is very useful for deriving turbulent closures and developing simple predictive models. We extend this and test the hypothesis that zonal and temporal averages of local MAPE and of local EKE also scale linearly along the storm tracks, as they shift with climate; and that their maxima are approximately collocated in space. This extension would suggest that changes in the position of the maximum of MAPE help determine the changes in the position of the maximum of EKE.

MS13's simulations show tandem shifts of the Hadley cell terminus and the storm tracks, in agreement with the results of Kang and Polvani (2011) and Ceppi and Hartmann (2013). Hadley cell expansion with warming is another robust response of models and of observations (Hu and Fu, 2007; Seidel and Randel, 2007; Lu et al., 2007; Seidel et al., 2008; Korty and Schneider, 2008; Adam et al., 2014; Levine and Schneider, 2015); although the Hadley cell contracts under warming confined to the tropics, e.g., El Niño (Seager et al., 2003; Tandon et al., 2012; Adam et al., 2014).

The first part of this chapter gives a brief overview of the methods and simulations used in this study, explaining how we identify storm tracks and the idea of using MAPE to understand storm track response to perturbations in climate. This is followed by an analysis of simulation results, and by a discussion and synthesis of

our key findings.

3.2 Methods and simulations

3.2.1 Idealized dry general circulation model

We build upon the work of MS13 and use an idealized dry general circulation model (GCM). This model contains no hydrological cycle or topography and thus allows us to test theories on storm tracks in an environment within which changes in mean temperature are decoupled from changes in stability. Otherwise, changes in mean temperature are coupled to changes in stability through moist dynamics and latent heat release (Xu and Emanuel, 1989; Emanuel, 2007; Schneider and O'Gorman, 2008). Further, this idealized dry GCM, despite its simplicity, not only captures many salient features of the observed general circulation, but also many of the observed responses to warming: a poleward shift of storm tracks (Bender et al., 2012), a rise in the height of the tropopause (Santer et al., 2003), and an expansion of the Hadley cell, with increasing mean temperature or decreasing midlatitude meridional temperature gradients (Hu and Fu, 2007; Adam et al., 2014).

The GCM is set up and forced in the same way as in MS13 (we use the simulation output from MS13 in our analysis); a detailed description of the model can be found in Chapter 2, Schneider (2004) and Schneider and Walker (2006). Radiative and surface fluxes in the model are parameterized using Newtonian relaxation toward a radiative-equilibrium profile. Example climates produced by this model are described in MS13.

The horizontal resolution of the model is about 1.5°, with 30 vertical sigma levels. A quasi-equilibrium dry convection scheme relaxes temperatures in an atmospheric column to a specified, but constant, lapse rate, $\Gamma_{\rm conv} = \gamma\Gamma_{\rm d}$. If a parcel raised from the surface has convective available potential energy relative to the convective lapse rate $\Gamma_{\rm d}$, its convective available potential energy is relaxed to zero within a specified timescale $\tau_{\rm conv}$, which is 4 hrs in this study. Within the fixed planetary boundary layer (surface up to $\sigma = 0.84$), there is vertical diffusion of momentum and dry static energy, $M = c_p\ T + g\ z$. In the remainder of the atmosphere, horizontal hyper-diffusion acts to dissipate momentum and energy at the smallest resolved scales.

Although this GCM has been used in several studies on storm track and related questions (Kushner and Polvani, 2004; Chen and Held, 2007; Butler et al., 2010), in this study, as in MS13, it is forced in a unique way. The model domain is partitioned into a deep tropical ($\gamma_{\rm e}$) and extratropical ($\gamma_{\rm x}$) zone, each with its own independently varied convective lapse rate. In this study, we analyze the simulations conducted by MS13, in which storm track response to mean radiative-equilibrium temperature changes and to global and deep tropical convective stability changes is described (see Table 1 in MS13 for a list of the variables and their values in the six simulated convection scenarios).

Of course, the results found herein are strictly applicable to planets with dry atmospheres. Uncertainty remains about how moist dynamics will affect the results. Nonetheless, dry atmospheres represent a good starting point to theorize about Earth's atmosphere. Indeed, much progress has been made by extending dry theories

to moist atmospheres.

3.2.2 Midlatitude storm tracks

To theorize about midlatitude storm tracks requires a way of identifying them in idealized simulations. Several proxies have been used in the literature to reason about storm tracks, see Chang et al. (2002) for a review. For example, band-pass filtered eddy fields represent a good storm track proxy, when taking a synoptic view of storm tracks (Blackmon, 1976; Blackmon et al., 1977; Hoskins and Valdes, 1990). Synoptic feature tracking (Murray and Simmonds, 1991; Hoskins and Hodges, 2002) also continues to be used. Band-pass filtered eddy fields are also useful for investigating storm track climatology and its response to climate change (Yin, 2005).

In this study, we are interested in storm track response on climatological time scales and identify storm tracks with the maxima of the zonal and temporal averages of EKE[1] (Eqn. 3.2). That is, we identify storm tracks from averages of many synoptic systems over many years. This circumvents the complexity of analyzing individual synoptic systems, assuming that larger-scale dynamics control their response to perturbations in climate. Our results are crosschecked using alternative proxies: surface zonal-mean zonal wind, and meridional and vertical eddy heat flux.

We define the various forms of kinetic energy used in this study: mean kinetic energy (MKE, Eqn. 3.1), eddy kinetic energy (EKE, Eqn. 3.2), barotropic eddy kinetic

[1]Unless otherwise specified, $\overline{(\cdot)}$ represents an arithmetic mean along a latitude circle and in time.

energy ($\mathrm{EKE_{bt}}$, Eqn. 3.3), and baroclinic eddy kinetic energy ($\mathrm{EKE_{bc}}$, Eqn. 3.4).

$$\mathrm{MKE}(\varphi) = \frac{p_0}{2g} \int_0^1 \left(\overline{u^2} + \overline{v^2} \right) d\sigma, \tag{3.1}$$

$$\mathrm{EKE}(\varphi) = \frac{p_0}{2g} \int_0^1 \left(\overline{u'^2} + \overline{v'^2} \right) d\sigma, \tag{3.2}$$

$$\mathrm{EKE_{bt}}(\varphi) = \frac{p_0}{2g} \left[\overline{\left(\int_0^1 u' \, d\sigma \right)^2} + \overline{\left(\int_0^1 v' \, d\sigma \right)^2} \right], \tag{3.3}$$

$$\mathrm{EKE_{bc}}(\varphi) = \mathrm{EKE}(\varphi) - \mathrm{EKE_{bt}}(\varphi). \tag{3.4}$$

where φ is latitude.

Although storm tracks are three-dimensional structures within the general circulation, we neglect asymmetries within a latitude circle, which are most prominent in the Northern Hemisphere—storm tracks are more zonally localized there. MS13 take some of the vertical structure of storm tracks into account by using barotropic EKE and demonstrating poleward storm track shifts with increasing mean radiative-equilibrium temperature or convective stability. However, in Earth-like configurations, EKE generally attains a maximum in the upper troposphere (Ait-Chaalal and Schneider, 2015) and stratospheric dynamics could influence barotropic measures of EKE. Hence, changes in the structure of barotropic EKE with climate could be biased toward upper-tropospheric, and in some cases, stratospheric changes, resulting in a possible divergence from near-surface kinetic energy response. Therefore, we use near-surface EKE to identify storm tracks.

In Fig. 3.1, we show the response of several measures of EKE to mean radiative-equilibrium temperature variations for simulations in which the tropics are compar-

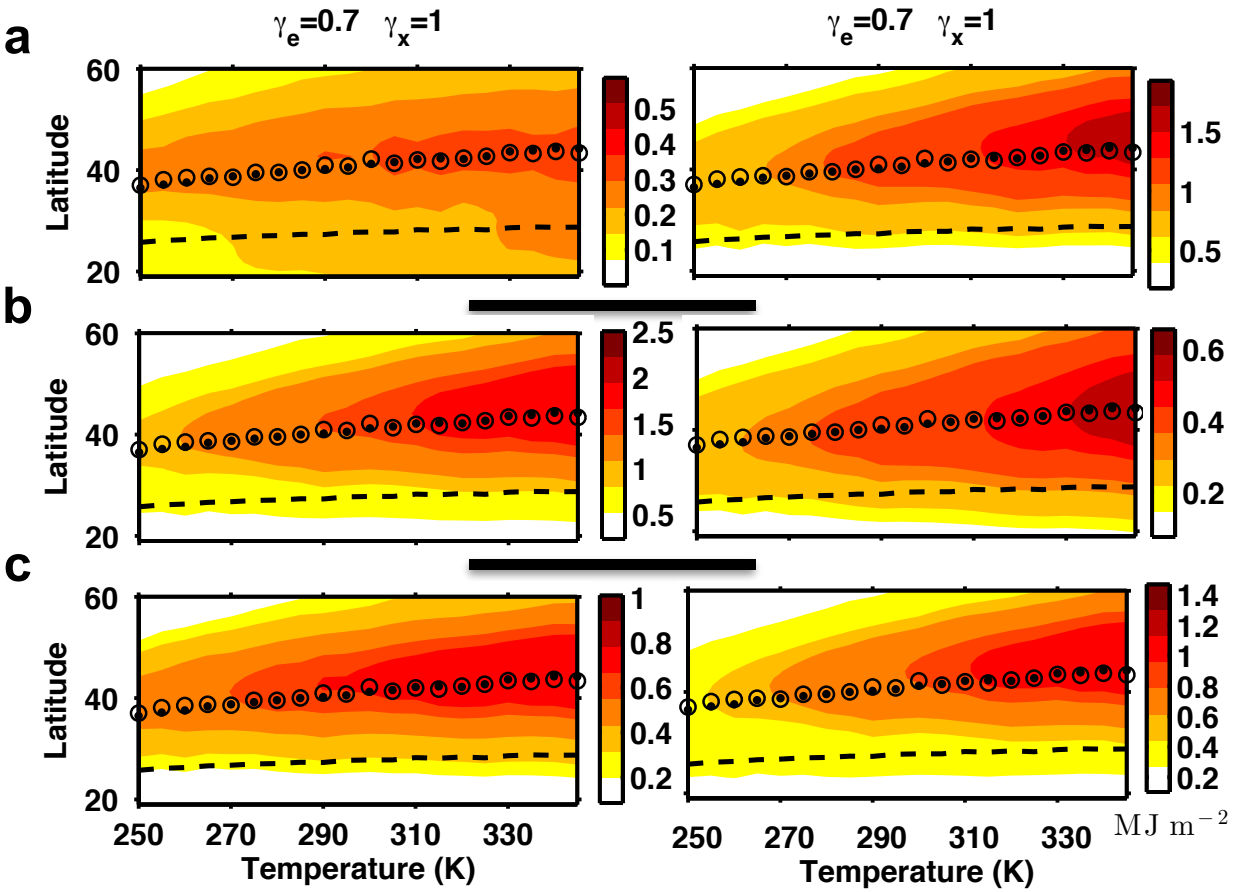

Figure 3.1: Kinetic energy response to mean radiative-equilibrium temperature variations, shown for simulations in which the tropics are more stable than the extratropics. (a) Baroclinic (left) and barotropic (right) EKE. (b) Integrated total EKE from the surface to the tropopause (left) and from the surface to about $\sigma = 0.6$ (herein referred to as near-surface EKE; right). (c) Total EKE, integrated on the interval of about $\sigma = (0.6, 0.4)$ (left) and on the interval of about $\sigma = (0.4, 0.2)$ (right). In these simulations, the structure of the response is, for the most part, unchanged; but, this is not always the case. The following convention is used throughout this chapter: the black dots represent the storm tracks identified as maximum near-surface EKE; the dashed black line represents the terminus of the Hadley cell circulation; and the black circles represent the maximum MAPE in each climate.

atively more stable than the extratropics. Indeed, for this set of simulations, all measures of EKE exhibit the same response; thus, in this case, using barotropic EKE to identify storm tracks gives similar results. In all figures in this chapter, the black dots represent the storm tracks measured as maxima of near-surface EKE; the dashed

black line represents the terminus of the Hadley cell circulation; and the black circles represent the maximum MAPE in each climate.

The most notable examples of when barotropic and near-surface EKE give different storm track responses come from changes in global convective stability. As the global convective stability increases, the upper-tropospheric storm track continues its poleward migration while the mid- and lower-tropospheric storm tracks and Hadley cell terminus cease their poleward expansion. This vertical tilting of the storm tracks as the climate changes is not well captured using only barotropic EKE—it follows the upper-tropospheric response. Since we are particularly interested in how tropospheric EKE responds to changes in climate, we use near-surface total EKE to identify storm tracks and employ it to help build a theory on storm track response to perturbations in climate.

3.2.3 Mean available potential energy

Mean available potential energy, in the sense described by Lorenz (1955), refers to the energy obtained from a difference between the current state of a system and one obtained from an adiabatic redistribution of mass, to a minimum energy state—a horizontally stable stratification in Lorenz's case [see Dutton and Johnson (1967) and Tailleux (2013) for reviews of available potential energy]. In essence, it describes the amount of potential energy available for conversion into kinetic energy and depends on the variance of pressure on isentropic surfaces. It can be approximated by the

variance of entropy on isobaric surfaces (Lorenz, 1955):

$$\overline{A} = 2^{-1}\ \kappa\ c_p\ g^{-1}\ p_0^{-\kappa}\ \int_{p_0}^{0}\ \overline{p}^{\kappa-1}\left(\partial_p\overline{\theta}\right)^{-1}\overline{\theta'^2}\ dp, \tag{3.5}$$

where the over bars represent a global mean on an isobaric surface and the prime a departure therefrom. EAPE is determined from departures of potential temperature from the zonal mean (square brackets) on isobars (Lorenz, 1955):

$$\overline{E} = 2^{-1}\ \kappa\ c_p\ g^{-1}\ p_0^{-\kappa}\ \int_{p_0}^{0}\ \overline{p}^{\kappa-1}\left(\partial_p\overline{\theta}\right)^{-1}\overline{[\theta^{*2}]}\ dp. \tag{3.6}$$

Available potential energy is generated through any perturbation away from the minimum energy state. In Earth's atmosphere, the main source of available potential energy is the differential solar heating and long-wave cooling of the planet. It can be partitioned into MAPE and EAPE [see Lorenz (1955) and Phillips (1956) for a discussion of available energies and their generation and conversion to kinetic energy]. Midlatitude eddies can extract both eddy and mean available potential energy and convert it to kinetic energy. This is accomplished predominantly through baroclinic conversion in strongly baroclinic regions (APE $\rightarrow$ EKE), though barotropic conversion (MKE $\rightarrow$ EKE) also contributes (Orlanski and Katzfey, 1991; Chang et al., 2002). A baroclinic region on a rotating sphere is one of strong meridional temperature gradients, implying vertical shear in the velocity field. There are several sources of local baroclinic regions, including land-sea thermal contrasts, ocean currents and general

ocean dynamics, and storm track eddies themselves (Chang et al., 2002; Brayshaw et al., 2009, 2011).

In his seminal work, Lorenz' available potential energy takes on meaning within the context of a (closed) system, i.e., the entire atmosphere. This restriction to closed systems has been documented as one of the drawbacks of MAPE as defined by Lorenz (Holliday and McIntyre, 1981). [Additionally, his defined minimum energy state is unrealizable in Earth-like configurations (Dutton and Johnson, 1967).] Nonetheless, we expand upon Lorenz' work and apply the concept of MAPE in a local framework, using the approximation first derived in Schneider (1984) and later in Schneider and Walker (2008) (see appendix):

$$\text{MAPE} = \frac{\kappa\ (\overline{p_t} - \overline{p_s})(L_z\ \partial_y \overline{\theta}_s)^2}{(24\ p_0\ \Gamma_d\ \overline{\partial_p \theta}_s)}. \tag{3.7}$$

The idea of local measures of available potential energy is not new. Several authors have come up with local adaptations to Lorenz' bulk measure (Holliday and McIntyre, 1981; Andrews, 1981; Kang and Fringer, 2010; Tailleux, 2013). In the appendix, we describe a simple adaptation to Lorenz' equation to obtain another measure of local available potential energy. Eqn. 3.7, like Lorenz (1955), highlights important quantities for reasoning about changes in available potential energy: the depth of the troposphere $\overline{p}_s - \overline{p}_t$, the meridional temperature gradient, $\partial_y \overline{\theta}$ or, through the thermal wind relationship, the vertical shear, $\partial_p \overline{u}$, and the static stability, $\partial_p \overline{\theta}$. The latter two of these quantities appear in other important composite quantities,

e.g., the Eady growth rate, $0.3\frac{f}{N}\frac{\partial_z u}{}$ (Lindzen and Farrel, 1980; Hoskins and Valdes, 1990), supercriticality, $-\frac{f}{\beta}\frac{\partial_y \overline{\theta}}{\Delta_v}$, (Schneider and Walker, 2006; O'Gorman, 2011), and isentropic slopes, $\frac{\partial_y \overline{\theta}}{\partial_p \overline{\theta}}$, (Held and Schneider, 1999; Schneider and Walker, 2006; Butler et al., 2011; Thompson and Birner, 2012).

In addition to being a possible unifying quantity, MAPE is useful because it is a mean-flow quantity, allowing for ease of computation from resolved model output or observations, and for possible predictive applications. Further, a full mechanistic link can be traced between potential energy generation by insolation and kinetic energy dissipation by viscosity and friction. Given that MAPE and EKE are largely related through baroclinic conversion, one can hypothesize that some scaling relationship exists between the two and it may be possible to use such a scaling to further understand storm track dynamics.

Prior studies have shown linear scaling relations between bulk measures of MAPE and of EKE (Schneider and Walker, 2006, 2008; O'Gorman and Schneider, 2008b; O'Gorman, 2010). Such scaling relations were shown to hold over a wide range of eddy energies and dynamical flow regimes. We extend this work by exploiting possible scaling between local measures of MAPE and EKE. Should they scale and their maxima collocate, then it becomes possible to make inferences about storm tracks using MAPE.

3.3 Simulation results

3.3.1 Storm track proxy responses

Surface zonal-mean winds and vertically integrated (between $\sigma = 0.8$ and $\sigma = 0.2$) eddy meridional and vertical heat flux (not shown) all shift poleward as the mean radiative-equilibrium temperature is increased (Fig. 3.2). A poleward shift of the maximum in surface westerlies implies a concomitant poleward shift of maximum vertically integrated meridional eddy momentum flux convergence $\left(\partial_y \overline{u'v'}\right)$ within the troposphere and of the near-surface meridional temperature gradients maximum $\left(\partial_y \overline{\theta}_s\right)$. There is only a small increase in the magnitude of maximum surface westerlies, along the storm tracks. Instead, a greater change in magnitude is experienced at constant latitude. Latitudes poleward of the storm tracks (within the band of near-surface westerlies) see increased westerly wind speeds with warming, while latitudes equatorward of the storm tracks experience a decrease. The largest shift of surface westerlies occurs when the extratropics are comparatively more stable than the deep tropics (Fig. 3.2a, top right).

If one fixes the mean radiative-equilibrium temperature, then one finds that the mean surface zonal-mean winds shift poleward with increased convective stability (Fig. 3.3). The largest increase in magnitude of the surface westerlies occurs when varying the global convective stability (Fig. 3.3a, left). Here, the magnitude of the zonal-mean westerlies is inversely proportional to the degree of stability. This convection regime sees the most rapid reduction in the mean near-surface isentropic

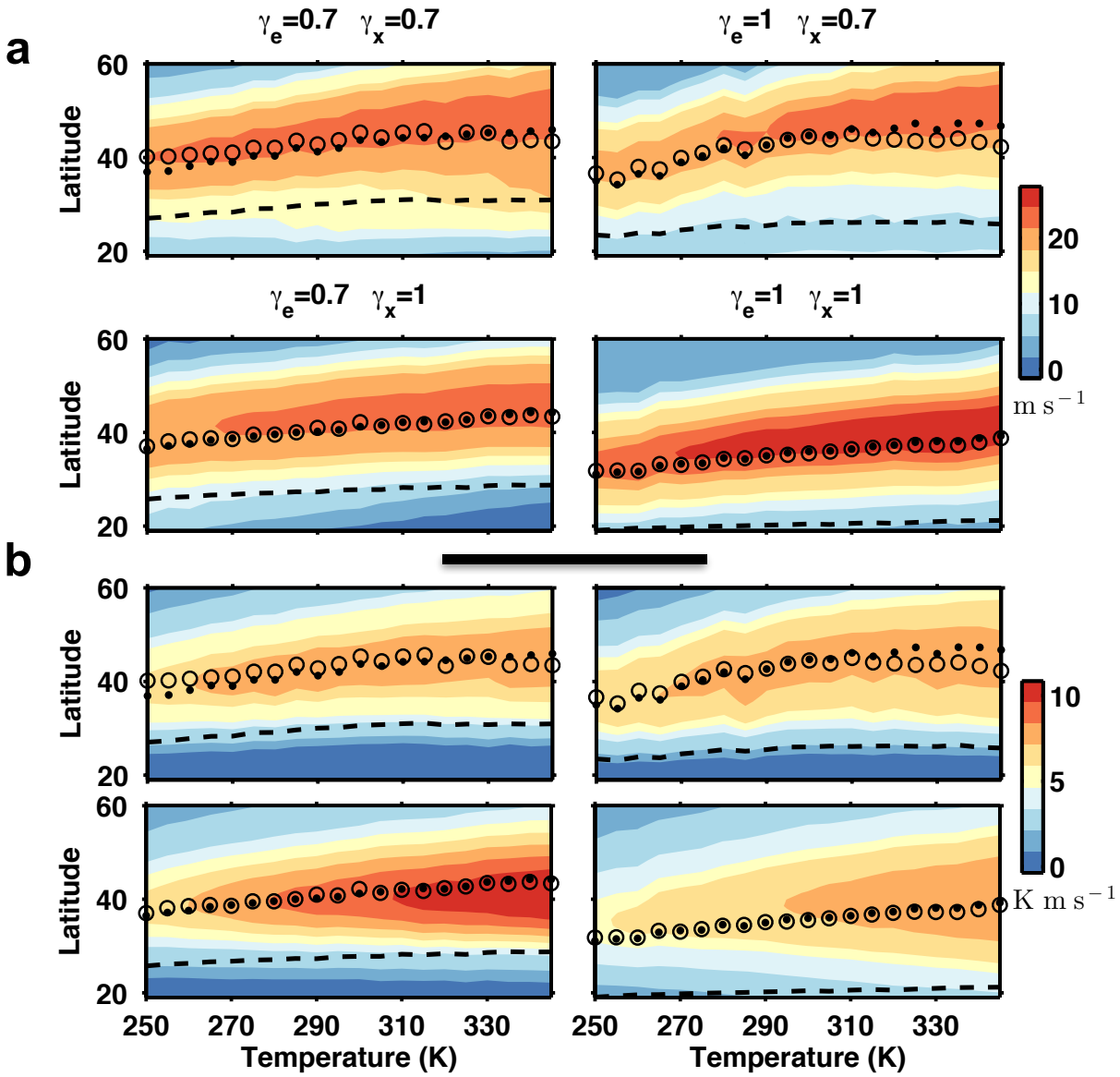

Figure 3.2: Fields of (a) near-surface zonal-mean zonal wind $\overline{u}$ and (b) vertically integrated (between $\sigma = 0.8$ and $\sigma = 0.2$ meridional eddy heat flux $\overline{v'T'}$ for simulations varying mean radiative-equilibrium temperature. There is general agreement among the different storm track proxy responses to mean radiative-equilibrium temperature variations: they all shift poleward with warming and generally in tandem with the terminus of the Hadley cell circulation.

slope, $\overline{I} = \partial_y \overline{\Theta} \; / \; \overline{\partial_p \Theta}$ (Held and Schneider, 1999; Schneider and Walker, 2006), along the storm tracks, with changing climate (decreasing near-surface meridional

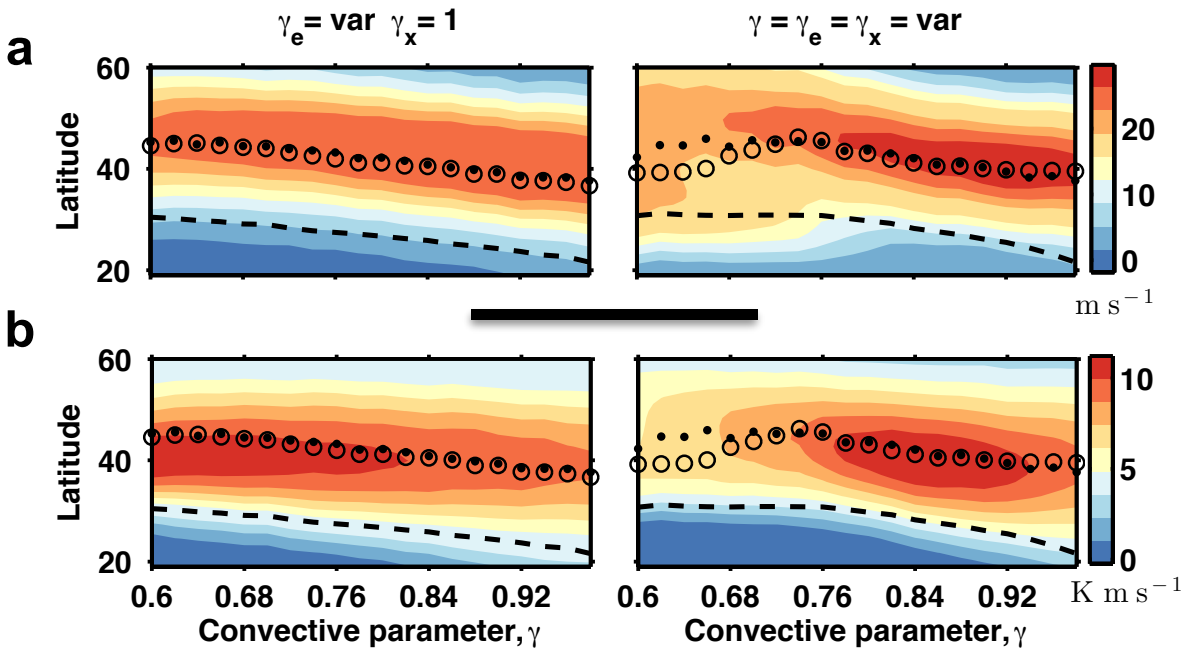

Figure 3.3: Same as in Fig. 3.2, but for simulations varying deep tropical (left) and global (right) convective stability. Meridional eddy heat fluxes (panel b) exhibit a local maximum centered at 40° latitude and a global convective lapse rate of about 8.5 K km^{-1}. There is agreement among the different storm track proxy responses to increases in convective stability (deep tropical or global): they all shift poleward and generally in tandem with the edge of the Hadley cell.

temperature gradients with increasing near-surface static stability). The near-surface isentropic slope along the storm tracks also decreases in simulations varying the deep tropical convective stability; however, this occurs because the reduction in the near-surface meridional temperature gradients outpaces the reduction in static stability. The mean radiative-equilibrium temperature simulations show changes in the near-surface meridional temperature gradients and static stability in the same sense; however, decreases in static stability, with warming, outpace decreases in near-surface meridional temperature gradients. This implies that isentropic slopes decrease along the storm tracks with increasing mean radiative-equilibrium temperature.

Maximum meridional eddy heat flux generally collocates in latitude with maximum EKE. But, there are some climates in which its maximum sits equatorward of the EKE maximum. Further, in the global convective stability variation simulations, meridional eddy heat flux exhibits a local maximum, in the climate-latitude space centered at ($\gamma = 0.85,\ 40°$). This local maximum implies, assuming constant diffusivity, a saddle point in the temperature-gradient field. As the convective stability increases everywhere, the maximum temperature gradient shifts from the midlatitudes to the subtropics near the Hadley cell terminus. In those climates of strong global static stability, within which eddies are comparatively weaker, the thermally driven subtropical jet dominates the dynamics—accounting for the broadening of surface westerlies seen in those climates.

All proxies shift poleward as the climate warms or as global or deep tropical convective stability increases. With few exceptions, all metrics shift in tandem with the Hadley cell terminus, suggesting that the Hadley cell circulation may play a role in facilitating the shifts seen in some of these simulations (Mbengue and Schneider, 2013).

3.3.2 Relationships among eddy kinetic energies and MAPE

In our simulations, we find that when averaged over a baroclinic zone, (15° about the latitude of maximum eddy potential to kinetic energy conversion; see appendix), bulk measures of EKE scale with bulk measures of MAPE. These findings demonstrate that the simulations conducted in this study obey the scalings found in prior studies

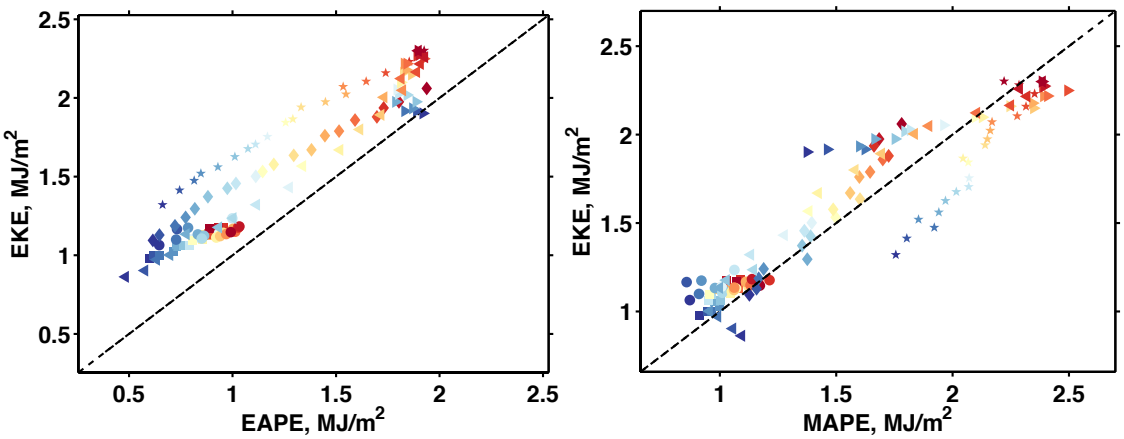

Figure 3.4: Relationship between MAPE and near-surface EKE. Not only do the bulk scalings demonstrated in previous dry macroturbulent studies hold in this study; but they are also extended to apply along the storm tracks.

(Schneider and Walker, 2006, 2008). We take this scaling a step further and show that both MAPE and EAPE scale linearly with near-surface EKE along the storm tracks, Fig. 3.4. This is a new and exciting result because we use this eventuality to help justify using MAPE, a mean-flow variable, to infer about shifts in EKE , a turbulent quantity, i.e., the storm tracks, with changing climate.

Fig. 3.5 shows the field of EAPE (Fig. 3.5a) and MAPE (Fig. 3.5b) for variations in mean radiative-equilibrium temperature. The responses to variations in tropical and global convective stability are shown in Fig. 3.6. For the most part, available potential energy along the storm tracks increases with increasing mean radiative-equilibrium temperature; albeit less so in simulations with comparatively more convectively stable extratropics, i.e., the top row of figures. The increase in available potential energy is largely due to decreasing midlatitude stability and is supplemented by increases in the height of the tropopause. The most severe increase in available potential energy occurs when the midlatitudes are least stable (analogous to a northern hemispheric

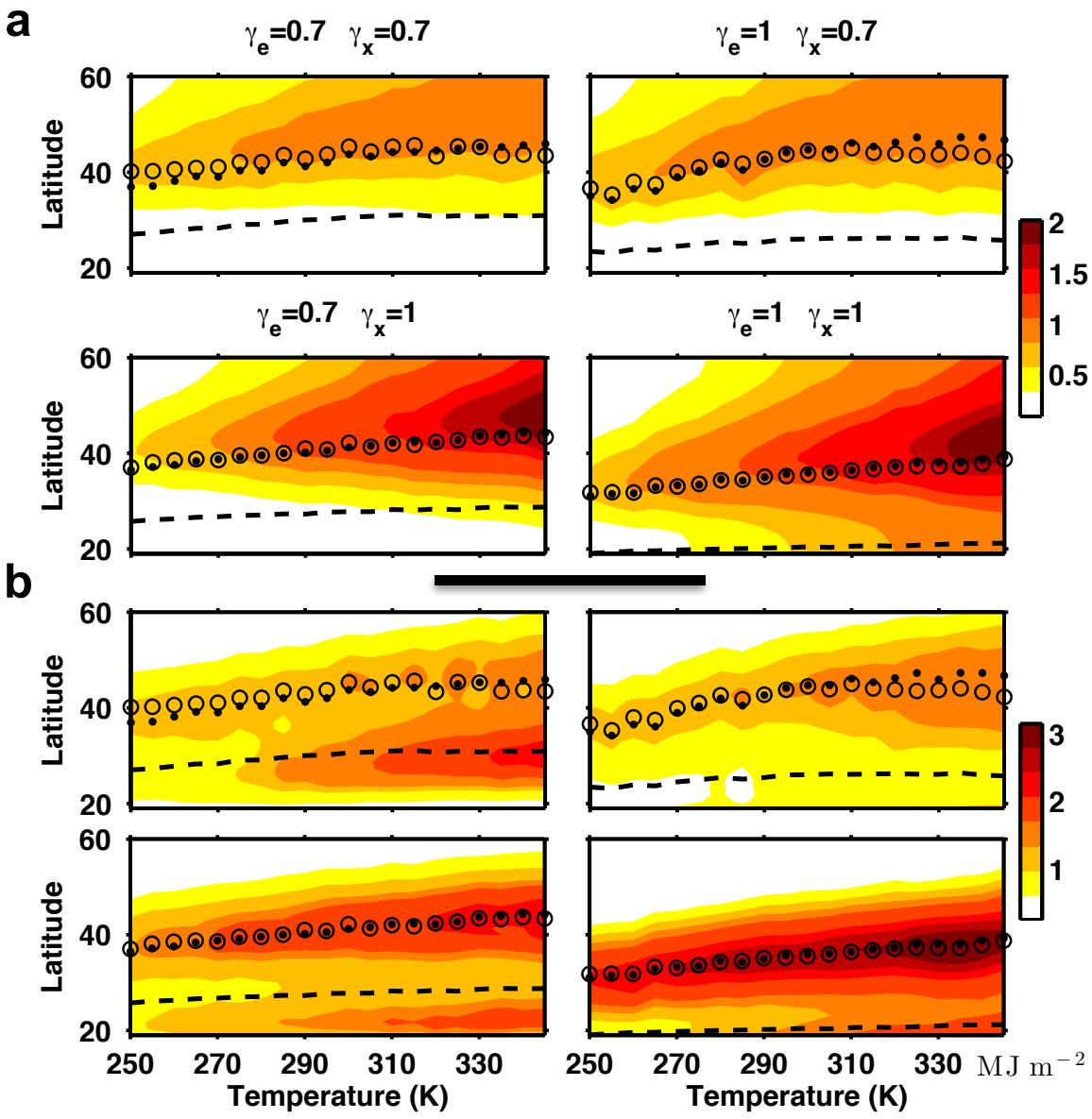

Figure 3.5: Field of (a) local eddy and of (b) mean available potential energy for simulations varying mean radiative-equilibrium temperature. Maxima of MAPE collocate with maxima of near-surface EKE, i.e., the storm tracks. Maxima of EAPE tend to sit a few degrees poleward of EKE maxima, in these simulations.

marine wintertime environment). Here, changes in EAPE are greatest where changes in static stability dominate changes in temperature variance. Increasing deep tropical convective stability leads to a poleward shift in EAPE with negligible changes in

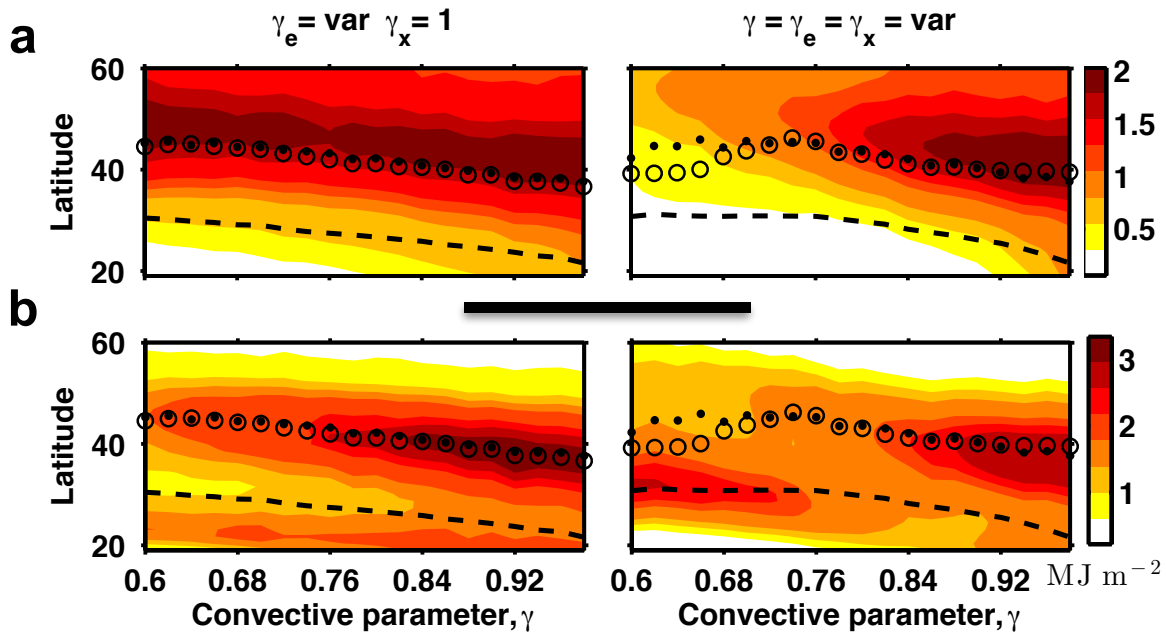

Figure 3.6: Same as in Fig. 3.5, but for simulations varying deep tropical (left) and global (right) convective stability. Similarly (save for the five most stable global convective stability simulations), maxima of MAPE collocate with the storm tracks, while maxima of EAPE sit a few degrees poleward of the storm tracks.

its magnitude, along the storm tracks (Fig. 3.6a, left). More generally, maximum available potential energy shifts poleward in tandem with maximum EKE. Increasing global convective stability leads not only to a poleward shift in EAPE, but also to a progressive decrease in its magnitude. MAPE, on the other hand, increases with increasing mean radiative-equilibrium temperature or decreasing convective stability.

An important finding of this work is that the latitude of local maxima of MAPE (black circles in the figures) collocates with the latitude of local maxima of near-surface EKE (black dots in the figures), as the climate changes. In some climates, the latitude of maximum MAPE, in a statistically steady state, does not lie exactly at the latitude of maximum EKE; however, they always lie within a few degrees of each other and shift in tandem. In these simulations, it is likely that eddies consume

available potential energy at that position faster than it can be restored by large-scale forcing. Also, as noted earlier, where the subtropical jet dominates the dynamics, the midlatitude maximum in MAPE is, in fact, a secondary maximum.

3.4 Synthesis

MAPE and EKE not only collocate locally in space, but they also scale linearly in a bulk sense and along the storm tracks. Using this result, we suggest that shifts in MAPE can be used to understand shifts in the midlatitude storm tracks.

3.4.1 MAPE decomposition

The results obtained thus far suggest that decomposing MAPE into its component parts may yield useful insight into storm track response to perturbations in the climate system. Using Eqn. 3.7, we decompose normalized MAPE into the normalized square of near-surface meridional temperature gradients, the normalized near-surface inverse static stability, and the normalized depth of the troposphere.

We now explicate a novel method for decomposing the field of a composite quantity (MAPE in this example) in the midlatitudes. Using Eqn. 3.7 and assuming a constant baroclinic width, the only variables left in MAPE are the square of the near-surface meridional temperature gradient, the inverse of the near-surface static stability, and the depth of the troposphere. First, take the natural logarithm of Eqn. 3.7, where ξ

consolidates all constants:

$$ln\overline{A} = ln\ \frac{\xi\ \overline{\Delta p}\ \left(\partial_y\overline{\theta_s}\right)^2}{\overline{\partial_p\theta_s}}, \tag{3.8}$$

$$= ln\ \xi + ln\ \overline{\Delta p} + ln\ \left(\partial_y\overline{\theta_s}\right)^2 - ln\ \overline{\partial_p\theta_s}.$$

It is reasonable to expect that a long-term, statistically-equilibrated midlatitude climatology of the zonal-mean near-surface meridional temperature gradient and near-surface static stability to be everywhere positive. Thus, we normalize MAPE by a somewhat fictitious, yet mathematically expedient, climate: the geometric mean[2], $(\cdot)^*$, of MAPE in the full climate-latitude space,

$$ln\overline{A} - ln\overline{A}^* = ln\ \xi + ln\ \overline{\Delta p} + ln\ \left(\partial_y\overline{\theta_s}\right)^2 - ln\ \overline{\partial_p\theta_s} - ln\overline{A}^* \tag{3.9}$$

$$ln\frac{\overline{A}}{\overline{A}^*} = ln\ \xi + ln\ \overline{\Delta p} + ln\ \left(\partial_y\overline{\theta_s}\right)^2 - ln\ \overline{\partial_p\theta_s} - ln\overline{A}^*.$$

Since the product of the geometric mean is the geometric mean of the product, we obtain the following useful decomposition of MAPE (Eqn. 3.10).

$$ln\frac{\overline{A}}{\overline{A}^*} = ln\ \xi + ln\ \overline{\Delta p} + ln\ \left(\partial_y\overline{\theta_s}\right)^2 - ln\ \overline{\partial_p\theta_s} - ln\ \xi - ln\ \overline{\Delta p}^* - ln\ \left(\partial_y\overline{\theta_s}\right)^{2*} + ln\ \overline{\partial_p\theta_s}^*,$$

$$= ln\ \frac{\overline{\Delta p}}{\overline{\Delta p}^*} + ln\ \frac{\left(\partial_y\overline{\theta_s}\right)^2}{\left(\partial_y\overline{\theta_s}\right)^{2*}} + ln\ \frac{\overline{\partial_p\theta_s}^*}{\overline{\partial_p\theta_s}}. \tag{3.10}$$

The above decomposition allows us to investigate how each of the normalized components of MAPE change with climate. This decomposition is exact and does not suffer

[2]For a set x_1 ... x_M, the geometric mean is given by, $\left(\prod_{j=1}^{M}\ x_j\right)^{1/M}$.

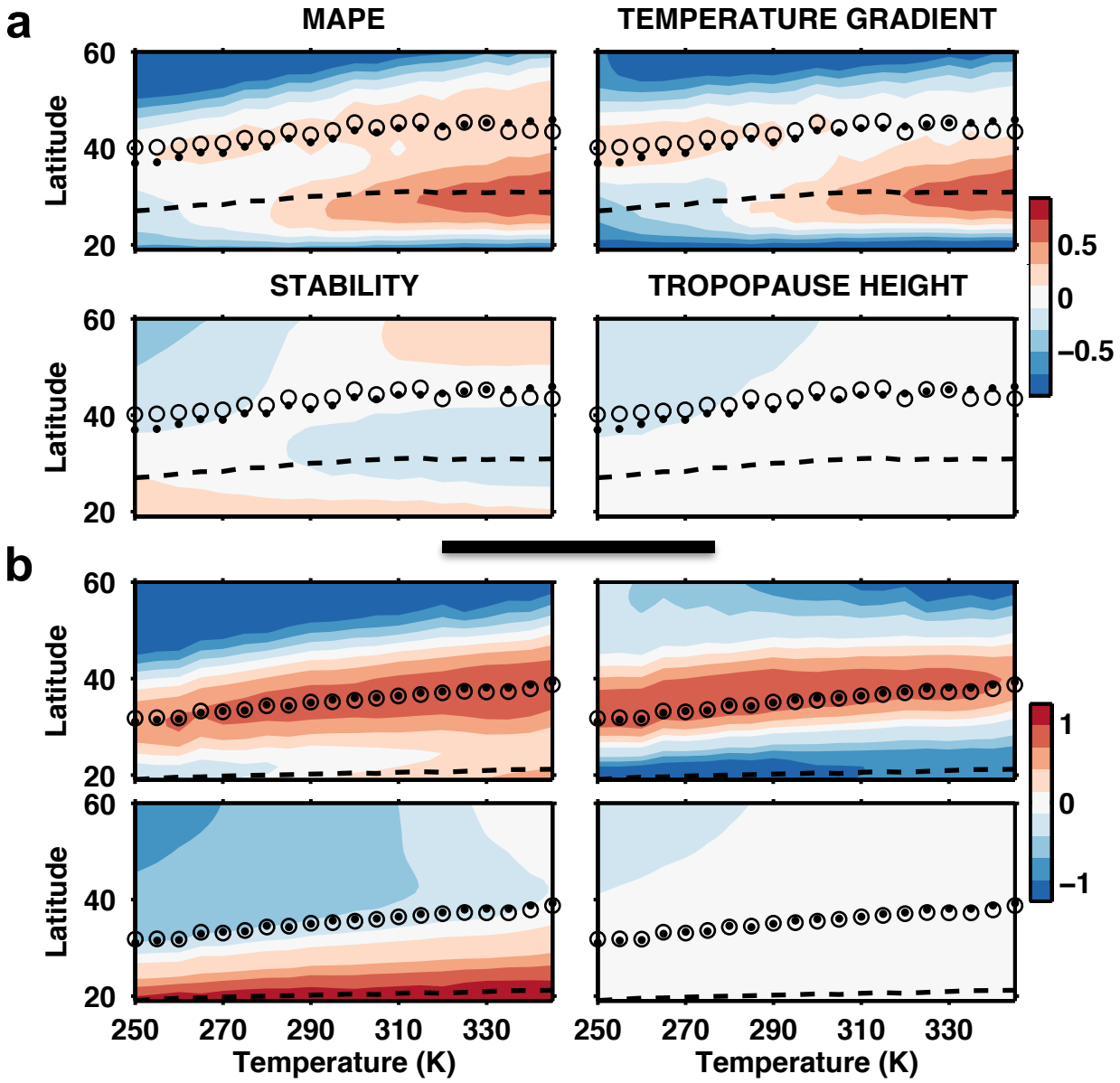

Figure 3.7: Normalized MAPE decomposed into its constituents for simulations varying mean radiative-equilibrium temperature. In these simulations, the convective stability is the same throughout the globe: (a) $\gamma = 0.7$ and (b) $\gamma = 1$. The latitude of maximum normalized MAPE, indicative of the storm track latitude, is largely determined by the latitude of maximum near-surface temperature gradients. This implies that explaining shifts in near-surface meridional temperature gradients could help explain part of the storm track shift seen in dry atmospheres.

from the approximate nature of truncated derivatives about a reference climate. The main drawback, however, is that the reference climate is not a simulated climate.

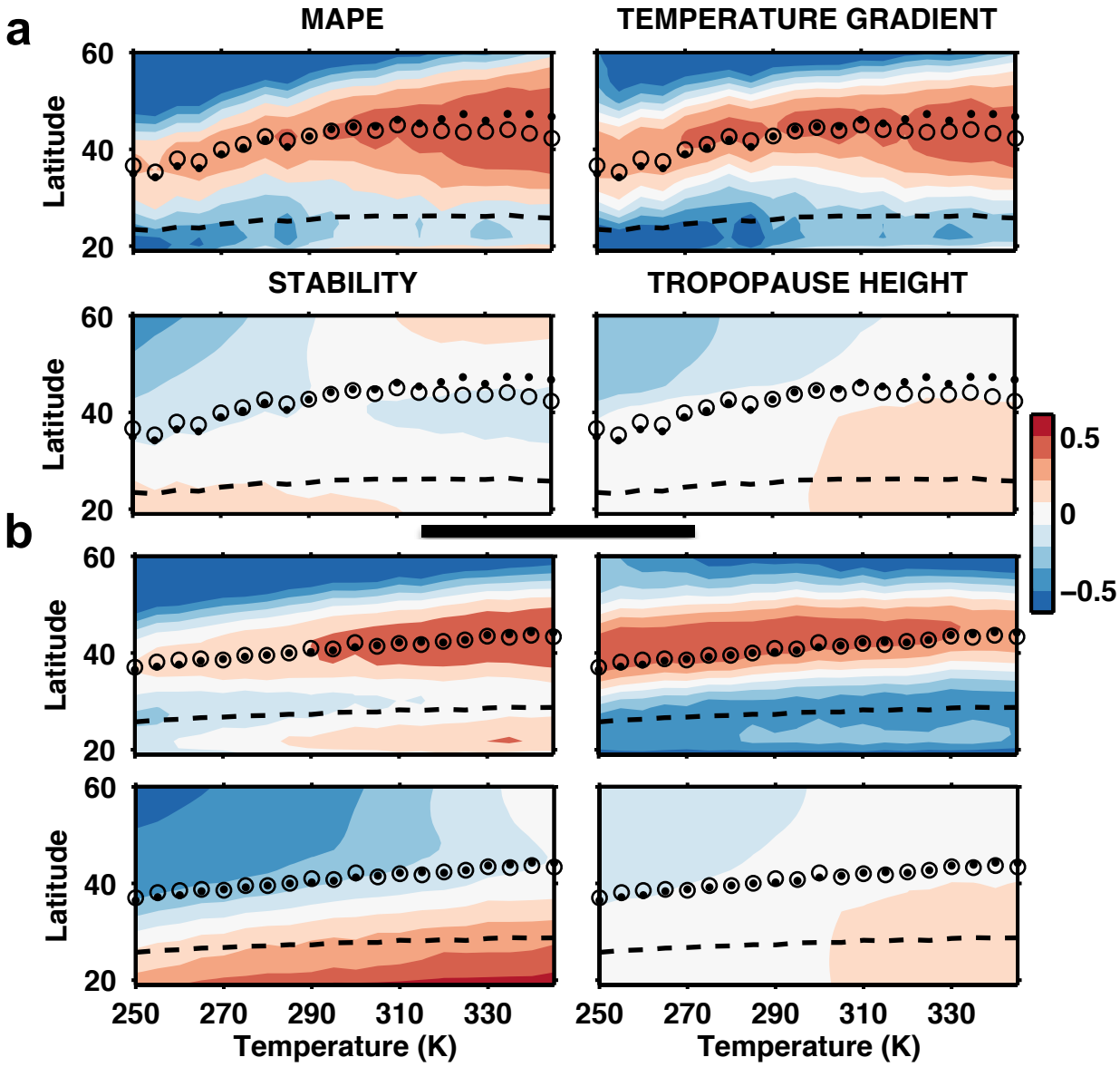

Figure 3.8: Normalized MAPE decomposed into its constituents for simulations in which mean radiative-equilibrium temperature is varied. (a) $\gamma = 0.7$ (extratropics) and $\gamma = 1$ (tropics), that is the extratropics are more convectively stable compared to the deep tropics. (b) $\gamma = 1$ (extratropics) and $\gamma = 0.7$ (tropics), that is the deep tropics ($\pm 10°$) are more stable.

In Fig. 3.7, we show the response of normalized MAPE and each of its components to variations in mean radiative-equilibrium temperature. Fig. 3.7a shows the decomposition for simulations that are the most stable globally, and Fig. 3.7b shows

it for the convectively near-neutral simulations. Fig. 3.8, on the other hand, shows the MAPE decomposition for simulations in which mean radiative-equilibrium temperature is varied and where the extratropics are comparatively more stable than the tropics (Fig. 3.8a) and comparatively less stable (Fig. 3.8b). By construction (see the appendix), the sum of the latter three diagrams in each panel yields the first diagram. From the figures, it is apparent that the location of maximum MAPE, in the mid-latitudes, is largely determined by the location of maximum near-surface meridional temperature gradients, although the structure of MAPE may not necessarily be well captured by it alone.

In this study, we treat the width of the baroclinic zone as constant across climates. Simulations in which the baroclinic zone width is allowed to vary show that it contributes little to changes in MAPE with respect to climate, and makes no contribution (by construction) to changes with respect to latitude. Changes in tropopause height contribute the least to changes in the field of MAPE; however, they make the largest contribution in simulations varying the convective stability.

Changes in normalized MAPE with climate result from a delicate interplay between normalized near-surface meridional temperature gradients and normalized near-surface static stability. Generally, local maximum temperature gradients decrease with increasing mean radiative-equilibrium temperature. The statistically steady-state dynamic pole-equator temperature contrast (as opposed to the radiative-equilibrium pole-equator temperature contrast, which is fixed in these simulations) also decreases with increasing mean radiative-equilibrium temperature. In these simulations, the

mid- and high-latitude steady-state static stability increases, while the tropical static stability decreases. The rate of change of tropical static stability with increasing mean radiative-equilibrium temperature is generally lower than the rate of change of midlatitude static stability.

Fig. 3.9 decomposes MAPE for simulations in which deep tropical convective stability (Fig. 3.9a) and global convective stability (Fig. 3.9b) are varied. It is clear, in these simulations, that midlatitude maxima of near-surface temperature gradients collocate with the storm tracks. Further, in these convective stability experiments, near-surface meridional temperature gradients capture both the structure and maxima of MAPE. In this case, near-surface meridional temperature gradients can be used as a proxy for MAPE, and more so than for simulations varying mean radiative-equilibrium temperature.

The bifurcation of the jets (separation of a merged zonal-mean jet stream into a distinct eddy driven and subtropical jet) and increasing strength of the subtropical jet is clearly visible in Fig. 3.9b. In this set of simulations, where we vary the global convective stability, the rate of change of tropical static stability outpaces the rate of change of mid- and high-latitude static stability; this contrasts with the mean radiative-equilibrium temperature simulations. Here, the Hadley cell shows a strong expansion with strong increases in tropical stability, while changes in the height of the tropopause have a negligible direct impact on the change in MAPE.

Although the near-surface meridional temperature gradient does not always reproduce the sense of the rate of change of MAPE with changing climate; it can be

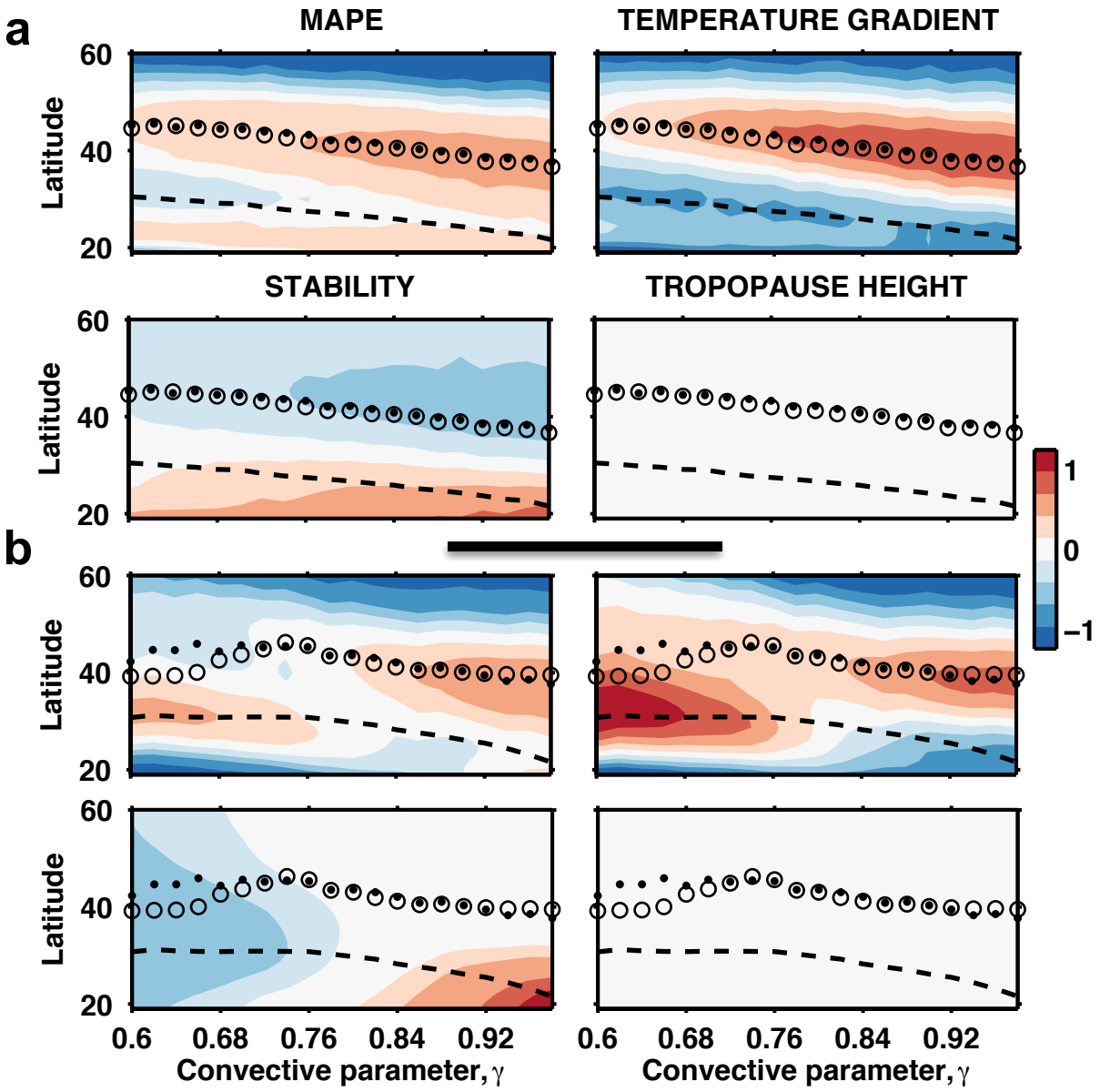

Figure 3.9: Normalized MAPE decomposed into its constituents for simulations in which (a) deep tropical and (b) global convective stability is varied. It can be seen that the local maximum of normalized near-surface meridional temperature gradients may be used as a proxy for maximum normalized local MAPE, in these simulations.

used to identify the location of the maximum in MAPE, as the climate changes; this cannot be done with the near-surface static stability in these sets of simulations—and is a significant find. Thus, the latitude of the storm tracks is largely determined

by the latitude of maximum near-surface temperature gradients. This implies that understanding shifts in near-surface meridional temperature gradients can go a long way in helping to understand the shifts in storm tracks.

To isolate the role of each component of normalized MAPE on the storm tracks, i.e., the latitude of maximum MAPE, we reconstruct MAPE using variations with climate of one component at a time, while the other two are held fixed at a reference value (Eqn. 3.11). For example, normalized MAPE reconstructed using the tropopause height is given by,

$$ln\ \frac{\overline{A}}{\overline{A}^*} = ln\ \frac{\overline{\Delta p}}{\overline{\Delta p}^*} + \left(ln\ \frac{(\partial_y \overline{\theta_s})^2}{(\partial_y \overline{\theta_s})^{2^*}} \right)_{ref} + \left(ln\ \frac{\overline{\partial_p \theta_s}^*}{\overline{\partial_p \theta_s}} \right)_{ref}. \tag{3.11}$$

Then, we compare the reconstructed MAPE maximum to the normalized MAPE maximum, as the climate changes. Therefore, the reconstructed MAPE maximum that most closely matches the normalized MAPE maximum reflects the component that exerts the most influence on the changes in the storm tracks, as the climate.

Fig. 3.10 shows the changes in latitude of maximum reconstructed MAPE for simulations varying mean radiative-equilibrium temperature (Fig. 3.10a) and convective stability (Fig. 3.10 b). Immediately clear from the figures is that most of the variability of the storm track shifts comes from variability in near-surface meridional temperature gradients. In the globally most stable climate, the reconstructed MAPE using static stability overshoots the full MAPE, while the one reconstructed using the near-surface meridional temperature gradient undershoots. Since the undershoot is greater, in absolute value, we conclude that the shift in MAPE with climate, in

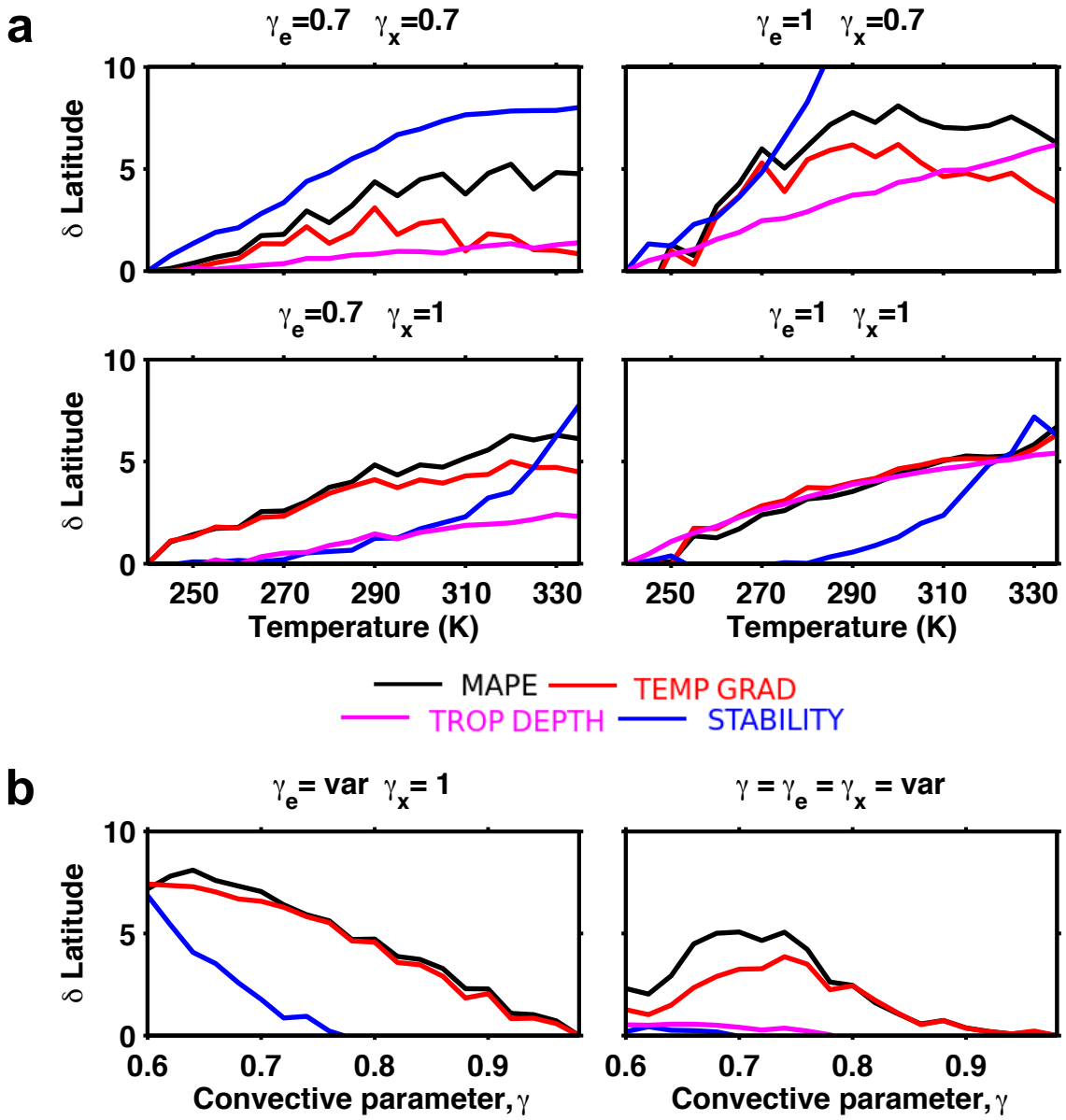

Figure 3.10: The evolution of latitude of maximum reconstructed MAPE (the storm tracks) with climate for (a) mean radiative-equilibrium temperature simulations and for (b) convective stability variations. Each line represents the maximum of MAPE computed when that component varies and the other two are fixed to reference values. For clarity, the latitude of the most equatorward MAPE maximum has been subtracted from each latitude. Generally, MAPE reconstructed with near-surface meridional temperature-gradient variations, using reference values for static stability and tropopause height (red line), produces the best representation of storm track shifts (black line) with climate.

this convection regime, is controlled by shifts in the near-surface stability. In all other convection regimes, shifts in the near-surface meridional temperature gradients dominate the shifts in maximum MAPE and thus, the midlatitude storm tracks. The tropopause height exerts little direct control on storm track latitude in all but the convectively near-neutral simulation (Fig. 3.10a, bottom left). Here, both changes in tropopause height and in near-surface meridional temperature gradients accurately reproduce the storm track response. The dominance of near-surface meridional temperature gradients along the storm tracks is nicely demonstrated in the convective stability simulations. When varying deep tropical stability, the static stability starts to influence a small subset of comparatively more stable climates. So, although varying the tropical static stability directly affects the Hadley circulation, especially its width, its effect on the position of the storm tracks comes about by changes in the extratropical near-surface meridional temperature gradients.

Fig. 3.11 shows the changes in the magnitude of MAPE and of reconstructed MAPE along the reconstructed storm tracks for simulations varying mean radiative-equilibrium temperature (Fig. 3.11a) and deep tropical and global convective stability (Fig. 3.11b). In the former set of simulations, near-surface static stability dominates the changes in the magnitude of MAPE with changing climate. It is supplemented by changes in the depth of the troposphere, which plays a greater role controlling the magnitude of MAPE with changing climate and less of a role in controlling the position of maximum MAPE.

The situation is somewhat different in simulations varying convective stability. Here, near-surface meridional temperature gradients dominate the decrease in MAPE with increasing convective stability. In these simulations, changes in the depth of the troposphere exert negligible control on the change in the magnitude of MAPE along the storm tracks. In simulations varying tropical stability, the inverse static stability acts in the opposite sense of the near-surface meridional temperature gradient, while they act in the same sense when changing deep tropical convective stability.

It is interesting, and indeed surprising, that even when changing deep tropical or global convective stability, it is the near-surface meridional temperature gradients that are directly responsible for changes in storm track position. This suggests that changes in deep tropical stability must be communicated to the extratropical storm tracks through another medium that can shift near-surface meridional temperature gradients. Therefore, one avenue for gaining some understanding about storm shifts is to explain how deep tropical stability changes can influence the midlatitude near-surface temperature gradients. We will follow this line of thinking to its conclusion.

In addition to the results contained herein, MS13 and others (Kang and Polvani, 2011; Ceppi and Hartmann, 2013) show that storm tracks expand in tandem with an expanding Hadley cell circulation. Indeed, MS13 showed that changes in deep tropical stability shifts both the Hadley cell edge and the midlatitude storm tracks. One outstanding question remains: how are the changes in deep tropical stability communicated to the midlatitudes.

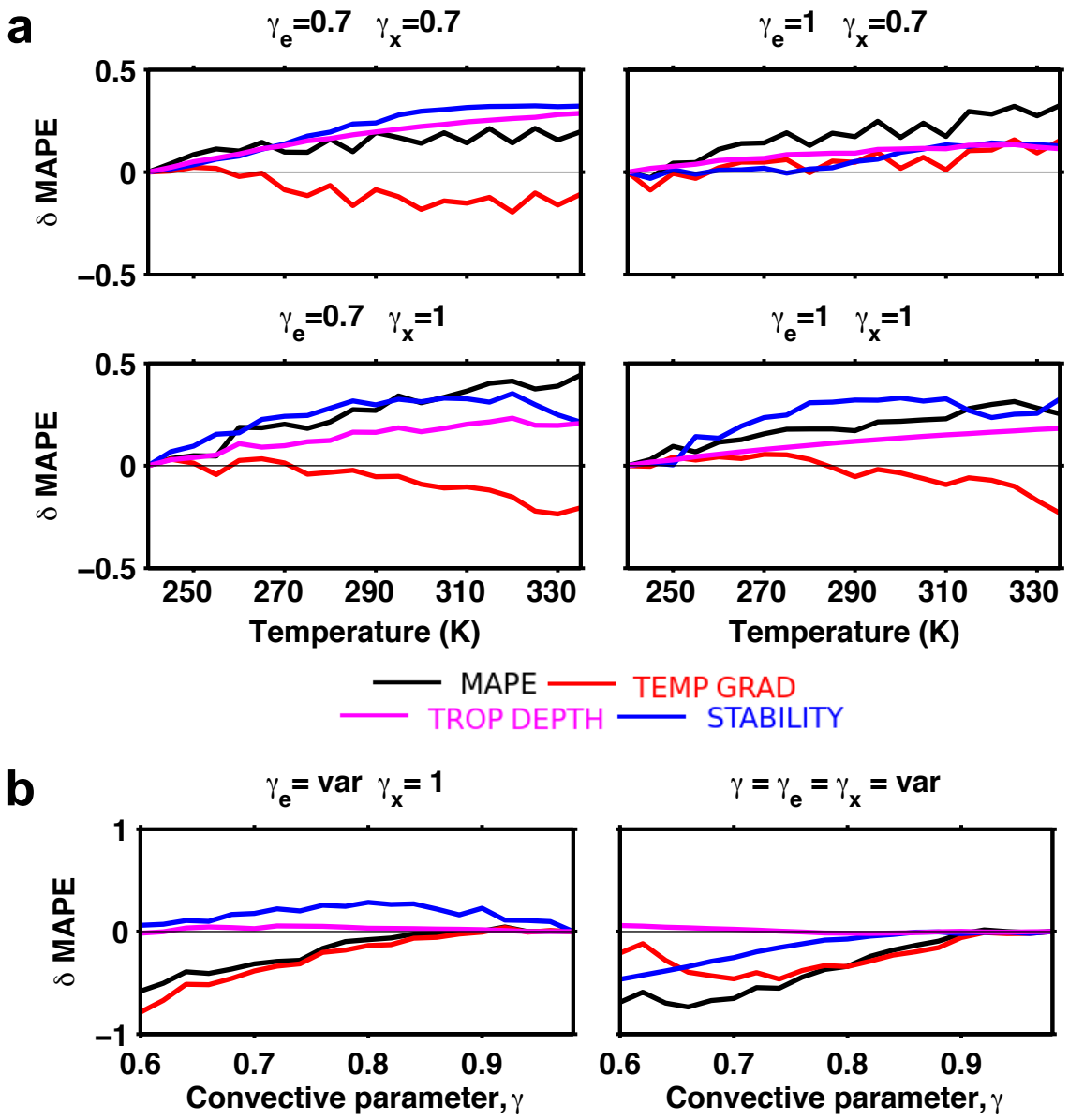

Figure 3.11: Similar to Fig. 3.10, but now considering how the magnitude of reconstructed MAPE changes with (a) mean radiative-equilibrium temperature and (b) convective stability. Static stability plays a much greater role when investigating how the magnitude of MAPE changes with climate (usually supplemented by a rise in the height of the tropopause). Nonetheless, it is worth noting that in simulations in which deep tropical stability is varied, near-surface meridional temperature gradients dominate not only how storm tracks change with latitude, but also the magnitude of the decrease with increasing stability.

Based on the results from MS13 and on the insights contained herein, we proffer the following hypotheses for the poleward shifts seen in their simulations. In the first set of simulations, in which MS13 vary mean radiative-equilibrium temperature independent of changes in stability, as the climate warms, the tropopause height increases (based on the fixed emission temperature of the model). This increase in the height of tropopause, when supplemented by an increase in the tropical static stability leads to an increase in the bulk stability. This increase in bulk stability drives an expansion of the Hadley circulation. As the Hadley cell expands, near-surface meridional temperature gradients are forced further poleward; as a result, storm tracks are forced further poleward.

In the simulations in which MS13 vary the convective stability for fixed mean radiative-equilibrium temperature, the situation is rather similar. Here, there is a marked reduction in the response of the height of the tropopause, but a significant increase in the tropical stability. Again, this serves to increase the bulk stability leading to an expansion of the Hadley cell circulation. As the Hadley cell terminus shifts poleward, so does the maximum meridional temperature gradients—and the storm tracks with them.

3.5 Conclusion

The midlatitude storm tracks respond in various ways to perturbations in the climate system. One robust response is the poleward shift of storm tracks with global warming. Since a generally accepted theory about how storm tracks shifts with cli-

mate change remains elusive, we analyze simulations from an idealized dry GCM to help develop such a theory from a simplified framework. By using such a framework, we isolate quantities believed to be key drivers of these shifts and vary them independently.

The results contained herein complement and extend the work of some previous studies. We show, consistent with prior studies that bulk measures of EKE, averaged over a baroclinic zone, scale linearly with similarly averaged bulk measures of MAPE. This result is extended upon and it is demonstrated that MAPE and near-surface EKE exhibit a similar linear scaling, along the storm track. The most important piece of this theoretical construct is the result that local maxima of MAPE and of EKE collocate in all climate change simulations. This result justifies using MAPE to help understand shifts in EKE—the storm tracks. We employ a mathematically expedient normalized decomposition of MAPE and show that the near-surface meridional temperature gradient is one of the most important quantities in *directly* determining how storm tracks shift when the climate is perturbed; while, near-surface static stability plays a greater role in determining the magnitude of energy available for potential to kinetic conversion and is perhaps more directly related to changes in storm track strength, though this is not the subject of this work. We suggest, consistent with previous work, that increases in the height of the tropopause is an important, but intermediate step in determining storm track shifts with changes in climate. MS13 showed that increases in deep tropical convective stability lead to a poleward shifts in storm tracks. Here, we extend upon this and show that these changes in deep tropical

stability must act through a dynamical intermediary, since near-surface meridional temperature gradient shifts directly control storm track shifts, in those simulations.

Another robust feature of the general circulation's response to warming is the general widening of the Hadley cell circulation. In all idealized simulations conducted herein and in MS13, all storm track proxies migrate poleward in near synchrony with the Hadley cell terminus. Synthesizing the results of this chapter with previous work, we proffer the following explanations for storm tracks shifts seen in the dry idealized context. For the simulations varying mean radiative-equilibrium temperature: as the climate warms, the tropical tropopause height increases. In the convection regimes in which the tropical stability also increases with warming, or decreases in such a way that the bulk stability still increases; then, this increase in bulk stability leads to an expansion of the Hadley cell circulation, which pushes out near-surface meridional temperature gradients, thus pushing storm tracks further poleward (in the convection regimes where there is a decrease in bulk stability; then, it is likely that a decrease in the dynamic pole-equator temperature contrast helps push near-surface meridional temperature gradients, along with the storm tracks, further poleward). In simulations varying the convective stability (both deep tropical and global), the tropical stability increases with a concomitant increase in tropopause height. This comparatively large increase in the bulk stability leads to an expansion of the width of the Hadley circulation, which again pushes near-surface meridional temperature gradients poleward, leading to a poleward shift of storm tracks.

3.6 Appendix

3.6.1 Local mean available potential energy

We use two methods to obtain a local measure of MAPE. The first assumes that MAPE is consumed by eddies of a finite length scale, and that the scale of variation of the meridional temperature gradients implied by large-scale forcing is larger than the eddy length scale[3]. Thus, a local MAPE can be defined at a latitude, ϕ_0, if in place of taking the mean pressure on an entire isentrope and then contrasting the pressure variance; the mean is defined on a segment of the isentrope about a fixed radius of latitude, ϕ_0, and the variance contrasted within that region. In practice, we use Eqn. 4 and replace the over bar with a compact averaging filter of radius ϕ_c about a critical radius at all latitudes (Eqn. 3.12).

$$\mathrm{lMAPE}(\phi) = \left((1+\kappa)\ \Gamma_d\ p_0^{\kappa}\right)^{-1} \int_0^{\infty} \left([p^{\kappa+1}] - [p]^{\kappa+1} \right)\ d\theta, \tag{3.12}$$

where

$$[\cdot] = \frac{\int_{\phi-\phi_c}^{\phi+\phi_c} [\cdot]\ \mathrm{K}(\phi')\ \mathrm{d}\phi'}{\int_{\phi-\phi_c}^{\phi+\phi_c} \mathrm{K}(\phi')\ \mathrm{d}\phi'}.$$

In this study, the critical radius is taken as 15° and a top-hat filter is used. The main drawback of this definition of local MAPE is that until the radius becomes half the length of an isentrope, it under estimates the actual available potential energy. An attractive property, on the other hand, is that the limits are realistic: the bulk MAPE

[3]These assumptions are similar to those used to justify diffusive closures near the Earth's surface (Held and Schneider, 1999)

on one end, and zero on the other.

Alternatively, an approximation to MAPE can be derived, as done in Schneider (1984) and Schneider and Walker (2006), from [Eqn. 8] in Lorenz (1955) by Taylor expanding the variance of potential temperature about a latitude band, ϕ_0 (this is the center of the baroclinic zone in Schneider and Walker (2006)), and assuming that the zonal- and temporal-mean potential temperature and meridional potential temperature gradient at that latitude is representative of those quantities over some delta neighborhood about ϕ_0. See appendix A in Schneider and Walker (2006) for further details and [Fig. A1] therein for a demonstration of the accuracy of this approximation. The only difference between Eqn. 3.7 and Eqn. 3 in Schneider and Walker (2006) is that we apply it locally here and do not average over the baroclinic region.

Eqn. 3.7 introduces the baroclinic width or eddy length scale, L_z, as a new dynamic quantity. In this study, L_z is fixed to 30°. We present our results using this definition of local MAPE.

3.6.2 Baroclinic zones

Unlike in Schneider and Walker (2006, 2008), where the baroclinic width varied with climate, this study follows O'Gorman (2011), and uses a fixed baroclinic width of 30°, an approximation of the maximum energy-containing eddy length scale, centered on the baroclinic latitude. In these simulations, the baroclinic latitude is diagnosed as the latitude of maximum vertically integrated eddy potential to kinetic energy conversion.

This expression can be derived by taking the temporal derivative of either EAPE or MAPE, see Lorenz (1955) Eqn. 26. If one performs the standard conversion from temperature to potential temperature, then one obtains an expression for conversion of MAPE to EAPE (Eqn. 3.13).

$$C_E = -R\ g^{-1}\ \int_0^1\ (p\ p_0^{-1})^{\kappa-1}\overline{\theta'\ w'}\ d\sigma. \tag{3.13}$$

All variables are output from the GCM.

3.6.3 Hadley cell terminus and storm track latitude

The following streamfunction can be derived from the mass conservation equation in the meridional-pressure plane,

$$\psi = \frac{2\ \pi\ R\ \cos\phi}{g} \int_0^p\ \overline{v}\ dp' \tag{3.14}$$

The Hadley cell terminus is computed by first diagnosing the isobar where the Eulerian mass streamfunction (Eqn. 3.14) attains it maximum value nearest to the equator, this is usually in the mid-troposphere, near 500 hPa. Then, the latitude along this isobar where the stream function first changes sign poleward of this maximum is used as the Hadley cell terminus.

Finally, the latitude of maximum of any field A(ϕ)(e.g., EKE for storm tracks),

in latitude, ϕ, is computed using Eqn. 3.15, with n = 16.

$$\phi_{max} = \frac{\int_{\phi_2}^{\phi_1} A^n \ \phi \ d\phi}{\int_{\phi_2}^{\phi_1} A^n \ d\phi} \tag{3.15}$$

Chapter 4

Linking Hadley circulation and storm tracks in an energy-balance model

4.1 Introduction

Earth's Hadley cell is hypothesized to exert control on the shifts of the midlatitude storm tracks. The storm tracks represent an important component of the Earth's general circulation: they redistribute large amounts of energy, moisture, and momentum within the atmosphere. It has been shown that the Hadley cell terminus shifts in tandem with the storm tracks (Kang and Polvani, 2011; Ceppi and Hartmann, 2013; Mbengue and Schneider, 2013), but the causal mechanism remains uncertain. Some studies suggest that extratropical eddy dynamics (the dynamics of their critical line) may control the Hadley cell terminus [see Lu et al. (2007)]. In essence, this means that shifts in the storm tracks lead to expansions or contractions of the Hadley cell. But strong evidence also exists showing that tropical processes and Hadley cell dynamics can exert control on the extratropical eddies (Nakamura, 1998). In this study, we test the idea that Hadley cell dynamics can exert causal control on the storm

track's mean latitude. To do so, we use a simple one-dimensional energy-balance model interactively with an idealized dry general circulation model. Here, we build on the work of Mbengue and Schneider (2013) and Mbengue and Schneider (2015) to construct a closed theory of the storm track shifts seen in the idealized dry context. We discuss extensions to moist, Earth-like atmospheres.

One-dimensional models are of significant pedagogical value in studying questions of climate change. Indeed, several insights have been derived from them, and they have a long history of use (Budyko, 1969; Sellers, 1969; North, 1975a,b; Roe and Lindzen, 2001; Ambaum and Novak, 2014). One interesting result, using a 1-D model, has been to investigate ice-albedo feedbacks and show that two stable equilibrium states exist with one unstable one (Budyko, 1969; Sellers, 1969; North, 1975a,b).

The macroturbulence in Earth's atmosphere, which is responsible for the majority of meridional energy transport from regions of net energy surplus to those of net deficit, arises from baroclinic instability of sheared zonal flow on a rotating sphere (Charney, 1947; Eady, 1949). Hence, diffusive parameterizations for meridional turbulent heat transports may seem questionable at first glance; that is, as opposed to using transports that depend, in some way, on the degree of baroclinic instability (Stone, 1978).

Nonetheless, diffusive parameterizations of energy transports have found widespread use in energy-balance models (Sellers, 1969; North, 1975a,b). One reason is because of mathematical expedience. Another is that these transports at any latitude can be thought of as random parcels of, on average, warmer (colder) air moving poleward

(equatorward), thus mimicking molecular diffusion (Lorenz, 1979). Furthermore, it has been found that the macroturbulence in Earth's atmosphere organizes itself into critical states in which non-linear eddy-eddy interactions are weak, explaining why linear theories have been rather successful at explaining some atmospheric phenomena (Schneider and Walker, 2006); thus, one may consider inter-scale energy transfer to be unimportant on these timescales, meaning that all response modes are forced by large-scale radiative forcing, which is strong and helps establish a well-defined background meridional temperature gradient, whose scale of variation is larger than the scale of eddies that act to dissipate them. Thus, to consider the eddy energy transports as diffusive in this context is reasonable (Held and Schneider, 1999; Held, 2000). Moreover, it has been shown that a diffusive parameterization can capture the physics of the atmosphere's forced response on climatological scales, while they do poorly when simulating shorter time scale responses or the atmosphere's free response to internal variability (Lorenz, 1979; Frierson et al., 2007; Roe et al., 2015).

The first part of this chapter presents the diffusive energy-balance model and the Hadley circulation parameterization. This is followed by a presentation of sensitivity tests using an analytical solution of the diffusive energy-balance model. A comparison of the results derived from the energy-balance model and solutions from a similarly forced idealized dry general circulation model follows. The last part of this chapter then synthesizes and discusses the implications of this work.

4.2 The diffusive energy-balance model

We construct a simple energy-balance model, Eqn. 4.1, that has simple representations of the elements we believe to be important for the shifts in storm tracks seen in the idealized dry GCM. Temperature in the model represents near-surface temperatures, i.e., just above the boundary layer. Since this is a dry, single-layer model, the diffusion can be thought of as diffusing dry static energy. This simple diffusive energy-balance model has been used before (Frierson et al., 2007). However, to our knowledge, it has never been used to idealize Hadley cell dynamics and study storm track response to changing climate before.

The storm tracks are identified as the maximum absolute value of the meridional temperature gradient within the domain. This model lacks other processes believed to be important for the storm track response to changing climate. The main advantage of this model is its simplicity. Building on previous work, the storm track problem has now been distilled to a question of near-surface meridional temperature gradients, Hadley cell dynamics, and eddy-energy transports. Within this context, any storm track shifts stand a better chance of being causally explained.

4.2.1 Energy-balance equation

The diffusive energy-balance model equation in one dimensional spherical coordinates is given by,

$$C_0\ \partial_t T(\varphi) = \frac{\partial_\varphi\ D(\varphi)\ \cos(\varphi)\ \partial_\varphi\ T(\varphi)}{R^2\ \cos(\varphi)} + \frac{E(\varphi) - T(\varphi)}{\tau_{\text{rad}}} + \frac{(T_0 - T(\varphi))\ \mathcal{H}\left(|\varphi_h| - |\varphi|\right)}{\tau_{\text{eq}}}, \tag{4.1}$$

and

$$\partial_\varphi T(-\pi/2) = \partial_\varphi T(\pi/2) = 0 \tag{4.2}$$

where $\mathcal{H}$ is the Heaviside function, φ is latitude, and T_0 is a dynamically determined energetically consistent temperature to which the Hadley cell adjusts tropical temperatures at each time step. $D(\varphi)$ is the diffusivity, which in this study, is constant; R is the radius of the Earth, $E(\varphi)$ is the radiative-equilibrium temperature profile, and τ_{rad} and τ_{eq} are the radiative relaxation and tropical relaxation timescales, respectively.

Eqn. 4.1 is a formal statement that the evolution of zonal-mean temperatures in a given latitude band (left hand side) is balanced by the energy flux out of that latitude band (first term on the right), the large-scale radiative heating in the latitude band (second composite term on the right), and, if it is a latitude band inside the Hadley cell circulation, the net cooling induced by the Hadley cell circulation (third composite term on the right). These terms are explored in more detail over the next few subsections.

4.2.1.1 Radiative forcing

Shortwave heating, long-wave cooling, sensible, latent, and turbulent energy fluxes are all parameterized as relaxation toward a prescribed radiative-equilibrium temperature profile (which resembles that of the Earth), $E(\varphi)$, over a prescribed radiative time scale, τ_{rad}. This forcing profile is exactly the same as the one used in the idealized dry GCM. The radiative-equilibrium temperature profile, $E(\varphi)$, is given by,

$$E(\varphi) = \overline{T}_E + \Delta_H \left(1/3 - \sin^2(\varphi)\right). \tag{4.3}$$

4.2.1.2 Meridional energy transports

The total meridional temperature flux is given by,

$$\overline{[v\ T]} = \overline{[v]}\ \overline{[T]} + \overline{[v]'\ [T]'} + [\overline{v}^*\ \overline{T}^*] + [\overline{v'^*\ T'^*}], \tag{4.4}$$

where the first term of the right hand side is the mean meridional energy flux, the second term is the transient eddy energy flux, the third is the stationary eddy energy flux, while the fourth is the transient asymmetric eddy energy fluxes. The over bar represents a temporal mean and the prime a departure therefrom. The square brackets represent a mean along a latitude circle and the asterisk a departure therefrom. The models we have used so far, and will use in this chapter, have no means to excite zonal asymmetries; hence, the latter two terms on the right hand side are zero. Thus, a

parameterization for the meridional energy transports requires finding as relationship for $\overline{[v\ T]} = \overline{[v]}\ \overline{[T]} + \overline{[v]'\ [T]'}$.

Transient energy transports in the model are parameterized as diffusive. We assume that these diffusive fluxes are proportional to the meridional temperature gradient,

$$dq(\varphi) = D(\varphi)\ R^{-1}\ \partial_\varphi\ T, \tag{4.5}$$

where $dq(\varphi)$ is the diffusive flux per unit latitude circle. For a latitude band of width, $\delta\varphi$, the diffusive fluxes at the boundaries are,

$$F(\varphi) = 2\ \pi\ \cos(\varphi)\ D(\varphi)\ \partial_\varphi\ T|_\varphi, \tag{4.6}$$

$$F(\varphi + \delta\varphi) = 2\ \pi\ \cos(\varphi + \delta\varphi)\ D(\varphi + \delta\varphi)\ \partial_\varphi\ T|_{\varphi+\delta\varphi}, \tag{4.7}$$

respectively. Then, the diffusive flux temperature tendency, $DQ(\varphi)$, follows from the flux difference divided by the latitude band area,

$$DQ(\varphi) = \frac{F(\varphi + \delta\varphi) - F(\varphi)}{2\ \pi\ R^2\ \cos(\varphi)\ \delta\varphi}, \tag{4.8}$$

$$= \frac{D\ (\varphi + \delta\varphi)\ \cos(\varphi + \delta\varphi)\ \partial_\varphi\ T|_{\varphi+\delta\varphi} - D\ (\varphi)\ \cos(\varphi)\ \partial_\varphi\ T|_\varphi}{R^2\ \cos(\varphi)\ \delta\varphi}, \tag{4.9}$$

$$= \frac{\partial_\varphi D(\varphi)\ \cos(\varphi)\ \partial_\varphi\ T}{R^2\ \cos(\varphi)}, \tag{4.10}$$

where the latter equation is obtained by taking the limit as the latitude band width

goes to zero. Therefore, in our model,

$$\partial_y \ \overline{[v]' \ [T]'} = \frac{\partial_\varphi D(\varphi) \ \cos(\varphi) \ \partial_\varphi \ T}{R^2 \ \cos(\varphi)}. \tag{4.11}$$

In the present study, we use a constant diffusivity, D, obtained from the mean near-surface diffusivity in GCM simulations. In this context, near-surface means a vertical average over a thin layer above the planetary boundary layer ($\sigma = 0.8$ to $\sigma = 0.7$). Since transient eddies dominate energy transport in the extratropics, this is an adequate representation of the total transport in the extratropics. However, in the tropics (within the Hadley cell) transports by the mean meridional circulation must also be considered.

4.2.1.3 Tropical to extratropical transition

If one subscribes to the perspective that the Hadley cell terminates where baroclinic eddies reach the tropopause, then one expects the supercriticality (the ratio of the vertical extent of baroclinic eddies to the vertical extent of the troposphere) (Eqn. 4.12) to be around one at the terminus of the Hadley cell edge [see Schneider and Walker (2006), Korty and Schneider (2008) and Levine and Schneider (2015) for further details].

$$sc(\varphi) = \frac{f}{\beta} \frac{\partial_y \overline{\theta}_s}{2 \ \overline{\partial_p \theta}_s \ (\overline{p}_s - \overline{p}_t)} = -\frac{f}{\beta} \frac{\partial_y \overline{\theta}_s}{\Delta_v}, \tag{4.12}$$

$$= -\tan(\varphi) \frac{\partial_\varphi \overline{\theta}_s}{\Delta_v}, \tag{4.13}$$

where f is the planetary vorticity, β is the planetary vorticity gradient, and Δ_v is the bulk stability. By construction, supercriticality cannot exceed one. But values less than one suggest that other processes, like convection, set the height of the tropopause. If one takes a slightly relaxed definition of supercriticality, say where baroclinic eddies dominate the dynamics, then one permits the Hadley cell to terminate at values less than one. In fact, Korty and Schneider (2008) and (O'Gorman, 2011) found the supercriticality computed at the location of the Hadley cell terminus to be less than one in the idealized dry context. Thus, we consider the supercriticality to take on a constant value, possibly less than one, at the terminus of the Hadley cell.

Since the supercriticality at the Hadley cell terminus is constant, then the Hadley cell terminus latitude, φ_H, is determined by the meridional temperature gradient and the bulk stability there. Since the bulk stability is our experimental parameter, the Hadley cell terminus is dynamically determined by the evolution of the meridional temperature gradient. Hence, the boundary between the tropics and the extratropics is given by,

$$\varphi_H = \tan^{-1}\left(-sc\,\frac{\Delta_v}{\partial_\varphi \theta}\right). \tag{4.14}$$

In the energy-balance model, Eqn. 4.14 is used to identify the Hadley cell terminus.

4.2.1.4 Hadley cell parameterization

Mbengue and Schneider (2013, 2015) hypothesized that the Hadley circulation plays a role in midlatitude storm track migrations. More specifically, they hypothesize that shifts in the Hadley cell terminus can cause shifts in the storm track's position.

Thus, to test this hypothesis and establish the degree to which shifts in the Hadley cell terminus can cause changes in the storm track position, we include a simple parameterization for the Hadley cell in the energy-balance model.

Considering the Hadley cell in its most basic role as one component, of several within the climate system, that transports energy from regions of net surplus to those of net deficit, then a simple first approximation of it, in a 1D energy-balance model, is as a mechanism to reduce temperature gradients over its domain of operation, which can change with climate, in an energetically consistent way. In essence, the parameterization will, at every time-step, determine the Hadley cell width and relax temperatures equatorward of this dynamically determined Hadley cell terminus toward an energetically consistent temperature, T_0.

Eqn. 4.27 provides the zonal-mean temperature profile, and, since it is smooth and continuous, all of its derivatives, at each time-step. The bulk stability, as mentioned earlier, is an experimental parameter, and the supercriticality is constant. Thus, we require another equation to close the system and dynamically determine T_0. We invoke tropical energy balance to do it. By that we mean that we allow the Hadley parameterization to relax tropical temperatures to the temperature T_0 that ensures a balance between the net radiative tropical heating and the net eddy energy fluxes into the extratropics. Thus, a relation is obtained by integrating Eqn. 4.27 from the

equator to the pole:

$$C_0 \int_0^{\pi/2} \partial_t T(\varphi)\ \cos(\varphi)\ d\varphi = \int_0^{\pi/2} \frac{\partial_\varphi\ D(\varphi)\ \cos(\varphi)\ \partial_\varphi\ T}{R^2}\ d\varphi \tag{4.15}$$
$$+ \int_0^{\pi/2} \frac{E(\varphi) - T(\varphi)}{\tau_{\text{rad}}}\ \cos(\varphi)\ d\varphi$$
$$+ \int_0^{\pi/2} \frac{(T_0 - T(\varphi))\ \mathcal{H}\left(|\varphi_h| - |\varphi|\right)}{\tau_{\text{eq}}}\ \cos(\varphi)\ d\varphi,$$

Assuming that a steady state has been reached and that the fluxes at the boundaries are zero, then we have,

$$\int_0^{\pi/2} \frac{T(\varphi) - E(\varphi)}{\tau_{\text{rad}}}\ \cos(\varphi)\ d\varphi \tag{4.16}$$
$$= \int_0^{\pi/2} \frac{(T_0 - T(\varphi))\ \mathcal{H}\left(|\varphi_h| - |\varphi|\right)}{\tau_{\text{eq}}}\ \cos(\varphi)\ d\varphi,$$

Eqn. 4.16 yields the following constraint on the temperature to which the Hadley circulation can relax the tropics while still maintaining energy balance,

$$T_0 = \text{cosec}(\varphi_H)\ \frac{\tau_{\text{eq}}}{\tau_{\text{rad}}} \int_0^{\pi/2} \left(T(\varphi) - E(\varphi)\right))\ \cos(\varphi)\ d\varphi \tag{4.17}$$
$$+ \text{cosec}(\varphi_H)\ \int_0^{\pi/2} T(\varphi)\ \mathcal{H}\left(|\varphi_h| - |\varphi|\right)\ \cos(\varphi)\ d\varphi,$$

Thus, the model proceeds as follows. At each time step, the Hadley cell terminus is computed from Eqn. 4.14 using the temperature-gradient profile computed from the previous step. Then, T_0 is computed from Eqn. 4.17, after which the model is stepped forward in time. At the end of the simulation, the storm track latitude is computed.

4.2.1.5 Storm tracks

The storm track latitude is identified as the maximum absolute value of the meridional temperature gradient. After the simulation is completed, a top hat filter of width 42° is applied to the temperature gradient before computing the storm track latitude. This physically motivated step ensures that synoptic eddies feel the changes in the width of the Hadley cell. If the filter width is too small, then the storm track shift in response to the Hadley cell expansion is reduced.

4.3 Simulations

Table 4.1 lists the reference parameters and their values used throughout this study. Unless otherwise stated, they are the default values used in the energy-balance model. Most values are the same as those used in forcing the idealized dry general circulation model, especially the radiative parameters.

Eqn. 4.1 is solved on numerically on a domain with 1° resolution (the GCM has a meridional resolution of about 1.5°). Simulations are run forward in time, using a forward Euler numerical scheme, until a steady state in temperature is reached (for further details, please see the appendix). Table 4.2 details the simulation variables for the sensitivity study and the numerical energy-balance model simulations.

Table 4.1: Simulation and reference parameters

Parameter	Symbol	Value
	Planet and fluid	
Heat capacity	C_0	1.8×10^8 J m^{-2} K^{-1}
Specific Heat	c_p	1004 J kg^{-1} K^{-1}
Diffusivity	D_0	2.1×10^6 m^2 s^{-1}
Hadley cell extent	Had_{ex}	30°
Planetary radius	R	6.365×10^6 m
Supercriticality	sc	0.5
Tropopause pressure	ΔP	800 hPa
Density	ρ	1.0 kg m^{-3}
Convective lapse rate	$\gamma\Gamma_d$	6.9 K km^{-1}
	Diabatic processes	
Radiative-equilibrium mean temperature	$\overline{T}_{eq}$	288 K
Pole-equator temp. contrast	Δ_H	120 K
	Relaxation timescales	
Extratropical	τ_{rad}	50 days
Deep tropical	τ_{eq}	4 days

4.4 Results

In this section, results from an analytical and numerical solution to the energy-balance model are presented and then compared to the idealized dry GCM.

4.4.1 Eddy-diffusivity and its implications

Fig. 4.1 shows the response of near-surface eddy-diffusivity, $D = -\left\langle \overline{v'\theta'} \cos(\varphi)/\partial_y\theta \right\rangle$ in the idealized dry GCM. The angled bracket means a near-surface vertical average between $\sigma = 0.8$ and $\sigma = 1$. On the left shows variations in diffusivity for simulations varying mean radiative-equilibrium temperature in a convection regime in which deep tropical temperatures are relaxed toward an Earth-like moist-adiabatic-type value

Table 4.2: Simulation parameters for sensitivity tests using the analytical solution and for the numerical simulations [min : step : max]

Experimental Parameter	Symbol	Value
	Sensitivity study with analytical model	
Dry eddy efficiency	$\zeta = 86400\ D_0\ \tau_{rad}\ R^{-2}$	0 : 0.1 : 1
Pole-equator temp. contrast	Δ_{H}	20 : 5 : 300 K
Dry static energy flux @ HC	F	−100 : 5 : 0 K
	Numerical simulations	
Convective parameter	γ	0.6 : 0.02 : 0.98

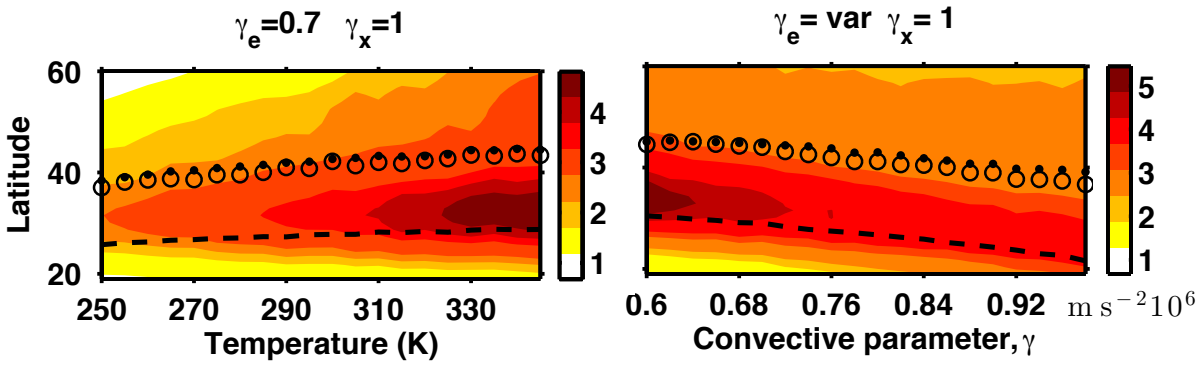

Figure 4.1: Response of near-surface eddy diffusivity ($D = \left\langle \overline{v'\theta'}\ \cos(\varphi)/\partial_y\theta \right\rangle$) for simulations varying mean radiative-equilibrium temperature in a convection regime where deep tropical temperatures are relaxed toward a moist adiabatic value ($\gamma = 0.7$), while temperatures outside of this region toward a dry adiabatic one ($\gamma = 1$) (left) and deep tropical convective stability (right). There is stronger variation in eddy diffusivity with latitude than with climate, and stronger variation with climate near the Hadley cell terminus than along the midlatitude storm tracks. The angled bracket means a vertical average between $\sigma = 0.8$ and $\sigma = 1$.

($\gamma = 0.7$), while temperatures outside of this region are relaxed toward a dry adiabatic one ($\gamma = 1$). On the right shows diffusivity response to changes in deep tropical convective stability. There is stronger variation in diffusivity with latitude than with climate, and stronger variation with climate near the Hadley cell terminus than along the midlatitude storm tracks.

The variation of diffusivity with latitude justifies using a model diffusivity that is a function of meridional temperature gradients, $\partial_y \overline{\theta}$, or of temperature curvature, $\partial_{yy} \overline{\theta}$. By definition $\partial_y \overline{\theta}$ attains a maximum absolute value at the storm tracks, while $\partial_{yy} \overline{\theta}$ attains an absolute minimum closer to the Hadley cell and is zero at the storm tracks.

It is apparent from Fig. 4.1 that the maximum near-surface eddy diffusivity, in both simulations, sits just outside the Hadley cell terminus, implying enhanced eddy transports there. There is a modest poleward shift in the maximum near-surface eddy diffusivity with increasing mean radiative-equilibrium temperature and a significant poleward expansion with deep tropical convective stability. The magnitude also increases as mean radiative-equilibrium temperature increases or as the convective stability increases. In some simulations, the Hadley cell expanded but the temperature gradients at its terminus remained relatively fixed. The enhanced eddy-transport outside the Hadley cell suggests a mechanism for this to occur. Because, in its absence, the Hadley cell terminus would experience an increased meridional temperature gradient implied by the imposed large-scale radiative forcing.

4.4.2 Analytical solution of the energy-balance model

It is possible to solve Eqn. 4.1 analytically [see appendix] from the frame of reference of the Hadley cell edge. Thus, the Hadley cell edge is considered the boundary across which eddy energy fluxes are specified. Energy fluxes at the poles are assumed to be zero. The analytical solution of the energy-balance model does not contain a Hadley

cell parameterization, since iterations would then be necessary to enforce continuous temperatures and temperature gradients at the Hadley cell terminus—this is done numerically in the full energy-balance model solution. Nonetheless, some insight is possible, even in the absence of an explicit Hadley circulation parameterization. We find that storm tracks migrate even in this simple model and it is useful to understand why this occurs. Thus, we explore a two-mode approximation to the solution of energy-balance model without any Hadley circulation parameterization and perform several sensitivity tests.

Fig. 4.2 (top) shows the zonal-mean temperature profile for a two-mode solution of the analytical model. Here, the Hadley cell edge sits at the point $\varphi = 0$. This can be thought of as simulations in which one sits on the Hadley cell edge and observes the changes in extra-tropical meridional temperature profile as the flux across it is varied. The end-conditions are symmetric and the fluxes there are zero. Increasing the amplitude of the flux across the Hadley cell edge implies an increase in the pole-equator temperature contrast. Weaker fluxes imply flatter temperatures in the tropics, i.e., equatorward of the Hadley cell.

The large arrows in the top panel of Fig. 4.2 represent the Hadley circulation. The poleward flow occurs in the upper troposphere, while the return flow occurs near the surface. Of course, there is net poleward transport of dry static energy, $c_p\ T + g\ z$.

The zonal-mean meridional temperature-gradient profile is shown in bottom of Fig. 4.2, for the two-mode analytical solution. It is clear from this figure that the solution satisfies the boundary conditions of this problem. Storm tracks are ideal-

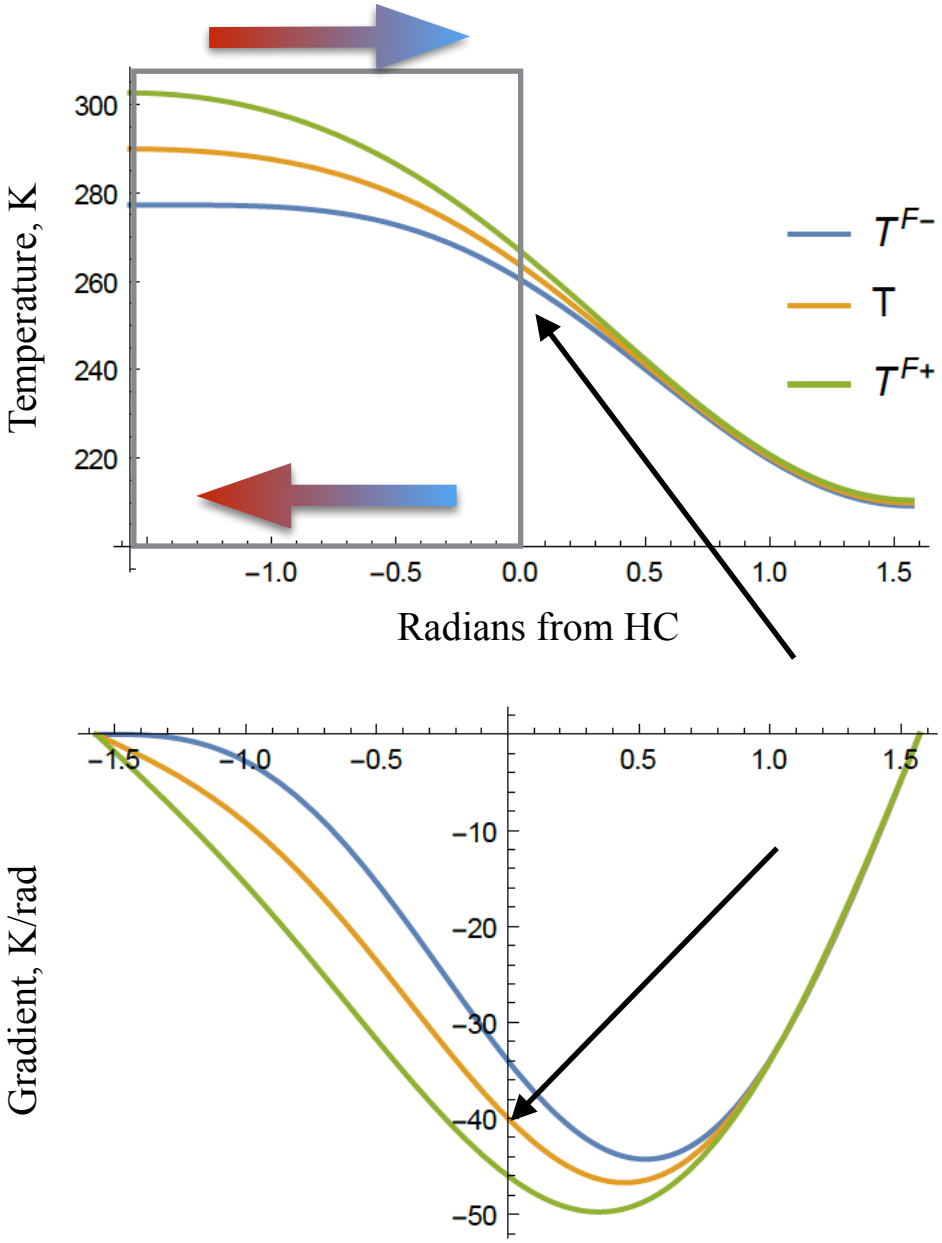

Figure 4.2: Top: zonal-mean temperature profile for a two-mode approximation of the analytical solution. The large arrows show the Hadley circulation, while the black arrow points to the Hadley terminus. Bottom: meridional temperature-gradient profile. Storm tracks are identified as global maxima of the absolute value of near-surface meridional temperature gradients. Increasing the flux across the Hadley cell edge shifts the storm tracks equatorward, relative to the Hadley cell extent.

ized as global minima in the Northern Hemisphere meridional temperature-gradient profile, or more generally as the maximum absolute value of meridional temperature gradients. From this simple model, a first mode of storm track shift is previewed, and will be further discussed later. As the flux across the boundary of the Hadley circulation increases in magnitude, i.e., becomes more negative, storm tracks within this simple configuration shift equatorward. A 12 K/rad change in the flux across the Hadley cell implies about a 7-degree change in the latitude position of the storm tracks.

The zonal-mean temperature curvature profile for a two-mode approximation of the analytical solution is shown in Fig. 4.3. Shifts in the storm tracks are easily identified as zero-crossings of each graph, the black arrow points to them. Diffusive transport divergence is proportional to the curvature of temperature. Like in Fig. 4.1, the maximum diffusion sits equatorward of the storm tracks and shifts poleward as they shift poleward. This result is similar to the one seen in the dry GCM, except that there the maximum diffusivity sits between the Hadley cell terminus and the storm tracks, while here the maximum absolute value of the temperature curvature sits inside the Hadley cell.

The red arrow in Fig. 4.3 represents the implied transient eddy fluxes across the Hadley cell terminus. In essence, this is the boundary condition of the analytical solution to the energy-balance model. It is a transient flux because the mean meridional velocity is zero at the Hadley cell terminus, and there are no zonal asymmetries in the model to excite stationary eddy fluxes.

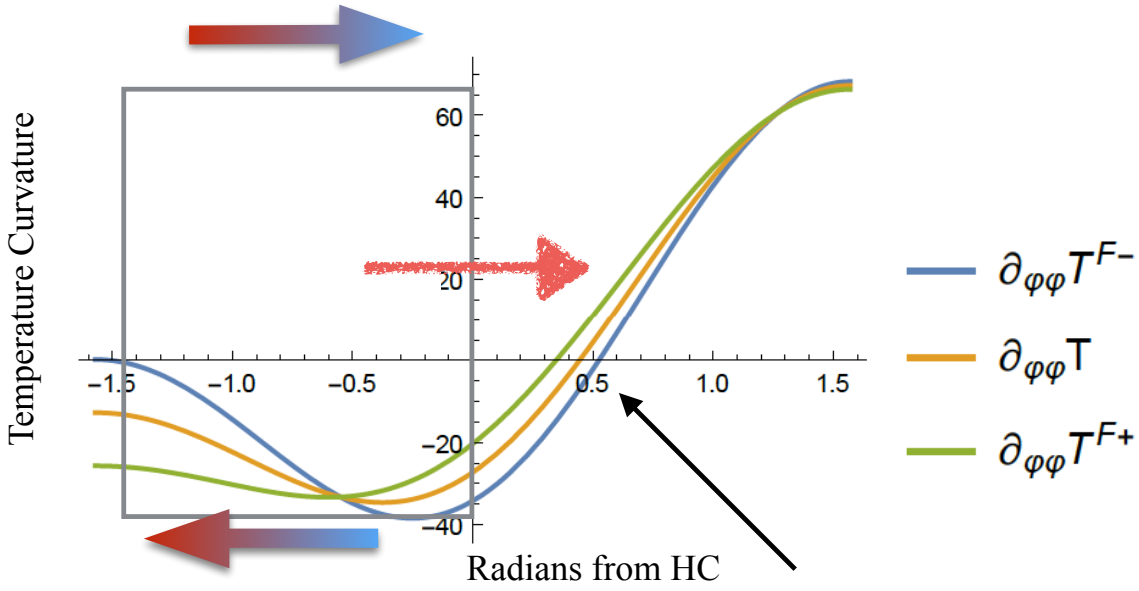

Figure 4.3: Zonal-mean meridional temperature curvature profile for a two-mode solution of the analytical model. Shifts in the storm tracks with climate are easily identified by the zero-crossings of each graph (black arrow). Maximum diffusive transport sits equatorward of the storm tracks, as seen in the GCM results. The gray box and the arrows show the Hadley cell circulation, while the red arrow shows the implied eddy transports from the tropics to the midlatitudes. The equator is at -1.5 and the Hadley cell terminus at 0.

Using the two-mode approximation of the analytical solution (see appendix), four sensitivity tests are conducted. These results are shown in Fig. 4.4. The top left panel shows storm track sensitivity to variations in the pole-equator temperature contrast. The response is logarithmic. As the pole-equator temperature contrast increases, for fixed Hadley-cell terminus flux and dry eddy efficiency, the storm tracks shift poleward, but saturate at high latitudes. The saturation is toward the forcing-imposed storm track latitude.

The dry eddy efficiency, ζ, is the ratio of the inverse diffusive time-scale to the inverse radiative time scale. If the diffusive time-scale decreases relative to the radiative time-scale, then eddies are considered to have increased their efficiency, likewise if the

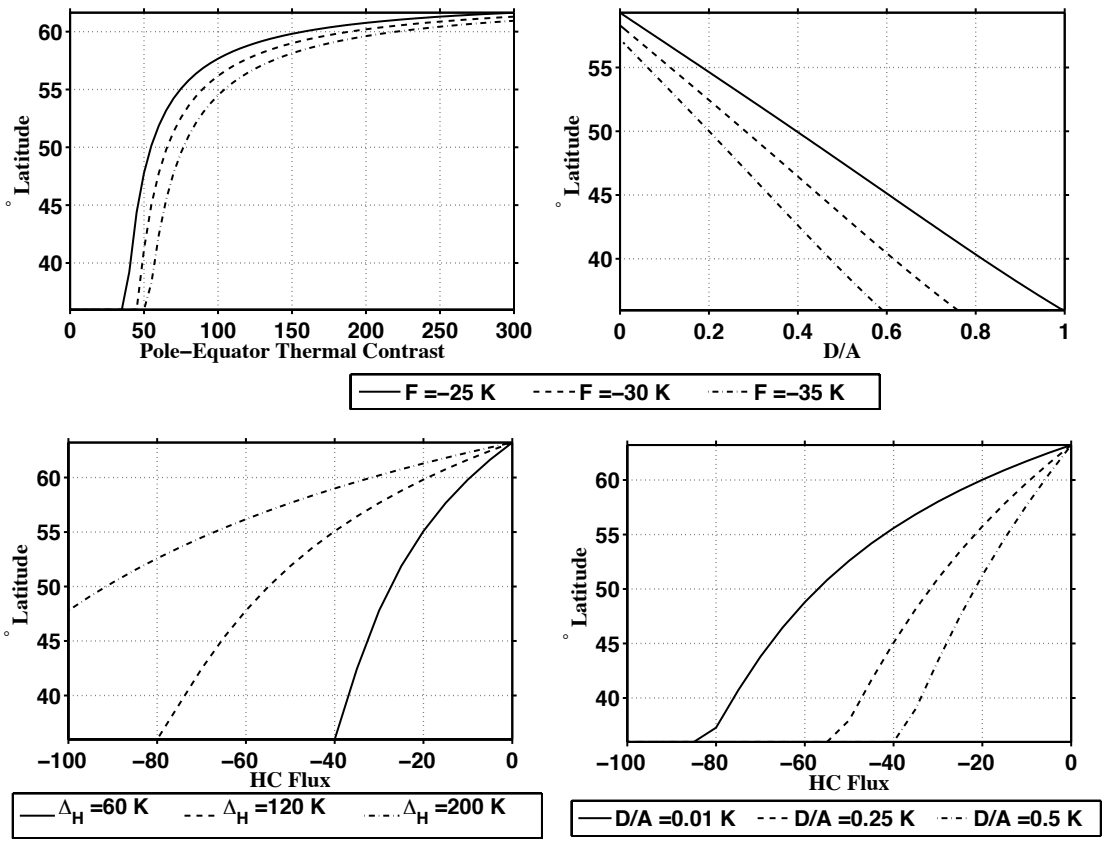

Figure 4.4: Storm track latitude sensitivity tests conducted with the analytical solution of the energy-balance model. Top left: storm track sensitivity to the pole-equator thermal contrast for three values of the Hadley cell terminus flux, F. Top right: sensitivity to dry eddy efficiency, D/A, for three values of Hadley cell terminus flux. Finally, the bottom panels show storm track sensitivity to Hadley cell terminus flux for three values of the pole-equator thermal contrast (left) and dry eddy efficiency (right).

radiative time-scale (forcing) increases relative to the diffusive time-scale. Thus, eddy efficiency decreases as (D/A) gets smaller. In this case, storm tracks move closer to the externally imposed storm track latitude, as seen in Fig. 4.4 (top left).

The bottom panels highlight an important result. That is, as the flux at the Hadley cell terminus decreases, the storm tracks migrate poleward. The left panel of Fig. 4.4 implies that storm track sensitivity to the flux at the Hadley cell boundary

decreases as the pole-equator thermal contrast increases. Similarly, as the dry eddy efficiency increases, the poleward shift induced by a change in the flux at the Hadley cell terminus increases.

This result uncovers two modes of storm track shifts. The first is through the change in the flux at the Hadley cell terminus. All else being equal, an increase in the flux there leads to an equatorward shift of storm tracks, while a decrease leads to a poleward shift. The second results if the flux at the Hadley cell terminus remains constant. Consider a reference and a perturbed climate. In the reference climate, the storm tracks will sit at a fix distance from the Hadley cell edge, let us call this distance the baroclinic length-scale. According to our model, in the perturbed climate, this length scale remains the same if the flux at the Hadley terminus remains the same. Therefore, if the perturbed climate experienced a change in the bulk stability that lead to a shift in the Hadley cell terminus, but negligible change in the flux at the terminus, then any latitudinal shifts in the storm tracks must result from shifts in the Hadley cell terminus itself. This suggests a possible mechanism by which deep tropical convection can influence storm track position: through Hadley cell dynamics.

4.4.3 Numerical solution of the full energy-balance model

The full energy-balance model is solved numerically. The zonal-mean temperature profile (left) and meridional temperature gradient (right) profile are shown in Fig. 4.5. The Hadley cell parameterization flattens temperatures in the tropics, as is apparent from the figure.

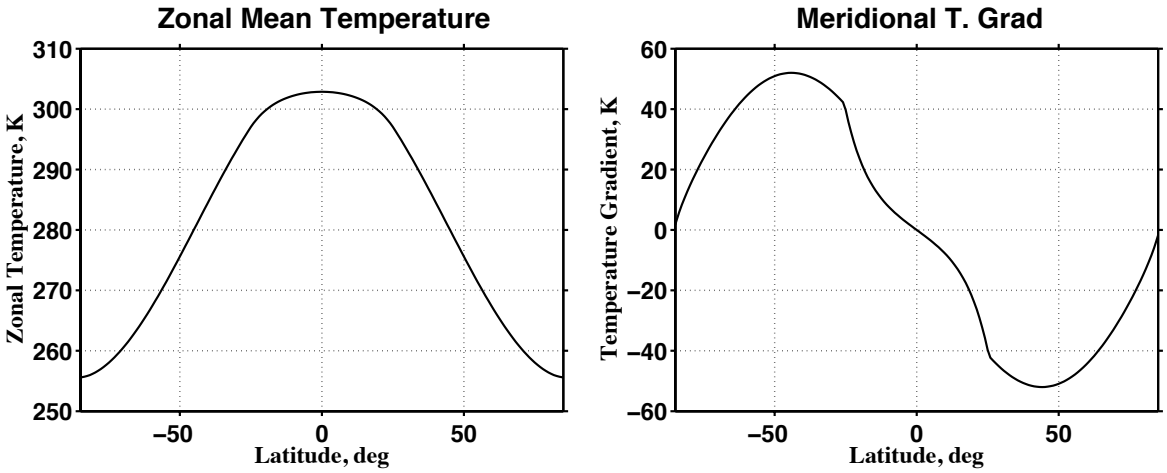

Figure 4.5: A numerical solution of the full energy-balance model. On the left is the zonal-mean temperature profile, and on the right is the zonal-mean temperature-gradient profile.

The Hadley cell width is determined by the supercriticality criterion and is largely dependent on the bulk stability and the meridional temperature gradients. For fixed meridional temperature gradients and supercriticality, increasing the bulk stability leads to a poleward expansion of the Hadley cell. We test the hypothesis that the Hadley cell width expansion can cause a shift in the storm tracks by varying the bulk stability through the convective lapse rate. The responses of the Hadley cell terminus and the storm tracks to changes in the convective stability are shown in Fig. 4.6.

The energy-balance model's response is qualitatively similar to the response seen in the idealized dry GCM: generally, as the convective stability increases, the midlatitude storm tracks migrate poleward in tandem with the Hadley cell terminus. This suggests that the energy-balance model captures the important mechanisms controlling storm track shifts in the dry idealized context.

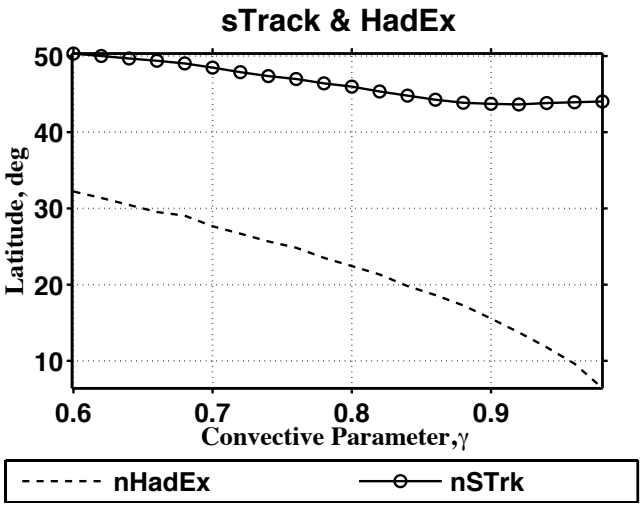

Figure 4.6: Response of the energy-balance model to changes in convective stability. The dashed line shows the Hadley cell terminus, while the solid line with the circle shows the storm tracks. As the convective stability increases (convective parameter decreases), the Hadley cell terminus shifts poleward. Likewise, from about $\gamma = 0.88$, the storm tracks shift poleward and in tandem with the Hadley cell terminus.

In low stability climates, the distance from the storm tracks to the Hadley cell edge seems too large for the expansion of the Hadley cell to be communicated to synoptic eddies in the midlatitudes. At about $\gamma \leq 0.88$, synoptic eddies begin to feel the influence of the expanding Hadley cell and commence their poleward migration. Note that the poleward expansion of the storm tracks slows at high convective stabilities. In this model, this is because of the increasing flux at the Hadley cell terminus.

Forced on its own, the energy-balance model produces results similar to the GCM and validates the hypothesis that shifts in the Hadley cell terminus can push storm tracks poleward. Next, the energy-balance model is forced with variables computed from the GCM and the two are compared.

4.4.4 Comparing the energy-balance model to the GCM

The results from the energy-balance model, forced with the bulk stability and the diffusivity computed from the dry GCM[1], is compared to the GCM results in figure Fig. 4.7. The zonal-mean temperature profiles agree, to a reasonable extent, with the largest discrepancy nearest to the poles. There are also some errors near the GCM's storm tracks. The meridional temperature-gradient profile shows that the energy-balance model does not capture the rich structure of the GCM's profile. This is because we have used a constant diffusivity versus one that is a function of latitude. There are clearly latitudes where the model is too diffusive and others where it appears not diffusive enough. We proceed with constant diffusivity to help control for the structure of eddy transports within the atmosphere. In so doing, one ascertains the degree to which shifts in the storm tracks and the Hadley cell terminus are independent of it. In future work, the idea of using a diffusivity that is a function of latitude will be explored.

The energy-balance model captures the salient features of the GCM's mean temperature and temperature-gradient profile. Importantly, in this reference simulation, the energy-balance model produces a midlatitude maximum in meridional temperature gradients near to that of the GCM ($\approx 3^\circ$ poleward of it). The models are forced in the same way and occupy different levels in the hierarchy of models. Hence, one can perturb the energy-balance model's climate to help understand the shifts in storm tracks seen in the idealized dry context. In this simplified frame-work, making

[1]The bulk stability uses near-surface values (just above the planetary boundary layer) and diffusivity is a near-surface vertical average.

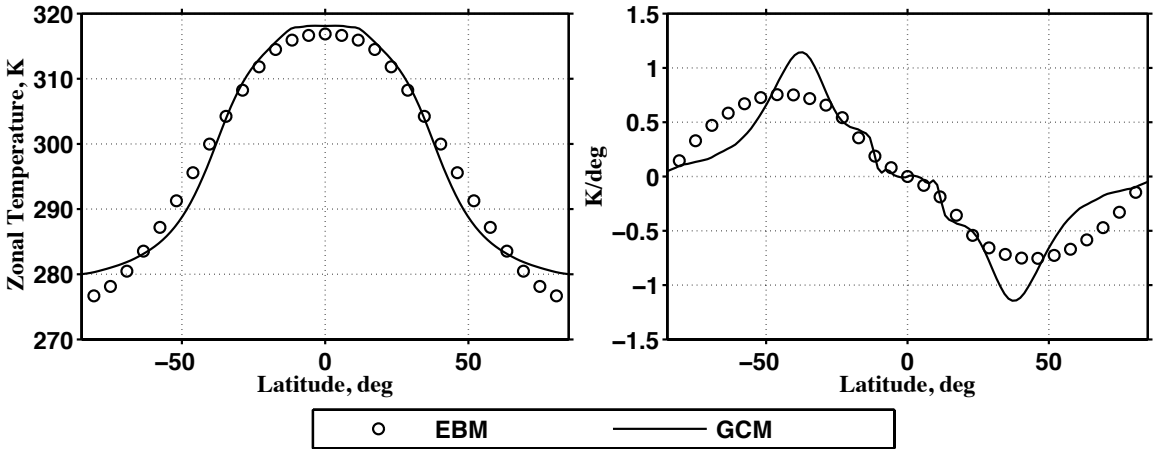

Figure 4.7: Comparing the zonal-mean temperature (left) and temperature-gradient (right) profiles from the GCM (solid lines) and the energy-balance model (circles). The zonal-mean temperatures agree. The energy-balance model is unable to capture the rich structure of the GCM's equilibrium temperature-gradient profile largely because it is forced with constant diffusivity.

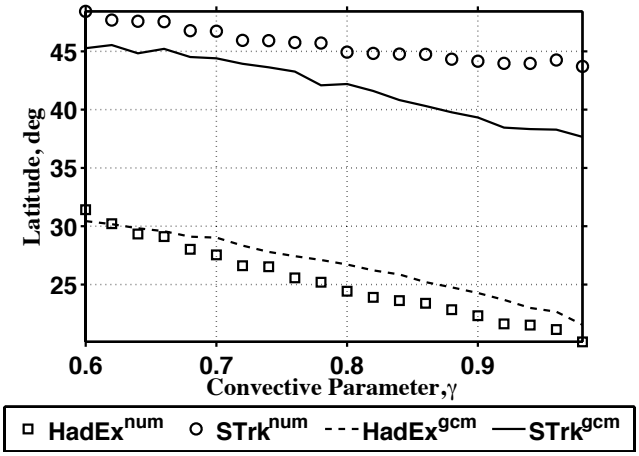

Figure 4.8: Storm track response to changes in deep tropical convective stability in the idealized dry GCM (solid black line) and in the full energy-balance model (circles). Note that deep tropical stability is inversely proportional to the convective parameter, γ. The dashed line shows the Hadley cell terminus in the GCM and the squares show it for the energy-balance model. The energy-balance model verifies that the Hadley cell's expansion can act to push storm tracks further poleward.

causal links becomes easier.

Fig. 4.8 compares storm track and Hadley terminus responses to changes in convective stability. Both models show a poleward shift of the storm tracks with increasing convective stability, and the shift occurs in tandem with the Hadley cell terminus. In the most unstable climates, the separation between the Hadley cell and the storm tracks is too large for the storm tracks to feel the impact of the expanding Hadley cell. Therefore, there is little shifting of the storm tracks in those climates. As the separation distance between the Hadley cell and the storm tracks comes to within roughly a synoptic wavelength, the storm tracks commence their tandem poleward migration with the Hadley cell edge. Thus, as seen in the figure, the total Hadley cell shift is greater than the storm track's total shift in the energy-balance model. This behavior has been seen, to some extent, in simulations using the idealized dry GCM.

4.5 Discussion and synthesis

We use a simple energy-balance model to help simplify and distill the question of storm track shifts with changing climate into its basic elements. We do this because progress in understanding storm track shifts has been hampered by the fact that many mechanisms are acting simultaneously and sometimes in canceling ways—making establishing cause and effect particularly challenging. Simple models can assist in this regard as they can be used to exclude both actual and hypothesized secondary phenomena.

This simple energy-balance model controls for some proposed mechanisms cited in the literature. The energy-balance model contains no explicit wave activity, yet

demonstrates storm track shifts similar to those seen in the idealized dry GCM. This suggests that there are modes of storm track shifts that are independent of extratropical dynamics and that changes in deep tropical stability can shift the storm tracks poleward or equatorward by changing the width of the Hadley circulation.

4.5.1 Theory

1. Storm tracks can shift simply due to expansions or contractions of the Hadley circulations, if the storm track length scale remains fixed.

2. Storm tracks can shift in response to changes in the flux at the Hadley cell edge.

An expression for the storm track latitude can be obtained from Eqn. 4.42, by setting the temperature curvature to zero.

$$0 = -F\ \sin(\varphi_{stk}) + \frac{2\ \Delta_H\ \left(7\ \sin^2(\varphi_H) + \sin(\varphi_H) - 8\right) - 15\ F\ (2\ \zeta + 1)}{8\ (6\ \zeta + 1)}\ \cos(2\ \varphi_{stk}), \tag{4.18}$$

which can be solved to obtain the storm track latitude,

$$\sin(\varphi_{stk}) = \frac{-F \pm \sqrt{F^2 + 8\ A^2}}{4A}, \tag{4.19}$$

where

$$A = \frac{2\ \Delta_H\ \left(7\ \sin^2(\varphi_H) + \sin(\varphi_H) - 8\right) - 15\ F\ (2\ \zeta + 1)}{8\ (6\ \zeta + 1)}. \tag{4.20}$$

The sensitivity of storm track position to each of the parameters is presented in Fig. 4.4. Nonetheless, the aforementioned statements are immediate from Eqn. 4.19. Note that in the analytical solution, φ_H is a radiative forcing parameter. It helps define the radiative forcing in the extratropics.

4.5.2 Model limitations

The energy-balance model used in this study has several limitations which need to be borne in mind when interpreting these results. The energy-balance model resolves a single vertical level. It lacks vertical transport which occurs in a real atmosphere. Therefore, it becomes challenging to apply and interpret dynamical parameterizations, like the convective transports in the tropics. Also, the model cannot simultaneously represent near-surface properties, where the diffusive nature of the model is most valid, and top-of-the-atmosphere properties, where terrestrial radiative loss occurs and where an important radiative balance applies. Nonetheless, the error associated with this eventuality does not grossly affect the conclusions drawn from this analysis, as a comparison to the results to the full idealized GCM output shows.

Furthermore, there is no reason to suppose that energy transports are diffusive at all latitudes; this is likely to fail in the deep tropics. Moreover, ocean transports and latent transports are not explicitly represented. Inter-scale interactions are not represented, though this may be represented by adding a stochastic element to the diffusive-transport parameterization (Lorenz, 1979). Finally, and perhaps most importantly, this model contains no moist-thermodynamics or transports. However, to

first order, the effects of moisture can be thought of as modifying eddy efficiency and tropospheric stability.

Nonetheless, the simplicity of this model is its greatest utility. Experiments are simple to perform and easy to interpret. It is true that many real-world processes are missing in the energy-balance model. However, the model captures the basic physics of the temporal scale that we are interested in, and, should the phenomenon of interest still manifest (i.e., should storm tracks migrate poleward), then it provides evidence that unrepresented processes may be secondary. Therefore, used in concert with a hierarchy of models, energy-balance models become good tools to gain insights into storm track dynamics, and climate dynamics in general.

4.5.3 Hypothesis validation

The results of this study support the hypothesis of Mbengue and Schneider (2013) and Mbengue and Schneider (2015). The mechanism for the storm track shifts seen in the idealized dry GCM can be summarized as follows, for simulations in which mean radiative-equilibrium temperature is varied: as the climate warms, the tropopause height increases (for fixed emission temperature), the bulk stability increases leading to an expansion of the Hadley cell; as the Hadley cell expands, near-surface temperature gradients are pushed further poleward, thus pushing the storm tracks further poleward. Fig. 4.9 summarizes this mechanism.

A similar mechanism explains the shift seen in Mbengue and Schneider's (2013) deep tropical convective stability simulations: as the deep tropical convective stability

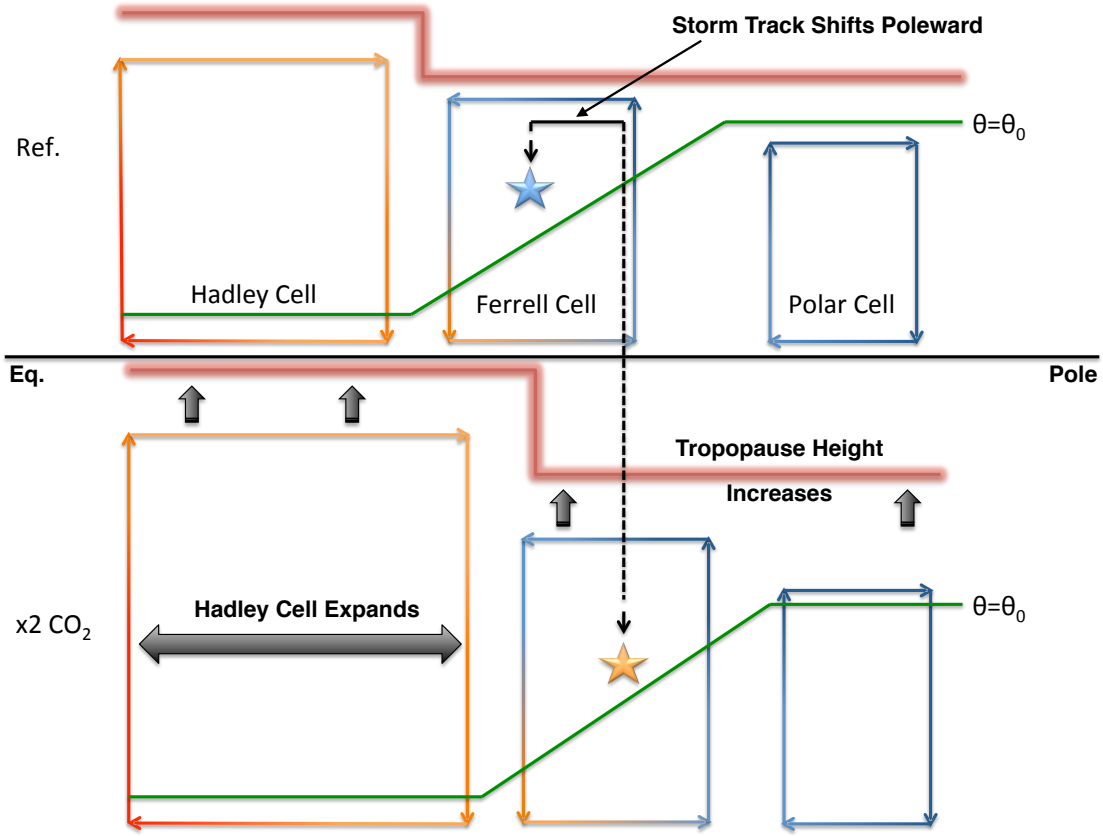

Figure 4.9: Schematic of our proposed storm track shift mechanism. The stars represent the storm track latitude in each climate. The top figure represents the control climate, while the bottom represents the perturbed climate. As the climate warms, the tropopause (red line) height increases (black arrows), indicative of an increase in the bulk stability. The Hadley cell expands and expels near-surface meridional temperature (green line) gradients farther poleward. As a result, storm tracks are forced farther poleward.

increases, the bulk stability increases (through increases in the convective stability and tropopause height), which leads to an expansion of the Hadley cell. Again, the expanding Hadley cell pushes near-surface temperature gradients outward shifting the storm tracks further poleward.

The tandem translation of the Hadley cell terminus and the storm tracks has been noted before. But, until now causality was difficult to establish; here, we uncover one

mode of tropical control of the storm track shifts with changing climate.

The second mode of storm track shifts seen in our simple model does not conflict with previous work on extratropical control of storm tracks shifts. We find that changes in the flux across the Hadley cell boundary can lead to shifts in the storm tracks. Both tropical and extratropical dynamics can influence the energy flux across the Hadley cell. For example, midlatitude waves propagating equatorward and breaking near their critical line (axis where the phase speed equals the background flow speed), which would be in the vicinity of the Hadley cell terminus, would decelerate the upper-level flow, leading to a reduction in the shear and an implied reduction in the near-surface temperature gradients. In accordance with our findings, this scenario would lead to a poleward shift in the storm tracks if the Hadley cell does not contract enough to compensate.

4.5.4 Relation to prior work

Prior studies have posited that poleward shifts of the storm tracks are solely due to changes in the height of the tropopause (Williams, 2006; Lorenz and DeWeaver, 2007). We complete their mechanism by showing that increases in the height of the tropical tropopause leads to an increase in the bulk stability and to an expansion of the Hadley cell, which pushes out near-surface temperature gradients—and thus, the storm tracks.

In some of MS13's simulations, the storm tracks did not exactly parallel the expanding storm tracks. This could be due to both mechanisms highlighted here acting

together. Validation of this hypothesis is left for future work.

Studies of inter-annual variability of storm tracks show that they migrate equatorward during the El Niño phase of the Southern Oscillation (while the opposite is true during the La Niña phase) (Chang et al., 2002). During El Niño, tropical temperatures increase. Given the observed contraction of the Hadley cell during El Niño (Seager et al., 2003; Adam et al., 2014) and the increase in meridional temperature gradients, our theory predicts an equatorward shift of the storm tracks in agreement with observations.

Observations of the seasonal cycle of the Northern Hemisphere storm tracks show that they migrate equatorward during the winter (Chang et al., 2002). The Northern Hemisphere winter is the time when the region is the most baroclinically unstable, marked by strong temperature gradients and vertical shear. Indeed, the increasing midlatitude/subtropical temperature gradients is sufficient to pull storm tracks equatorward—as is any contraction of the Hadley cell terminus.

Ice-albedo feedbacks suggests that in a warming Earth-like environment, the poles will heat more than the equator in a phenomenon known as polar amplification. In this context, the reduction of midlatitude and subtropical temperature gradients imply an enhanced poleward migration of storm tracks with polar amplification.

All of these observations must be placed within context. The storm tracks are strongly influenced by stationary eddy activity (Kaspi and Schneider, 2011, 2013) and the climate system has many feedbacks not accounted for in the simple model presented here. Nonetheless, we have shown two modes for storm track shifts that

are largely consistent with what is observed and with what has been found before.

4.6 Conclusion

A generally agreed upon theory of storm track shifts with climate change remains elusive. This is likely because there are many competing mechanisms acting in sometimes canceling ways. This issue is exacerbated by using complex simulations or observations in isolation to try to understand the mechanisms driving storm track response.

We use several numerical models of varying complexity to develop a theory of storm track shifts with changing climate. These models are used in an interdependent way, e.g., we use the dry GCM to help force the diffusive energy-balance model. Moreover, by using simple models, we isolate quantities believed to be important drivers of the storm tracks and vary them independently.

Although others have used models similar to those we have employed, this is the first time, to our knowledge, that an energy-balance model is used with a simple parameterization of the Hadley cell. Additionally, we now provide a closed theory for the storm track response seen in Mbengue and Schneider (2013) and support for the hypotheses made in Mbengue and Schneider (2015).

We showed that there are two modes of storm track shifts. The first is one in which the Hadley cell acts to push near-surface meridional temperature gradients farther poleward, when the storm track length scale remains fixed. Second, changes in the flux across the Hadley cell can lead to changes in the storm track length scale

and the storm track position.

Sensitivity tests conducted with the analytical model show that it is possible for the storm tracks to shift due to changes in eddy transport efficiency. In the presence of strong radiative forcing, storm tracks would sit near the radiatively-forced latitude. Eddy activity transports energy and dissipates the radiatively produced meridional temperature gradients, which are constantly restored by large-scale radiative forcing. These large-scale processes, in concert with eddy activity, conspire to set the steady-state zonal-mean storm track position. As the climate changes, eddy effectiveness can be changed by processes that increase the eddies' workload; for example, increases in the meridional temperature gradients or reduction in the large-scale thermal restoration time-scale. Climate change can also result in increases in eddy efficiency. For example, as the climate warms, eddies ladened with more latent energy because of increased evaporation are more efficient at poleward energy transport (Pierrehumbert, 2002; Caballero and Langen, 2005; O'Gorman and Schneider, 2008a; Cabellero and Hanley, 2012).

The simple model used in this study does not contain any information about the structure of eddies themselves, although the second mode uncovered provides an avenue for them to act. Nevertheless, we find clear evidence that near-surface dynamics are likely driving the shifts in storm tracks.

We started with the observed poleward shift of the midlatitude storm tracks with warming. Recognizing the complexity of the problem, we simplified it by isolating variations in mean temperature from those of stability. In so doing, we discovered

that changes in deep tropical convective stability (tropical convection) could shift the midlatitude storm tracks poleward. This lead us to search for mechanisms that could communicate changes in stability in the deep tropics to shifts in the extratropical storm tracks. One candidate that stood out was the tandem migrating Hadley cell circulation. Hence, we tested the hypothesis that the Hadley cell can cause shifts in the storm tracks and confirmed that it does.

4.7 Appendix

4.7.1 Numerics

The base code of the energy-balance model was written by Tapio Schneider, while the parameterizations were written by Cheikh Mbengue.

4.7.2 Boundary conditions

To enforce Neumann boundary conditions at the end points, reflection boundary points are used such that,

$$T_1 = T_3; \qquad T_n = T_{n-2} \tag{4.21}$$

$$D_1 = D_3; \qquad D_n = D_{n-2} \tag{4.22}$$

where n is the number of grid points and D represents the diffusivity for the case of variable diffusivity.

4.7.2.1 Diffusive energy fluxes

The diffusive-flux operator is discretized as follows,

$$\mathcal{D}_j = {}^1\!/_2((D_{j+1} + D_j)(T_{j+1} - T_j) - (D_{j-1} + D_j)(T_j - T_{j-1}))\Delta\varphi^{-2}, \tag{4.23}$$

where j represent spatial grid points.

4.7.2.2 Time stepping

The discretized energy-balance equation is given by,

$$T_j^{n+1} = T^n + \frac{\mathcal{D}_j}{R^2 cos(\varphi_j)}\ \Delta t + {}^1/_{\tau_{rad}}(E_j - T_j^n)\ \Delta t \qquad (4.24)$$
$$+ {}^1/_{\tau_{eq}}(T_0^n - T_j^n)\ \mathcal{H}\left(|\varphi_h| - |\varphi_j|\right)\ \Delta t,$$

where n represents the temporal level and φ_h is the Hadley terminus latitude.

The time step, dt, is limited to maintain the stability of the simulations. It depends on the grid spacing, $\Delta\varphi$, the diffusivity, D_0, and the heat capacity, C_0. It is formally expressed as,

$$dt = 0.49\ \frac{\Delta\varphi^2\ max[R^2\ C_0\ \cos(\varphi_j)]}{D_0\ C_0}. \qquad (4.25)$$

The diffusive cfl number is 0.49.

4.7.3 Radiative forcing in the analytical solution

The radiative forcing profile, $E(\varphi)$, to which temperatures are relaxed is hemispherically symmetric. The domain of the analytical solution to the energy-balance model is one hemisphere, yet the equator represents the Hadley cell terminus and the pole is still the pole. Therefore, the radiative profile of the analytical solution must be transformed to reflect this. The transformation is given as,

$$E(\varphi) = \overline{T}_E + \Delta_H \left(1/3 - (\sin(\varphi_H) + (1 - \sin(\varphi_H))\ \sin(\varphi))^2\right), \qquad (4.26)$$

where φ_H is the latitude of the Hadley cell terminus.

4.7.4 1D energy-balance model: the analytical solution

Starting with the partial differential equation (PDE) for a one-dimensional diffusive energy-balance model without the Hadley circulation parameterization,

$$\partial_t \check{T}(\mu,t) = \partial_\mu \left(1-\mu^2\right) D \; \partial_\mu \check{T}(\mu,t) + A\left(E(\mu) - \check{T}(\mu,t)\right), \tag{4.27}$$

where φ is latitude, $\mu = \sin(\varphi)$, D is a constant diffusion of dry static energy, A is the inverse of a constant radiative time scale, i.e., $A = 1/\tau_{rad}$, and $E(\mu)$ is the meridional radiative-equilibrium temperature profile. We specify Neumann boundary conditions at the Hadley cell edge ($\mu = 0$) and at the pole ($\mu = 1$)

$$\begin{aligned} \partial_\mu \check{T}(0,t) &= F \\ \partial_\mu \check{T}(1,t) &= 0. \end{aligned} \tag{4.28}$$

F in Eqn. 4.28 specifies the flux across the terminus of the Hadley cell. The initial condition is an arbitrary function of latitude whose form is inconsequential, since we will ultimately be interested in steady-state solutions,

$$\check{T}(\mu,0) = \check{\psi}(\mu). \tag{4.29}$$

This PDE can be solved analytically. First, we homogenize boundary conditions by defining a new temperature, $\acute{T}(\mu,t) = \check{T}(\mu,t) - F\,(\mu + 2^{-1}\mu^2)$. Using $\acute{T}$ in the original PDE yields the transformed pde,

$$\begin{aligned}
\partial_t \acute{T}(\mu,t) &= \partial_\mu \left(1-\mu^2\right) D\ \partial_\mu \acute{T}(\mu,t) - A\ \acute{T}(\mu,t) + \acute{S}(\mu),\\
\partial_\mu \acute{T}(0,t) &= 0,\\
\partial_\mu \acute{T}(1,t) &= 0,\\
\acute{T}(\mu,0) &= \psi(\mu),
\end{aligned} \tag{4.30}$$

where $\acute{S}(\mu) = D\ F\,(1-3\mu^2-2\mu) - A\ F\,(\mu+2^{-1}\mu^2) + A\ E(\mu)$ and $\psi(\mu) = \check{\psi}(\mu) - F\,(\mu+2^{-1}\mu^2)$. A final simplification is made by specifying temperature, $T(\mu,t) = e^{A\ t}\ \acute{T}(\mu,t)$, and substituting it into the transformed PDE, we obtain,

$$\begin{aligned}
\partial_t T(\mu,t) &= \partial_\mu \left(1-\mu^2\right) D\ \partial_\mu T(\mu,t) + S(\mu,t),\\
\partial_\mu T(0,t) &= 0,\\
\partial_\mu T(1,t) &= 0,\\
T(\mu,0) &= \psi(\mu),
\end{aligned} \tag{4.31}$$

where $S(\mu,t) = \acute{S}(\mu)e^{A\ t} = \left[D\ F\,(1-3\mu^2-2\mu) - A\ F\,(\mu+2^{-1}\mu^2) + A\ E(\mu)\right] e^{A\ t}$. Noting that the diffusive operator is the Legendre differential operator, with solution $-D\ n(n+1)P_n(\mu)\ \forall\ n \in (0,\mathbb{N})$, where $P_n(\mu)$ are Legendre polynomials. One can now employ an eigenfunction expansion of the PDE in terms of Legendre polynomials.

Thus, if we let $T(\mu,t) = \sum_n \tau_n(t)P_n(\mu)$ and $S(\mu,t) = \sum_n s_n(t)P_n(\mu)$, then our PDE transforms into the ODE,

$$\partial_t \tau_n(t) + D\ n(n+1)\tau_n(t) = s_n(t), \tag{4.32}$$

$$\tau_n(0) = (2n+1)\int_0^1 \psi(\mu)P_n(\mu)\ d\mu, \tag{4.33}$$

$$s_n(t) = (2n+1)\int_0^1 S(\mu,t)P_n(\mu)\ d\mu, \tag{4.34}$$

where we have used the orthogonality property of Legendre polynomials,

$$\int_0^1 P_m(\mu)P_n(\mu)\ d\mu = (2n+1)^{-1}\delta_{mn}, \tag{4.35}$$

to obtain Eqns. 4.33 and 4.34. We use an integrating factor to solve Eqn. 4.32,

$$\tau_n(t) = \int_0^t s_n(\hat{t})e^{D\ n(n+1)(\hat{t}-t)}\ d\hat{t} + \tau_n(0)e^{-D\ n(n+1)t}. \tag{4.36}$$

Since, the time dependence of $s_n(t)$ is known,

$$s_n(t) = (2n+1)\int_0^1 S(\mu,t)P_n(\mu)\ d\mu = e^{A\ t}(2n+1)\int_0^1 \acute{S}(\mu)P_n(\mu)\ d\mu = e^{A\ t}s_n,$$

then, we can perform the integral to obtain:

$$\tau_n(t) = \frac{s_n}{D\ n(n+1)+A}e^{A\ t} + \left(\tau_n(0) - \frac{s_n}{D\ n(n+1)+A}\right)e^{-D\ n(n+1)t}.$$

This implies,

$$T(\mu,t) = \sum_n \frac{s_n}{D\ n(n+1)+A} P_n(\mu) e^{A\ t} + \left(\tau_n(0) - \frac{s_n}{D\ n(n+1)+A}\right) P_n(\mu) e^{-D\ n(n+1)t}$$

and further implies,

$$\acute{T}(\mu,t) = \sum_n \frac{s_n}{D\ n(n+1)+A} P_n(\mu) + \left(\tau_n(0) - \frac{s_n}{D\ n(n+1)+A}\right) P_n(\mu) e^{-[D\ n(n+1)+A]t}.$$

Thus, we obtain the solution to Eqn. 4.27, which is the near-surface meridional temperature profile,

$$\check{T}(\mu,t) = F\left(\mu + 2^{-1}\mu^2\right) + \sum_n \frac{s_n}{D\ n(n+1)+A} P_n(\mu) + \left(\tau_n(0) - \frac{s_n}{D\ n(n+1)+A}\right) P_n(\mu) e^{-[D\ n(n+1)+A]t}. \tag{4.37}$$

The first two terms yield the steady-state solution which, to satisfy the boundary conditions, only admits even Legendre polynomials:

$$\check{T}(\mu) = F\left(\mu + 2^{-1}\mu^2\right) + \sum_{2n} \frac{s_n}{D\ n(n+1)+A} P_n(\mu). \tag{4.38}$$

We use the same radiative-equilibrium temperature profile as found in the idealized dry GCM,

$$E(\mu) = \overline{T}_E + \Delta_H \left(1/3 - \left(\mu_H + (1-\mu_H)\ \mu\right)^2\right), \tag{4.39}$$

Where σ is the mean radiative-equilibrium temperature and Δ_h is the pole-equator temperature contrast. Using Eqns. 4.38 and 4.39 we obtain a steady-state two-mode solution,

$$\begin{aligned}\check{T}(\varphi) = \sigma - \frac{F\ (23+78\ \zeta) - 2\ \Delta_H\ \left(7\ \sin^2(\varphi_H) + \sin(\varphi_H) - 8\right)}{48\ (6\ \zeta+1)} \left(3\ \sin^2(\varphi) - 1\right) \\ + F\ \sin(\varphi)(1 + 2^{-1}\sin(\varphi)) - F\,(2/3+\zeta) - \sin(\varphi)\ \Delta_H\ (1+\sin(\varphi))\,/3,\end{aligned} \tag{4.40}$$

$$\partial_\phi \check{T}(\varphi) = F\ \cos(\varphi) + \frac{2\ \Delta_H\ \left(7\ \sin^2(\varphi_H) + \sin(\varphi_H) - 8\right) - 15\ F\ (2\ \zeta+1)}{16\ (6\ \zeta+1)}\ \sin(2\ \varphi), \tag{4.41}$$

$$\partial_{\phi\phi} \check{T}(\varphi) = -F\ \sin(\varphi) + \frac{2\ \Delta_H\ \left(7\ \sin^2(\varphi_H) + \sin(\varphi_H) - 8\right) - 15\ F\ (2\ \zeta+1)}{8\ (6\ \zeta+1)}\ \cos(2\ \varphi), \tag{4.42}$$

where ζ is the dry eddy efficiency, given by $\zeta = D/A = 86400\ D_0\ \tau_{rad}\ R^{-2}$.

Using Legendre polynomials as eigenfunctions in the solution of a 1-D energy-balance equation to infer about climate change can be traced back to the work of North (1975a) and North (1975b).

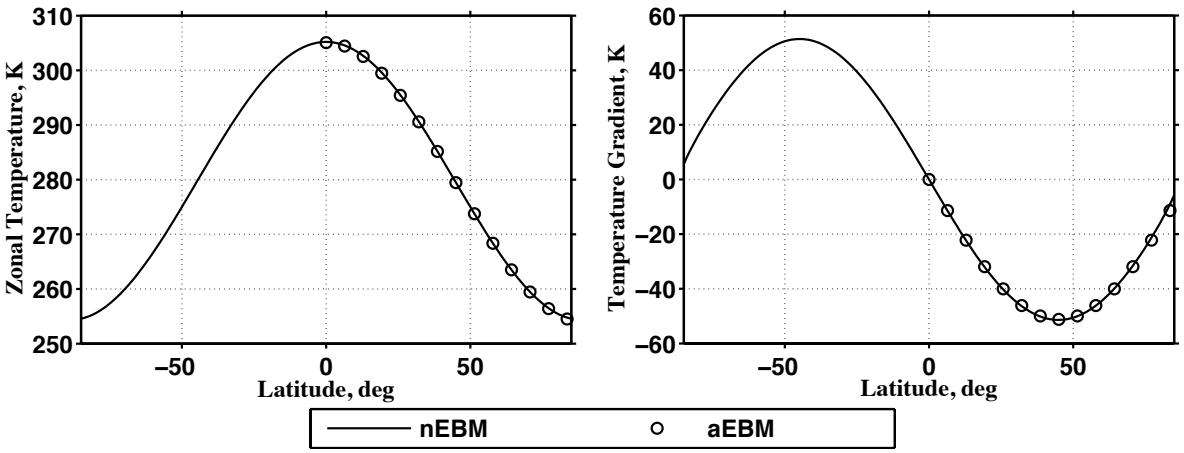

Figure 4.10: Zonal-mean temperature profile (left) and meridional temperature-gradient profile (right) for the numerical solution of the energy-balance model (solid line) and for the analytical solution(circles). The models are forced with the same parameters and boundary conditions. This is done to cross validate the models. The models produce the same solution.

4.7.5 Model cross validation

The truncated two-mode and the numerical solution are forced with the same (default) parameters and compared in Fig. 4.10. The boundary conditions for the analytical solution are 0 flux at the equator and at the pole. There is no Hadley cell parameterization for the cross validation. Both models agree on the solution, thus verifying their accuracy.

Chapter 5

Conclusion

Midlatitude storm tracks are an important medium for energy and angular momentum redistribution within Earth's atmosphere, and they will change as the climate changes. Climate models, supported by a growing body of observational data, have demonstrated that storm tracks shift poleward as the climate warms. But the dynamical mechanisms responsible for this shift remain unclear.

To isolate what portion of the storm track shift may be accounted for by large-scale dry dynamics alone, disregarding the latent heat released in phase changes of water, chapter 2 investigated the storm track shift under various kinds of climate change in an idealized dry general circulation model (GCM) with an adjustable but constant convective stability. It was found that increasing the mean surface temperature or the convective stability led to poleward shifts of storm tracks, even if the convective stability was increased only in a narrow band around the equator. Under warming and convective stability changes roughly corresponding to a doubling of CO_2 concentrations from a present-day Earth-like climate, storm tracks shift about 0.8° poleward, somewhat less than but in qualitative agreement with studies using moist GCMs. Five eighths of the poleward shift was shown to be caused by tropical

convective stability variations.

This demonstrated that tropical processes alone (the increased dry static stability of a warmer moist adiabat) can account for part of the poleward shift of storm tracks under global warming. This poleward shift generally occurred in tandem with a poleward expansion of the Hadley circulation; however, the Hadley circulation expansion did not always parallel the storm track shift.

Chapter 2 showed that zonal-mean storm track shifts in response to perturbations in climate occur even in very idealized simulations: dry atmospheres with axisymmetric forcing. In chapter three, it was demonstrated that the eddy kinetic energy in a storm track is linearly related to the local mean available potential energy (MAPE) and that maxima of the two generally are collocated in latitude.

Changes in local mean available potential energy with climate were then decomposed into components. It was shown that, for the simulations here, changes in the latitude of maximum local MAPE are dominated by changes in near-surface meridional temperature gradients. By contrast, changes in the magnitude of local MAPE are largely determined by changes in static stability and in the depth of the troposphere. Therefore, a theory of storm track shifts may build on these findings and need primarily to explain meridional changes in near-surface meridional temperature gradients. The Hadley circulation has been shown to shift in tandem with the storm tracks and was hypothesized to play an important role in facilitating the storm track shifts seen in this idealized dry context, especially in simulations where increases in deep tropical convective stability shift storm tracks poleward.

In chapter 3, we showed that near-surface meridional temperature gradients were important for understanding storm track shifts. We noted, consistent with similar studies (Kang and Polvani, 2011; Ceppi and Hartmann, 2013), the tandem shifts of the storm tracks and the Hadley cell terminus. In chapter 4, we tested the idea that expansions of the Hadley circulation contribute to shifts in the storm tracks. We used a diffusive energy-balance model forced by Newtonian relaxation toward radiative equilibrium. The model contained a simple Hadley cell parameterization that strongly reduces temperature gradients within the Hadley cell. The termination latitude of the Hadley cell was determined based on a criterion that quantifies where baroclinic eddies become deep enough to reach the tropopause.

This work demonstrates a clear link between Hadley circulation dynamics and storm track position. The energy-balance model is very simple and contains few parameters; however, they are all physically motivated. The results show that expansions of the Hadley cell, induced, for example, by increases in tropical static stability, can shift the storm tracks poleward. This explains the majority of the shift in the storm tracks seen in an idealized dry GCM. Storm track sensitivity to several other quantities in dry climates is also elucidated.

With the aid of a hierarchy of models, we obtain a closed theory of storm track shifts in dry climates. One can begin to generalize the results contained herein to moist atmospheres, to first order, by interpreting moisture transports as acting to increase the efficiency of dry eddy energy transports and as modifying the static stability of the atmosphere. Also, one would diffuse moist static energy instead of

dry static energy.

Bibliography

Adam, O., T. Schneider, and N. Harnik, 2014: Role of changes in mean temperatures versus temperature gradients in the recent widening of the Hadley circulation. *Journal of Climate*, **27**, 7450–7461.

Ait-Chaalal, F. and T. Schneider, 2015: Why eddy momentum fluxes are concentrated in the upper troposphere. *Journal of the Atmospheric Sciences*, **72**, 1585–1604.

Ambaum, M. H. P. and L. Novak, 2014: A nonlinear oscillator describing storm track variability. *Quarterly Journal of the Royal Meteorological Society*, **140**, 2680–2684.

Andrews, D. G., 1981: A note on potential energy density in a stratified compressible fluid. *J. Fluid Mech.*, **107**, 227–236.

Asselin, R., 1972: Frequency filter for time integrations. *Mon. Wea. Rev.*, **100**, 487–490.

Barnes, E. and L. M. Polvani, 2013: Response of the midlatitude jets and of their variability to increased greenhouse gases in the CMIP5 models. *Journal of Climate*.

Bender, F., V. Ramanathan, and G. Tselioudis, 2012: Changes in extratropical storm track cloudiness 1983-2008: observational support for a poleward shift. *Climate Dynamics*, **38**, 2037–2053.

Bengtsson, L., K. Hodges, and E. Roeckner, 2006: Storm tracks and climate change. *Journal of Climate*, **19**, 3518–3543.

Blackmon, M., 1976: A climatological spectral study of the 500mb geopotential height of the Northern Hemisphere. *Journal of the Atmospheric Sciences*, **33**, 1607–1623.

Blackmon, M., J. Wallace, N. Lau, and S. Mullen, 1977: An observational study of the Northern Hemisphere wintertime circulation. *Journal of the Atmospheric Sciences*, **34**, 1040–1053.

Brayshaw, D., B. Hoskins, and M. Blackburn, 2008: The storm-track response to idealized SST perturbations in an aqua-planet GCM. *Journal of the Atmospheric Sciences*, **65**, 2842–2860.

Brayshaw, D. J., B. Hoskins, and M. Blackburn, 2009: The basic ingredients of the North Atlantic storm track. Part I: land-sea contrast and orography. *Journal of the Atmospheric Sciences*, **66**, 2539–2558.

Brayshaw, D. J., B. Hoskins, and M. Blackburn, 2011: The basic ingredients of the North Atlantic storm track. Part II: sea surface temperatures. *Journal of the Atmospheric Sciences*, **68**, 1784–1805.

Budyko, M. I., 1969: The effect of solar radiation variations on the climate of the Earth. *Tellus*, **XXI**, 611–619.

Butler, A., D. Thompson, and T. Birner, 2011: Isentropic slopes, downgradient eddy fluxes, and the extratropical atmospheric circulation response to tropical tropospheric heating. *Journal of the Atmospheric Sciences*, **68**, 2292–2305.

Butler, A. H., W. J. Thompson, and R. Heikes, 2010: The steady-state atmospheric

circulation response to climate change-like thermal forcings in a simple general circulation model. *Journal of Climate*, **23**, 3474–3496.

Caballero, R. and P. Langen, 2005: The dynamic range of poleward energy transport in an atmospheric general circulation model. *Geophysical Research Letters*, **32**, L02 705, doi:10.1029/2004GL021 581.

Cabellero, R. and J. Hanley, 2012: Midlatitude eddies, storm-track diffusivity, and poleward moisture transport in warm climates. *Journal of the Atmospheric Sciences*, **69**, 3237–3250.

Ceppi, P. and D. L. Hartmann, 2013: On the speed of the eddy-driven jet and the width of the Hadley cell in the Southern Hemisphere. *Journal of Climate*, **26**, 3450–3465.

Chang, E., S. Lee, and K. Swanson, 2002: Storm track dynamics. *Journal of Climate*, **15**, 2163–2183.

Chang, E. K. M., 2013: CMIP5 projection of significant reduction in extratropical cyclone activity over North America. *Journal of Climate*, **26**, 9903–9922.

Charney, J. G., 1947: The dynamics of long waves in a baroclinic westerly current. *Journal of Meteorology*, **4 (5)**, 135–162.

Chen, G. and I. Held, 2007: Phase speed spectra and the recent poleward shift of Southern Hemisphere surface westerlies. *Geophysical Research Letters*, **34**, L21 805, doi:10.1029/2007GL031 200.

Chen, G., I. M. Held, and W. A. Robinson, 2007: Sensitivity of the latitude of the surface westerlies to surface friction. *Journal of the Atmospheric Sciences*, **64**, 2899–2915.

Chen, G., J. Lu, and D. Frierson, 2008: Phase speed spectra and the latitude of surface westerlies: interannual variability and global-warming trend. *Journal of Climate*, **21**, 5942–5959.

Dutton, J. A. and D. R. Johnson, 1967: The theory of available potential energy and a variational approach to atmospheric energetics. *Advances in Geophysics*, **12**, 333–436.

Eady, E. T., 1949: Long waves and cyclone waves. *Tellus*, **1**, 33–52.

Emanuel, K., 2007: Quasi-equilibrium dynamics of the tropical atmosphere. *The Global Circulation of the Atmosphere*, T. Schneider and A. Sobel, Eds., Princeton University Press, NJ, USA, 186–218.

Frierson, D. M. W., I. M. Held, and P. Zurita-Gotor, 2007: A gray-radiation aqua-planet moist GCM. Part II: energy transports in altered climates. *Journal of the Atmospheric Sciences*, **64**, 1680–1693.

Fyfe, J., 2003: Extratropical Southern Hemisphere cyclones: harbingers of climate change? *Journal of Climate*, **16**, 2802–2805.

Garfinkel, C. I., D. W. Waugh, and E. P. Gerber, 2012: The effect of tropospheric jet

latitude on coupling between the stratospheric polar vortex and the troposphere. *J. Climate*, **26**, 2077–2095.

Geng, Q. and M. Sugi, 2003: Possible change of extratropical cyclone activity due to enhanced greenhouse gases and sulfate aerosols—study with a high resolution AGCM. *Journal of Climate*, **16**, 2262–2274.

Hartmann, D. L., 1974: Time spectral analysis of mid-latitude disturbances. *Mon. Wea. Rev.*, **102**, 348–362.

Hartmann, D. L., 1994: *Global physical climatology*. Academic Press, CA, USA.

Held, I., 1982: On the height of the tropopause and the static stability of the troposphere. *Journal of the Atmospheric Sciences*, **39 (2)**, 228–241.

Held, I. and T. Schneider, 1999: The surface branch of the zonally averaged mass transport circulation in the troposphere. *Journal of the Atmospheric Sciences*, **56**, 1688–1697.

Held, I. M., 2000: The general circulation of the atmosphere. Wood Hole Oceanographic Institute.

Holliday, D. and M. E. McIntyre, 1981: On potential energy density in an incompressible, stratified fluid. *J. Fluid Mech.*, **107**, 221–225.

Holton, J., 2004: *An introduction to dynamic meteorology*. 4th ed., Elsevier Academic Press, MA, USA.

Hoskins, B. and K. Hodges, 2002: New perspectives on the Northern Hemisphere winter storm tracks. *Journal of the Atmospheric Sciences*, **59**, 1041–1061.

Hoskins, B. J. and P. J. Valdes, 1990: On the existence of storm-tracks. *Journal of the Atmospheric Sciences*, **47**, 1854–1864.

Hu, Y. and Q. Fu, 2007: Observed poleward expansion of the Hadley circulation since 1979. *Atmos. Chem. Phys.*, **7**, 5229–5236.

Kang, D. and O. Fringer, 2010: On the calculation of available potential energy in internal wave fields. *Journal of Physical Oceanography*, **40**, 2539–2545.

Kang, S. and L. M. Polvani, 2011: The interannual relationship between the latitude of the eddy-driven jet and the edge of the Hadley cell. *Journal of Climate*, **24**, 563–568.

Kaspi, Y. and T. Schneider, 2011: Downstream self-destruction of storm tracks. *Journal of the Atmospheric Sciences*, **68**, 2459–2464.

Kaspi, Y. and T. Schneider, 2013: The role of stationary eddies in shaping midlatitude storm tracks. *Journal of the Atmospheric Sciences*, **70**, 2596–2613.

Kidston, J., S. M. Dean, J. A. Renwick, and G. K. Vallis, 2010: A robust increase in the eddy length scale in the simulation of future climates. *Geophysical Research Letters*, **37**, L03 806, doi:10.1029/2009GL041 615.

Kidston, J. and E. P. Gerber, 2010: Intermodel variability of the poleward shift of the

austral jet stream in the CMIP3 integrations linked to biases in 20th-century climatology. *Geophysical Research Letters*, **37**, L09 708, doi:10.1029/2010GL042 873.

Korty, R. L. and T. Schneider, 2008: Extent of Hadley circulations in dry atmospheres. *Geophysical Research Letters*, **35, L23803, doi:10.1029/2008GL035847**.

Kushner, P. J. and L. M. Polvani, 2004: Stratosphere-troposphere coupling in a relatively simple AGCM: the role of eddies. *Journal of Climate*, **17**, 629–639.

Levine, X. and T. Schneider, 2015: Baroclinic eddies and the extent of the Hadley circulation: an idealized GCM study. *Journal of the Atmospheric Sciences*, **00**, 0000–0000.

Lindzen, R. and B. Farrel, 1980: A simple approximate result for the maximum growth rate of baroclinic instabilities. *Journal of the Atmospheric Sciences*, **37**, 1648–1654.

Lorenz, D. J., 2014: Understanding midlatitude jet variability and change using Rossby wave chromatography: wave-mean flow interaction. *Journal of the Atmospheric Sciences*, **71**, 3684–3705.

Lorenz, D. J. and E. T. DeWeaver, 2007: Tropopause height and zonal wind response to global warming in the IPCC scenario integrations. *Journal of Geophysical Research*, **112**, D10 119, doi:10.1029/2006JD008 087.

Lorenz, E., 1955: Available potential energy and the maintenance of the general circulation. *Tellus*, **VII (2)**, 157–167.

Lorenz, E. N., 1979: Forced and free variations of weather and climate. *Journal of the Atmospheric Sciences*, **36**, 1367–1376.

Lu, J., G. Chen, and D. Frierson, 2010: The position of the midlatitude storm track and eddy-driven westerlies in aquaplanet AGCM. *Journal of the Atmospheric Sciences*, **67**, 3984–4000.

Lu, J., A. G. Vecchi, and T. Reichler, 2007: Expansion of the Hadley cell under global warming. *Geophysical Research Letters*, **34**, doi: 10.1029/2006GL028 443.

Mbengue, C. and T. Schneider, 2013: Storm track shifts under climate change: what can be learned from large-scale dry dynamics. *Journal of Climate*, **26**, 9923–9930.

Mbengue, C. and T. Schneider, 2015: Storm track shifts under climate change: toward a mechanistic understanding using local measures of mean available potential energy. In prep.

Mellor, G. L. and T. Yamada, 1982: Development of a turbulence closure model for geophysical fluid problems. *Rev. Geophys. Space Phys.*, **20**, 851–871.

Murray, R. J. and I. Simmonds, 1991: A numerical scheme for tracking cyclone centers from digital data. Part I: development and operation of the scheme. *Aust Met. Mag.*, **39**, 155–166.

Nakamura, H., 1992: Midwinter suppression of baroclinic wave activity in the Pacific. *Journal of the Atmospheric Sciences*, **49**, 1629–1642.

Nakamura, H., 1998: Hadley circulation as a modulator of the extratropical climate. *Journal of the Atmospheric Sciences*, **49**, 2437–2457.

NOAA/GFDL, cited 2015: The spectral dynamical core [Available online at `http://data1.gfdl.noaa.gov/~arl/pubrel/m/atm\_dycores/src/atmos\_spectral/documentation/spectral\_core.pdf`].

North, G. R., 1975a: Analytical solution to a simple climate model with diffusive heat transport. *Journal of the Atmospheric Sciences*, **32**, 1301–1307.

North, G. R., 1975b: Theory of energy-balance climate models. *Journal of the Atmospheric Sciences*, **32**, 2033–2043.

O'Gorman, P., 2010: Understanding the varied response of the extratropical storm tracks to climate change. *PNAS*, **107 (45)**, 19 176–19 180.

O'Gorman, P., 2011: The effective static stability experienced by eddies in a moist atmosphere. *Journal of the Atmospheric Sciences*, **68**, 75–90.

O'Gorman, P. and T. Schneider, 2008a: The hydrological cycle over a wide range of climates simulated with an idealized GCM. *Journal of Climate*, **21**, 3815–3832.

O'Gorman, P. and T. Schneider, 2008b: Weather-layer dynamics of baroclinic eddies and multiple jets in an idealized general circulation model. *Journal of the Atmospheric Sciences*, **65**, 524–535.

Orlanski, I. and J. Katzfey, 1991: The life cycle of a cyclone wave in the Southern Hemisphere. Part I: eddy energy budget. *Journal of the Atmospheric Sciences*, **48**, 1972–1998.

Peixoto, J. P. and A. H. Oort, 1992: *Physics of Climate*. Springer-Verlag, NY, USA.

Phillips, N., 1956: The general circulation of the atmosphere: a numerical experiment. *Quarterly Journal of the Royal Meteorological Society*, **82 (352)**, 123–164.

Pierrehumbert, R., 2002: The hydrologic cycle in deep-time climate problems. *Nature*, **419**.

Riviere, G., 2011: A dynamical interpretation of the poleward shift of the jet streams in global-warming scenarios. *Journal of the Atmospheric Sciences*, **68**, 1253–1272.

Robert, A. J., 1966: The integration of a low order spectral form of the primitive meteorological equations. *J. Meteor. Soc. Japan*, **44**, 237–245.

Roe, G. H., N. Feldl, K. C. Armour, Y. Hwang, and D. M. W. Frierson, 2015: The remote impacts of climate feedbacks on regional climate predictability. *Nature Geosci.*, **8**, 135–139.

Roe, G. H. and R. S. Lindzen, 2001: A one-dimensional model for the interaction between continental-scale ice sheets and atmospheric stationary waves. *Climate Dynamics*, **17**, 479–487.

Rogers, R. R. and M. K. Yau, 1989: *A short course in cloud physics*. 3d ed., Butterworth Heinemann, MA, USA.

Santer, B., R. Sausen, T. Wigley, and J. Boyle, 2003: Behavior of tropopause height and atmospheric temperature in models, reanalyses, and observations: decadal changes. *Journal of Geophysical Research*, **108**, D14 002, doi:10.1029/2002JD002 258.

Schneider, E. K., 1984: Some minimization calculations concerning the effect of horizontal eddy momentum fluxes on the equilibrium zonal-mean motions. *Journal of the Atmospheric Sciences*, **41**, 1640–1647.

Schneider, T., 2004: The tropopause and the thermal stratification in the extratropics of a dry atmosphere. *Journal of the Atmospheric Sciences*, **61**, 1317–1340.

Schneider, T., 2007: The thermal stratification of the extratropical troposphere. *The Global Circulation of the Atmosphere*, T. Schneider and A. Sobel, Eds., Princeton University Press, NJ, USA, 47–77.

Schneider, T. and P. O'Gorman, 2008: Moist convection and the thermal stratification of the extratropical troposphere. *Journal of the Atmospheric Sciences*, **65**, 3571–3583.

Schneider, T., P. O'Gorman, and X. Levine, 2010: Water vapor and the dynamics of climate changes. *Reviews of Geophysics*, **48**, RG3001, doi:10.1029/2009RG000 302.

Schneider, T. and C. Walker, 2006: Self-organization of atmospheric macroturbulence into critical states of weak nonlinear eddy-eddy interactions. *Journal of the Atmospheric Sciences*, **63**, 1569–1586.

Schneider, T. and C. Walker, 2008: Scaling laws and regime transitions of macroturbulence in dry atmospheres. *Journal of the Atmospheric Sciences*, **65**, 2153–2173.

Seager, R., N. Harnik, Y. Kushnir, W. Robinson, and J. Miller, 2003: Mechanisms of hemispherically symmetric climate variability. *J. Climate*, **16**, 2960–2978.

Seidel, D. J., Q. Fu, W. J. Randel, and T. J. Reichler, 2008: Widening of the tropical belt in a changing climate. *Nature Geosci.*, **1**, 21–24.

Seidel, D. J. and W. J. Randel, 2007: Recent widening of the tropical belt: evidence from tropopause observations. *Journal of Geophysical Research*, **112**, D20 113, doi:10.1029/2007JD008 861.

Sellers, W. D., 1969: A global climatic model based on the energy balance of the Earth-atmosphere system. *Journal of Applied Meteorology*, **8**, 392–400.

Smagorinsky, J., S. Manabe, and J. L. Holloway, 1965: Numerical results from a nine-level general circulation model of the atmosphere. *Mon. Wea. Rev.*, **93**, 727–768.

Stone, P. H., 1978: Baroclinic adjustment. *Journal of the Atmospheric Sciences*, **35**, 561–571.

Swart, N. and J. Fyfe, 2012: Observed and simulated changes in the Southern Hemisphere surface westerly wind-stress. *Geophysical Research Letters*, **39**, L16 711,doi:10.1029/2012GL052 810.

Tailleux, R., 2013: Available potential energy and exergy in stratified fluids. *Annu. Rev. Fluid Mech.*, **45**, 35–58.

Tandon, N. F., E. P. Gerber, A. H. Sobel, and L. M. Polvani, 2012: Understanding Hadley cell expansion versus contraction: Insights from simplified models and implications for recent observations. *Journal of Climate*, **26**, 4304–4321.

Thompson, D. W. J. and T. Birner, 2012: On the linkages between the tropospheric isentropic slope and eddy fluxes of heat during Northern Hemisphere winter. *Journal of the Atmospheric Sciences*, **69**, 1811–1823.

Tsushima, Y., et al., 2006: The importance of the mixed-phase cloud distribution in the control climate for assessing the response of clouds to carbon dioxide increase: a multi-model study. *Climate Dynamics*, **27**, 113–126.

Wallace, J. M., G. H. Lim, and M. L. Blackmon, 1988: Relationship between cyclone tracks, anticyclone tracks, and baroclinic wave guides. *Journal of the Atmospheric Sciences*, **45**, 439–462.

Williams, G. P., 2006: Circulation sensitivity to tropopause height. *Journal of the Atmospheric Sciences*, **63**, 1954–1961.

Williams, P. D., 2009: A proposed modification to the Robert-Asselin time filter. *Mon. Wea. Rev.*, **137**, 2538–2546.

Xu, K. and K. Emanuel, 1989: Is the tropical atmosphere conditionally unstable? *Mon. Wea. Rev*, **117**, 1471–1479.

Yin, J., 2005: A consistent poleward shift of the storm track in simu-

lations of 21st-century climate. *Geophysical Research Letters*, **32**, L18 701, doi:10.1029/2005GL023 684.